1-1-2016

Crossed Beam Imaging Of The Reaction Dynamics Of Halogen Atoms With Selected Hydrocarbons

Yuanyuan Shi
Wayne State University,

CROSSED BEAM IMAGING OF THE REACTION DYNAMICS OF HALOGEN ATOMS WITH SELECTED HYDROCARBONS

by

YUANYUAN SHI

DISSERTATION

Submitted to the Graduate School

of Wayne State University,

Detroit, Michigan

in partial fulfillment of the requirements

for the degree of

DOCTOR OF PHILOSOPHY

2016

MAJOR: CHEMISTRY (Physical)

Approved By:

_____

Advisor Date

_____

_____

_____

_____

DEDICATION

This dissertation is dedicated to

My father: Shi, Yining;

My mother: Zhuang, Xuemei;

My friend: Dai, Xinyuan.

ACKNOWLEDGEMENTS

It seems like everyone in his childhood would be asked a question like “what you want to do when you grow up?” I remembered my answer was, I wanted to be a scientist; although at that time I did not even have any clue of what does a scientist mean. After five years in graduate school, I gained some feeling of what the life of researchers can look like. This section is my part of expressing my forever gratitude to all who helped me going through my PhD degree.

The first person comes to my mind is my advisor, Prof. Arthur G. Suits, one of the best scientists in chemical reaction dynamics. He is always full of exciting ideas and has a never-ending passion for science. I am more than glad to have been allowed to join his group and work under his guidance. He is a great mentor with even greater personality, always patient and nice; he taught me a great deal and helped me to overcome many difficulties.

I am amazingly fortunate to be part of the crossed-beam team in Suits Lab. It is a very challenging project, but I owe deep thanks to a former postdoc, Dr. Baptiste Joalland. He gave me the beginner’s tutorial and taught me how to operate the machine. I also worked with a smart and hard-working student Alexander Kamasah. The Suits Lab has a big diversity and I would like to say thank you to all, past and present, for their contributions in making a wonderful group: Dr. Nuradhika Herath, Dr.Armando Estillore, Dr. James Oldham, Dr. Kirill Prozument, Dr. Arghya Dey, Richard Van Camp, Nitin Patel, Dr. Lu Yan, Dr. Bernadette Broderick, Dr. Fadia Cudry, Dr. Chamara Abeysekera, Yunmin Lee, Dr. Lindsay Zack, Nuwandi Ariyasingha, Chaya Amarasinghe, Chandika Amarasinghe, Dr. James Thompson and my good friend Dr. Ravin Fernando.

I would like to thank my dissertation committee members: Prof. Wen Li, Prof. H. Bernhard Schlegel, Prof. Young-Hoon Ahn and Prof. Guangzhao Mao for their suggestions in completing

this dissertation. I thank all Chemistry Department staff for their help, Melissa Barton, Erin Bachert, Deborah McCreless, Diane Kudla, Nester Ocampo and Mary Wood. Thanks to all my friends in the Chemistry Department, especially Yanlong Zhu and Chenchen He; the three of us come from the same college and they are like my brother and sister. They are always kind and generous to offer help to me. Thanks to Bishnu Thapa for helping me to figure out Gaussian calculations. Also special thanks to Xinyuan Dai, Yang Liu and Weiwei Li, who are always willing to listen to me and help me to build up my strength and recover courage to go through the PhD life.

Last but not least, I would give my acknowledgements to my parents. They support me to the best they can and I am proud of being their daughter. They take serious consideration of my thoughts and plans, and help me with any decisions I made; they teach me to live a happier life and become a better person. They share the happiness and sorrow of my study and life. I could not finish this PhD without their love and support.

PREFACE

This dissertation is based closely on the following refereed publications:

Chapter 1: Joalland, B.; Shi, Y.; Estillore, A. D.; Kamasah, A.; Mebel, A. M.; Suits, A. G., Dynamics of chlorine atom reactions with hydrocarbons: insights from imaging the radical product in crossed beams. *J Phys Chem A* **2014,** *118* (40), 9281-95. DOI**:** 10.1021/jp504804n

Chapter 2: Abeysekera, C.; Joalland, B.; Shi, Y.; Kamasah, A.; Oldham, J. M.; Suits, A. G., Note: A short-pulse high-intensity molecular beam valve based on a piezoelectric stack actuator. *Rev Sci Instrum* **2014,** *85* (11), 116107. DOI: 10.1063/1.4902153

Chapter 3: Joalland, B.; Shi, Y. Y.; Patel, N.; Van Camp, R.; Suits, A. G., Dynamics of Cl plus propane, butanes revisited: a crossed beam slice imaging study. *Phys Chem Chem Phys* **2014,** *16* (2), 414-420. DOI: 10.1039/c3cp51785c

Chapter 4: Joalland, B.; Van Camp, R. D.; Shi, Y.; Patel, N.; Suits, A. G., Crossed-beam slice imaging of Cl reaction dynamics with butene isomers. *J. Phys. Chem. A* **2013**.
DOI: 10.1021/jp403030s

Chapter 5: Joalland, B., Shi, Y., Kamasah, A., Suits, A. G., & Mebel, A. M. (2014). Roaming dynamics in radical addition–elimination reactions. *Nature communications*, 5. DOI: 10.1038/ncomms5064

Chapter 6: Shi, Y. Y.; Kamasah, A.; Joalland, B.; Suits, A. G., Crossed-beam DC slice imaging of fluorine atom reactions with linear alkanes. *Journal of Chemical Physics* **2015,** *142* (18). DOI: 10.1063/1.4919099

Chapter 7: paper just submitted to JPCA

The author of this dissertation performed the experiments, analyzed the data and wrote the papers above. Prof. Alexander Mebel did the calculations for Chapter 5. The advisor: Prof. Arthur G. Suits conceived and designed the experiments.

TABLE OF CONTENTS

LIST OF TABLES

LIST OF FIGURES

CHAPTER 1-INTRODUCTION

1.1 Crossed beam dc slice imaging on differential cross sections

Differential cross sections (DCSs) obtained in crossed molecular beam experiments provide a comprehensive picture of the intimate dynamics of molecular collisions. Reactive scattering distributions in particular provide extraordinary insight into reaction mechanisms and reveal how molecular forces influence the dynamics during the approach and separation from the transition-state (TS) region. Reactions of atomic chlorine with alkanes represent a rich and well-studied class of reactions where such complex interactions may be studied in exquisite detail. Dynamical studies on this family of reactions, as well as on chlorine reactions involving functionalized hydrocarbons, were comprehensively reviewed by Murray and Orr-Ewing[1], with a particular emphasis on insights provided by rotational state-selective detection of the HCl product.

State-to-state angular distributions obtained for reactions of atomic chlorine with methane and ethane enabled Zare and coworkers to "picture" the Cl-H-C TS region and the impact of vibrational excitation of the target reactant.[2-7] The measured rotational state distribution of the HCl ($v' = 0$) product was found cold and strongly backscattered for the ground state reaction, both behaviors being consistent with a narrow cone of acceptance and a collinear TS geometry. The angular distribution was however dramatically affected by vibrational enhancement of methane, suggesting an opening of the potential energy landscape: a broader cone of acceptance and the possibility for the TS geometry to be bent. These results were obtained with the PHOTOLOC technique, a single beam apparatus where reactions are initiated by the photodissociation of Cl_2 at 355 nm and angular distributions determined through product speed distribution measurements using the core extraction technique.[8, 9] In PHOTOLOC studies on Cl+alkane reactions involving larger hydrocarbons, for which the abstraction reactions become

more favorable and slightly exoergic, HCl (or DCl) (v' = 0) rotational distributions were also found cold and backscattered, expanding the Cl+methane/ethane ground state reaction picture to a more general agreement for Cl+alkane reactions.[10-13]

Crossed-beam experiments have the capability of allowing experimentalists to control the initial state (e.g. energize the reagents' mode independently) and reactants direction. Besides, radical and target molecules could be confined in separate supersonic beams, ensuring reactions at specified collision energies. [14, 15]And crossed-beam studies allow the measurements of angular and translational energy distributions, the so-called double DCSs, giving access to the coupling between scattering angles and the energy partitioning into translational and internal degrees of freedom of the co-products. While in the past it was necessary to extrapolate the full distributions in the scattering plane by convolution fits from time-of-flight measurements at selected angles, the combination of crossed beam experiments with ion imaging provides the possibility to measure the full angular and translational energy (E_T) distributions at once. In particular, the DC slice imaging technique allows for direct inversion of the experimental data with no assumptions about the associated dynamics, revealing the coupling of energy and angular distributions to appear in full detail. Crossed-beam imaging also allows for detection of any product mass and recoil energy combination without the kinematic constraints associated with measuring laboratory time-of-flight spectra to obtain the velocity-flux distributions. A related advantage is that the center of mass distributions are simply a linear offset of the laboratory distributions, with no associated transformation Jacobian. The slice images themselves embody the velocity-flux contour maps that directly reflect the underlying collision dynamics. In other words, ion imaging turns the spotlight directly on the molecular forces acting at the moment of chemical reactions.

1.2 Roaming Reaction Mechanisms

For a very long time the dissociation of isolated molecules was supposed to have two decomposition pathways. One is to form a pair of smaller molecules described by a tight saddle point transition state, the other is simply bond stretching before breaking and gives out highly reactive radical products. In 2004 the term 'roaming' was coined which described a third, complex decomposition pathway forming products distinctly different from the one described by a tight saddle point transition state; additionally it can generate another set of products by simple bond fission, which means it entangled with the conventional pathway.[16]

The reaction that motivated the roaming pathway and best illustrated it is the formaldehyde dissociation. Generally theoretical and experimental results were in good agreement in finding vibrationally ground state CO and H_2 while the rotational distribution maximum of CO is within 40-50 range and H_2 is moderately rotationally excited.[17-21] In 1993 Moore and coworkers performed experimental reaction dynamics study of formaldehyde dissociation and when they excited H_2CO with higher energy than the H + HCO radical threshold, they observed a small shoulder toward lower rotational levels in the CO rotationally distribution as well as the well understood major peak.[22] They proposed one reason for this anomaly to be some unknown interaction between radical pathway and molecular pathway; another explanation is the anharmonicity of the transition state. This issue was addressed by a combined experimental and theoretical investigation of H_2 and CO formation in H_2CO dissociation at energies just above the radical threshold.[16] Two distinct mechanisms were found with high-resolution state-resolved imaging measurement of CO velocity distributions. One involves the well-characterized transition state and produced rotationally excited CO and vibrationally cold H_2, as the conventional dissociation pathway; the other mechanism produced rotationally cold CO and

vibrationally excited H_2. Quasi-classical trajectory calculations ascribed the second one to be an intramolecular H abstraction, which is the so-called roaming mechanism.

The second reported experimental roaming system was acetaldehyde dissociation to CH_4 and CO.[23, 24] Further theoretical work on CH_3CHO dissociation confirmed the roaming mechanism and now it is clear roaming is the dominant pathway.[24-26] Molecular beam experiments on NO_3 and a variety of alkanes characterized roaming.[27-31] And roaming has been reported in numerous other systems such as propene, acetone, formic acid, ethyl radical, large aliphatic aldehydes etc.[32-36] Roaming is widely recognized as an important and long-overlooked mechanism of unimoleculer dissociation.[37, 38]

1.3 Halogen reactions with hydrocarbons

Reactions of chlorine atoms with polyatomic hydrocarbons represent a vast body of important chemical events in atmospheric chemistry, notably as a source to form complex and highly reactive hydrocarbon radicals via metathesis reactions.[39, 40] Chlorine atom is indeed a powerful oxydizing agent involved in some major environmental issues such as the ozone-destruction cycle,[41-43] the oxidation of volatile organic compounds in marine boundary layers[44, 45] and Polar regions,[46, 47] the burning of hazardous waste,[48, 49] and possibly the aging of organic aerosols by heterogeneous processes.[50-52] Numerous kinetics studies have shown evidence for the high efficiency of hydrocarbon decomposition by Cl atoms.[53, 54] These reactions are faster than those with the hydroxyl radical OH by at least one order of magnitude,[55] although OH is the primary daytime oxidant in the atmosphere. Interestingly, recent observations show evidence for an active chlorine chemistry in the interstellar medium, but its potential role in space has so far hardly been explored.[56, 57] Studying Cl + RH reactions is also useful to gain a detailed understanding of combustion chemistry as exemplars of

the free radical abstraction of hydrogen atoms in saturated hydrocarbons.[58, 59] The high dimensionality and complexity of the potential energy surfaces (PESs), combined with experimental feasibility, is finally a central motivation to undertake detailed dynamics studies for of Cl + RH reactions.[1, 60, 61]

Cl atom reactions with alkanes are prototypical direct H abstractions, with nearly no barrier from reactants to products. They lie in the intermediate regime, i.e., these reactions are close to isoergicity. Considerable effort has been devoted to understanding the dynamics of this family of reactions, especially in the case of methane, CH_4, and its isotopologues. [2-4, 8, 62, 63]Experimental outcomes with theoretical confirmation showed a cold vibrational and rotational state distribution in the nascent HCl/DCl (v',j') ascribed to a collinear C–H(D)–Cl transition state (TS), which turned out to be a universal signature of these reactions.[10, 11, 64] In contrast, reactions with alkenes leading to the formation of HCl are strongly exoergic owing to the formation of resonantly stabilized radical products. Overall, the potential energy landscape is strongly affected by the presence of the CC double bond with pronounced differences in reactive behavior for alkylic, allylic, or vinylic sites. The production of vibrationally excited HCl(v'=1) has been detected with 2,3-dimethyl-but-2-ene in chlorinated solvents.[65] Furthermore, the dynamics of these reactions is considerably obscured by the competition between direct and indirect reactions. HCl + C_nH_{2n-1} products can indeed be formed via a Cl addition – HCl elimination mechanism involving a long-lived $C_nH_{2n}Cl$ intermediate.[66, 67] The formation of HCl(v'=1) products has been attributed to direct reactions, whereas addition-elimination was assumed to give low vibrational excitation due to energy randomization in the long-lived adduct.[68]

The high reactivity of fluorine atoms with a range of species arises owing to the very strong

bonds it forms, which place it in a class by itself even in comparison to other halogens. This extraordinary reactivity along with its size, which permits high-level theoretical calculations, makes it a very interesting target for dynamical investigations. The F + H_2 reaction has long been a benchmark system for exploring the dynamics of reaction resonances. In 1984, Neumark *et al.* reported a groundbreaking crossed-molecular-beam experiment on the F + H_2 reaction. The intense forward scattering peaking the HF (v' = 3) product was attributed to the important role of a quantum dynamical resonance phenomenon. [69, 70] They also reported F + D_2/HD reactions, where DF (v' = 4) from F + D_2 reaction and HF (v' = 3) from F + HD reaction have strong forward scattering. [71, 72] Theoretical analysis based on the Start-Werner potential energy surface explains this step as a result of a reactive resonance. Measured differential cross sections for this reaction over a range of collision energies also display a resonance signature. [73, 74] Based on the excitation functions for F + p-H_2 and F + n-H_2, they conjured the existence of resonance in F + H_2 reaction. [75] Yang and co-workers studied the F + H_2 and F + HD reactions via the H Rydberg tagging TOF technique in a crossed beam apparatus combined with quantum dynamics calculations. At low collision energies two Feshbach resonances are important in F + H_2 reaction; at higher collision energies the HF (v' = 3) forward scattering is attributed to a slow-down mechanism over the exit barrier. [76] More recent work shows that at low collision energy, a dynamical resonance trapped in the HF (v' = 3)-D adiabatic potential well is prominent in the pathway of F + HD (v = 0) reaction. [76-78] In the study of F + HD (v' = 1) → D + HF, broad peaks for backward-scattered HF (v' = 2 and 3) products at E_C = 0.21 kcal.mol^{-1} and 0.62 kcal.mol^{-1} were observed, attributed to excited Feshbach resonances trapped in the HF (v' = 4) – D vibrationally adiabatic potential in the post barrier region. Quantum dynamics calculations show that these resonance states can only be accessed by the vibrationally excited HD reagent.

[79]

In this article, I would like to give a comprehensive overview on the reaction dynamics of halogen atoms with selected hydrocarbons and alcohol. The target systems are Cl + 1,1,1,3,3,3-propane-d_6, Cl + 2,2-propane-d_2, Cl + n-butane, Cl + 1-butene, Cl + trans-2-butene, Cl + cis-2-butene, Cl + isobutene, F + n-propane, F + n-butane, F + n-pentane, F + 1-propanol, F + 1-butene, F + 1-hexene. We use a unique experimental set-up based on the combination of crossed molecular beams and ion imaging techniques, with an emphasis on product radical detection. The reactive scattering raw images were recorded and after background subtraction and density-to-flux correction the product translational energy distributions, as well as the center of mass angular distributions were presented and discussed with related theoretical calculations.

CHAPTER 2-EXPERIMENTAL SETUP

2.1 General overview

The experimental apparatus is shown in Fig.2.1.[80] The machine is consisting of a reaction chamber and two perpendicular source chambers. The reaction chamber is evacuated to ~10^{-7} Torr to ensure single-collision requirements while the source chambers are differentially pumped to ~10^{-7} Torr base and ~10^{-5} Torr operational pressures by turbomolecular pumps. Piezoelectric valves and piezo stack valves pulsed at 10 Hz generate molecular beams and after supersonic expansions beams are skimmed upstream to enter the main chamber. Hydrocarbons and radical precursors are diluted in various carrier gases (He/Ne/Ar, based on the vapor pressure of the liquids the concentration varies, but maximum dilution percentage is 5%) to vary beam speed, thus changing the collision energy. The product radicals are ionized by a VUV excimer laser (F_2, 7.9 eV) after collision as soon as they exit the interaction region. The ions are then accelerated up via a set of four direct current slice ion optics, through a 70cm flight tube vertical to the reaction plane to impact on a dual microchannel plate (MCP) detector coupled to a P-47 phosphor screen. For Cl reaction with C3-C4 hydrocarbons, the front plate of the MCP assembly is held at constant potential while a negative high-voltage pulse is given to the back plate to 'gate' the central slice of the products at a certain m/z ratio; the condition for Cl reaction with cycloalkenes and F reactions is opposite, i.e. the voltage of MCP back plate is held constant while the front plate is pulsed. A CCD camera is used to record the raw images and the data acquisition program is NUACQ-2 with event-counting and centroiding. After background subtraction and density-to-flux correction, the experimental data is directly inverted to the uncoupled center-of-mass angular and translational energy distributions.

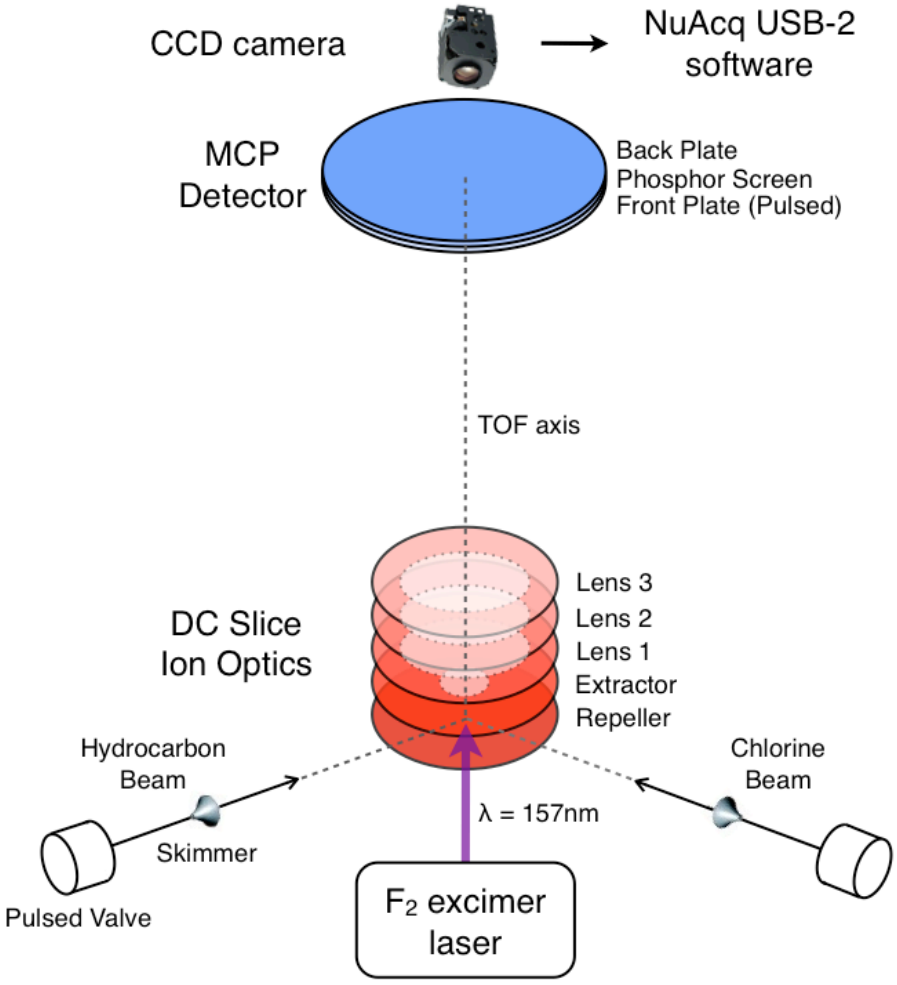

Figure 2.1: Schematic view of the crossed-molecular beam apparatus.

Ground electronic state Cl atoms are produced by the dissociation of Cl_2 from a piezoelectric disk valve and then photolyzed by the third harmonic at 355nm of a Nd:YAG laser (20mJ /pulse). The highlight of my sample preparation is the significant improvement of Cl beam density through overlapping photolysis region with an abalation plume.[81] We attached a cylindrical aluminum tube, 2 mm inner diameter; 5 cm length attached to the end of the valve nozzle and confined the molecular beam. On the side of the aluminum extension tube there is a conical aperture allowing focus the 355 nm laser beam just at the tip of the nozzle. The ratios between effective Cl populations for reaction versus the photochemical component were

enhanced greatly and would be shown in Chapter 3.

For F reaction with alkanes, we use a piezo stack valve (described in appendix) to generate 5% F_2 mixture in Helium and F atom was produced by a single state pulsed discharge. Two electrode plates were mounted in front of the nozzle to create the discharge. An insulation layer was placed between the first electrode and the ferrule to prevent unwanted discharge. The first electrode plate is held at ground while the other one is given a pulsed high voltage (+800 V); the pulse is 2 μs long and was set to discharge at the gas pulse's peak.[82]

These intense atom beams allow us to operate the VUV probe beam unfocused and our detection is highly selective with regards to the ionization energies (IEs) of the probed products. The radicals produced by photodissociation of parent hydrocarbon and alcohols can also participate in the reactive scattering signals, as a 157 nm photon can also generate signal from photodissociation of parents. We get rid of this by recording images with the 355 nm Nd-YAG laser off for chlorine reactions, discharge off for fluorine reactions and 157nm probe laser on. The integrated intensity of the background photochemistry signal is around 20% of the total in magnitude; thus it is straightforward to subtract the background reliably. Additionally, even if the background counts occur in different pixels for laser-off and laser-on images, a region containing only background could integrate to zero after correction because our subtracted images are signed values.

2.2 Direct current slice imaging

In many molecular reaction dynamics studies, a particle's speed and angular direction require simultaneous measurement. Molecular reaction studies, energy transfer processes and photodissociation can be fully understood only after specification of the velocities and internal energies of all products.[83] Product imaging, first performed by Chandler and Houston in 1987

on the photodissociation dynamics of methyl iodide, addresses the problem of simultaneous measurement by projecting the distribution of expanding photofragment onto a two-dimensional position sensitive detector and the original three-dimensional distributions were reconstructed by Abel inversion or other related techniques.[84] A major improvement of ion imaging was achieved by Eppink and Parker with the high resolution velocity map imaging based on the use of an electrostatic lens.[85] Since then this technique has become standard methods in molecular photodissociation and reactive scattering studies. However, it has two inherent shortcomings: introduction of artificial noise from inversion method and a requirement of cylindrical axis symmetry.[86] In 2001 Kitsopoulos and co-workers invoked a pulsed electric field to the expanding ionic fragment cloud followed by field free expansion. [87]Only the central 'slice' was allowed to be imaged directly, thus inverse Abel transformation can be eliminated and more polarization geometries and/or photofragment orientation become possible. Yet the introduction of a mesh grid blurred the observed image and caused a compromise with the imaging resolution.

Suits *et al.* published the direct current slice imaging method, imaging the central slice of the photofragment distribution directly without grids or pulsed electric fields.[86] The ion lens assembly is consist of a repeller plate and an extractor lens. Once the ratio of the voltage applied to the electrodes is decided particles of a certain mass with any velocity would be focused onto the same position on the detector for a given electrode system, thus reducing the image blur from molecular beam spatial spread and reaching good image resolution. Besides sharp velocity focusing, the velocity mapping apparatus also allows the spread in the arrival time at the detector of the expanding photofragment sphere to the order of several hundred nano-seconds. And a pulsed gate to the detector assembly with a 20-40ns width is quite feasible to record the distribution central slice independently.

2.3 Piezo Stack Valve

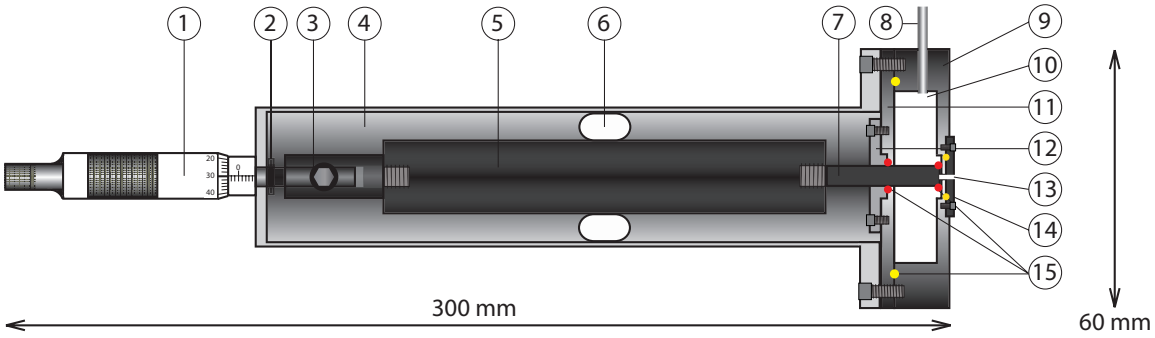

1	micrometer	6	teflon guide	11	chamber cap (SS)
2	nut	7	plunger (SS or Al)	12	ferrule (Al)
3	adapter (Al)	8	gas inlet (SS 1/16")	13	nozzle (SS 1mm)
4	half-cylinder (SS)	9	valve body (SS)	14	front plate (SS)
5	piezostack actuator	10	stagnation chamber	15	viton/kalrez o-ring

Figure 2.2: Schematic view of the valve assembly. The Piezostack actuator is mounted and aligned outside of a stainless steel valve body in a half-cylinder. The valve is scaled by Kalrez o-rings both at the tip and at half-length of the plunger. Other o-rings are shown in red.

In 1980s valves based on piezoelectric transducers were developed as molecular beam sources. Proch and Trickl's design is widely used and their design introduced a piezoelectric disk actuator.[88, 89] The requirements on fast opening times, high repetition rates and short durations calls for many improvements on the valve design, and valves based on a cantilever piezoactuator and magnetic or electromagnetic actuators were developed to address some limitations on the disk actuator acceleration force and gas throughput etc.[90-92] Recently there is a new, robust valve employing high-force piezoelectric stack actuators (Physik Instrumente, P-212.40) designed in our lab. Molecular beam characterization of dimers of 2,5-dimethylfuran (DMF_2) presents great improvements than disk translators both in pulse duration and molecular densities. [93]

Fig.2.2 is a schematic view of the valve assembly. Since any torques on the plunger can damage the piezo stack actuator (PSA), it must be mounted solely by the back; A thin-walled stainless steel cylinder, which is half open along its length, supports the PSA and one end of it is connected to the micrometer while the other to the valve base. The stack has a Teflon ring placed around it to form a snug fit with the inside of the cylinder, thus restrict all lateral movement and prevent any torque. Through a custom made adapter, the stack is connected to a fine micrometer head with a non-rotating spindle (Mitutoyo 110-102); the gas volume delivered through the nozzle orifice can be regulated through fine adjustments. The valve base is consists of a cylindrical stagnation chamber with 2.5 cm^3 volume, enclosing the plunger attached to the PSA. On the chamber cap there is a ferrule compressing an o-ring onto the plunger to seal the stagnation chamber; when the valve is closed there is another o-ring at the tip of the ferrule sealing the nozzle. As different PSAs from PI have different lengths but with the same diameter, switching to a PSA with higher force or farther travel distance only requires modify the length of the half-cylinder or the adapter. Additionally, this design protects the actuator from any contact with the corrosive gases that may reduce its lifetime. The segmented design of valve construction makes it easy to switch between different PSAs, plungers and nozzle plates, thus versatile for applications in various studies.

The valve is operated under the application of high-voltage pulse to the actuator. A voltage of +800 V is given to the PSA from a HV power supply (Kepco BHK 1000-0.2MG) via a LEMO connector to maintain the closed position. To open the valve, the actuator would be grounded by changing the actuator voltage to 0 V by a fast HV transistor switch (Behlke HTS 61-03 GSM) in a high capacitance RC circuit (R = 1Ω, C = 20 μF. In the valve paper we present the gas expanding through a 1 mm orifice in the nozzle plate. There is a rotary motion feedthrough

connected to the micrometer head to externally adjust the plunger after putting the valve into vacuum.

CHAPTER 3-REACTION DYNAMICS OF CHLORINE REACTION WITH PROPANE AND BUTANE ISOMERS

3.1 Introduction

Among alkanes, propane is the smallest one for which different and competing H abstraction sites exist. Primary abstraction to yield n-propyl and HCl is 2.0 kcal.mol^{-1} exoergic; secondary abstraction to yield isopropyl and HCl is 5.0 kcal.mol^{-1} exoergic ([94], reaction enthalpies measured at 298 K). Site-specific kinetics experiments with partially deuterated propane have revealed the "equal effectiveness" of both pathways, while primary abstraction has 3 times more H atom to occur.[10, 95] The C_4H_{10} system owns two isomers, namely n-butane ($CH_3CH_2CH_2CH_3$) and isobutane ($(CH_3)_3CH$). N-butane exhibits two primary and two secondary sites in a ratio of 3 to 2, and for isobutane three primary sites exist for only one tertiary site, with an H atom ratio of 9 to 1. Varley and Dagdigian measured a ratio of 3:1 for the cross sections of HCl(v' = 0) and DCl(v' = 0) products in the reaction of Cl atoms with labeled isobutane $(CH_3)_3CD$ despite the greater number of primary vs. tertiary hydrogens.[11] Dynamical insights on the Cl+propane abstraction reactions have been obtained using the crossed molecular beam technique in conjunction with a VUV synchrotron probe to ionize the propyl products ($h\nu$ = 9.5eV).[96] Laboratory TOF spectra and angular distributions were measured for a wide range of collision energies and, as mentioned above, the center-of-mass flux maps were interpolated from forward convolution fits to the laboratory distributions. The authors concluded on the existence of two distinct direct reaction mechanisms: a stripping mechanism characterized by a forward scattered distribution that they assigned to secondary abstraction, and a mechanism involving both primary and secondary abstractions, characterized by an impulsive product recoil that leads to the observed sideways/backward scattered components. The directions are here given with

respect to the hydrocarbon direction, as in the present study. The only existing direct measurement of DCSs associated to primary and secondary abstraction dynamics was undertaken in our group on selectively deuterated n-butane.[97] No significant differences were however observed in that study.

This chapter aims at revisiting Cl+alkane reactions for a set of intermediate C3 and C4 saturated hydrocarbons, propane and butane, using crossed beams combined with a universal detection scheme, DC slice imaging, and a high-density photolysis/ablation radical source. First I'll talk the improvements in experimental protocol, emphasizing the radical source development and its practical consequences on the data acquisition. Reactive scattering images and their derived double DCSs are presented later for a number of Cl+alkane abstraction reactions involving propane and its two partially deuterated isotopologues, namely 1,1,1,3,3,3-propane-d_6 ($CD_3CH_2CD_3$, hereafter **D1**) and 2,2-propane-d_2 ($CH_3CD_2CH_3$, **D2**), as well as n-butane and isobutene, followed by a discussion on the dynamical implications of these new results, in light of presented *ab initio* thermochemical data and previous work.

3.2 Experimental Setup

Experiments were conducted on our crossed molecular beam described in details in Chapter 2. Standard atomic radical sources such as photolysis or discharge usually suffer from poor densities and/or poor speed ratios. Here, atomic chlorine is generated by the 355 nm photolysis of a beam of 2% of Cl_2 seeded in He at a pulsed-valve pressure of 5 bar with a pulse duration of 100 μs. A significant improvement of the Cl beam density is achieved by overlapping the photolysis region located at the tip of the nozzle with an ablation plume. An aluminum extension tube of 2mm inner diameter and 5cm length along the propagation axis is mounted for this purpose, also confining the beam before it is skimmed. In this design, the focused laser beam (f =

350mm) is guided towards the tip of the nozzle of a pulsed piezoelectric valve by a conical aperture drilled in the extension tube. As photolysis and ablation are generated by a unique 355nm laser pulse, the Nd:YAG Q-switch is optimized to be fired 10μs earlier than for a standard photolysis. The speed ratios are equal to 9 and 6 with and without ablation, respectively (cf. Fig.3.1). Ablation drastically enhances the dissociation of Cl_2: the ratios between the effective Cl population in the interaction region and the photochemical component (cf. Fig.3.1a) due to the remaining Cl_2 population dissociated by the probe laser is changed from 1:1 to 5:1 with ablation at 20 mJ per pulse. Although the formation of spin-orbit excited state $Cl(^2P_{1/2})$ with ablation is a likely process its quenching to the ground state $Cl(^2P_{3/2})$ along the adiabatic expansion is believed to be as efficient as in the case of a conventional 355nm photolysis radical source. In any case, we intend to characterize this contribution in the future.

The resulting Cl beam is crossed at 90° by a 5% alkane pulsed beam seeded in He. Hydrocarbons were obtained from Sigma-Aldrich, with a stated isotopic purity of 98 atom % D for the two partially deuterated isotopologues of propane. To make certain that the ablated material does not imply any interfering reactions, we acquired data in similar conditions with the carrier gas only passing through the new radical source set-up: no scattering signal was observed.

Radical products are detected by single photon ionization with a VUV beam at 157nm generated by a F_2 excimer laser (GAM EX-10). The beam path is purged with N_2 and the power attenuated to ~0.5 mJ per pulse (except when probing the chlorine beam itself). The ionized cloud is accelerated and stretched by a set of four ion optics lenses and flies field-free along a 70cm flight tube oriented perpendicularly to the plane formed by the supersonic beams. It is detected on a 120mm diameter dual multi-channel plate coupled to a P-47 phosphor screen with a narrow (70 ns) gate pulse. Raw images are recorded using a CCD camera and our new

acquisition program NuAcq-2 at 768x768 pixels but centroided to 1536x1536 pixels. Direct inversion of the experimental data is then achieved after density-to-flux correction.

To be noticed is the gain in data accumulation that allows the improved Cl source: while more than an hour was necessary to reach satisfactory signal-to-noise ratio in previous similar experimental conditions, the present images were accumulated for 10 min with the probe laser unfocused. Only little density-to-flux correction was necessary. Moreover, the signal-to-noise levels with propane were too low to obtain adequate scattering images at all. The control of the experimental conditions is thus subsequently enhanced, and the interaction region is widely and *softly* illuminated. This avoids multiple photon ionizations to occur and, as we will see hereafter, to properly select the radical products with regard to their ionization energies.

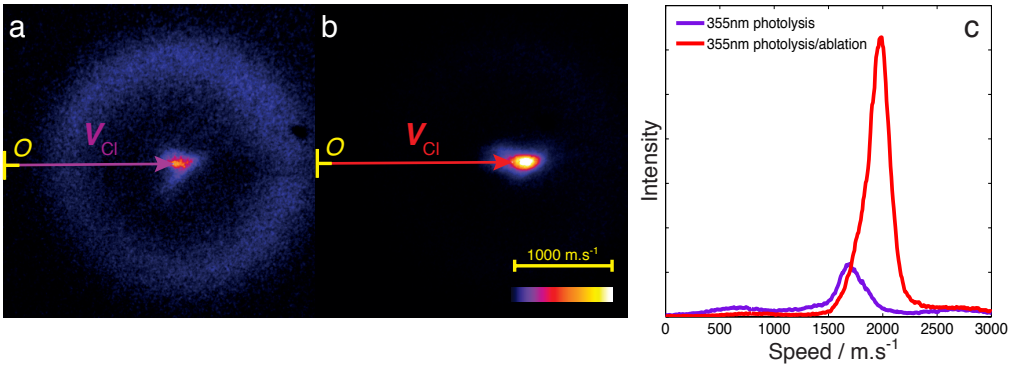

Figure 3.1: (a and b) Raw images at m/z = 35 without and with ablation, respectively, with signal intensity multiplied by 4 in image a. Chlorine speeds are 1680 m.s-1(a) and 1980 m.s-1(b). (c) Corresponding chlorine beam profiles.

3.3 Results

Reactive scattering images of the Cl+alkane reactions overlaid with their Newton diagrams are presented in Fig.3.2. The collision energies are equal to 11.6, 11.8, 12.1 kcal.mol^{-1} for propane, **D1**, and **D2** respectively, and 13.4 and 13.6 kcal.mol^{-1} for n-butane and isobutane. Scattering is seen broadly in all regions, with a tendency for peaking in the backward and forward directions. Propane images appear to show strong background interferences although the

integrations are done with signed data after subtraction. The photochemical propyl radical product scatters into a large region following 157nm dissociation, so that only data for angles larger than 30° will be analyzed. For butane, background is readily subtracted and the full scattering distributions can be analyzed.

Table 3.1: Bond dissociation energies (BDEs) and reaction enthalpies at 0K (ΔH(0K)) for all the possible H/D abstractions, and adiabatic and vertical energies of the corresponding products. Values calculated at the CBS-QB3 level of theory.

Reactant	Product	BDE kcal.mol^{-1}	ΔH(0K) kcal.mol^{-1}	Vertical IE eV	Adiabatic IE eV
propane **D1**, **D2**	n-propyl $CH_3CH_2CH_2$ $CD_3CH_2CD_2$ $CH_3CD_2CH_2$	100.6 103.1 100.6	-2.8 -1.5 -2.8	8.40 8.41 8.42	7.66 7.61 7.64
	isopropyl CH_3CHCH_3 CD_3CHCD_3 CH_3CDCH_3	97.0 97.3 99.4	-6.4 -6.1 -5.2	7.74 7.75 7.73	7.47 7.48 7.46
n-butane	n-butyl $CH_3CH_2CH_2CH_2$	100.5	-3.0	8.32	7.51
	2-butyl $CH_3CH_2CHCH_3$	97.3	-6.1	7.67	7.32
isobutane	2-methylene-propane $(CH_3)_2CHCH_2$	100.6	-2.8	8.33	6.64
	isobutyl $(CH_3)_3C$	95.3	-8.1	7.22	6.87

Table 3.2: Collision energies EC and available energies Etot for secondary and tertiary H/D abstractions, and average translational energy release. The latter is given along with the fractions

fC and ftot of collision energy EC and available energy Etot for indicated center-of-mass scattering regions, respectively.

	E_C kcal/mol	E_{tot} kcal/mol	**Total**			**Forward**		
			$\langle E_T \rangle$	f_C	f_{tot}	$\langle E_T \rangle$	f_C	f_{tot}
propane	11.6	17.9	7.8	0.67	0.43	7.9	0.68	0.44
D1	11.8	17.9	6.2	0.53	0.35	7.1	0.60	0.40
D2	12.1	17.4	7.9	0.65	0.45	8.6	0.71	0.49
n-butane	13.4	19.6	7.9	0.58	0.40	8.8	0.65	0.45
isobutane	13.6	21.6	7.6	0.56	0.35	8.6	0.64	0.40

	E_C kcal/mol	E_{tot} kcal/mol	**Sideways**			**Backward**		
			$\langle E_T \rangle$	f_C	f_{tot}	$\langle E_T \rangle$	f_C	f_{tot}
propane	11.6	17.9	7.9	0.68	0.44	7.5	0.65	0.42
D1	11.8	17.9	5.8	0.49	0.33	5.6	0.48	0.31
D2	12.1	17.4	7.6	0.62	0.44	7.4	0.61	0.43
n-butane	13.4	19.6	7.2	0.53	0.37	7.7	0.57	0.39
isobutane	13.6	21.6	6.9	0.51	0.32	7.2	0.53	0.33

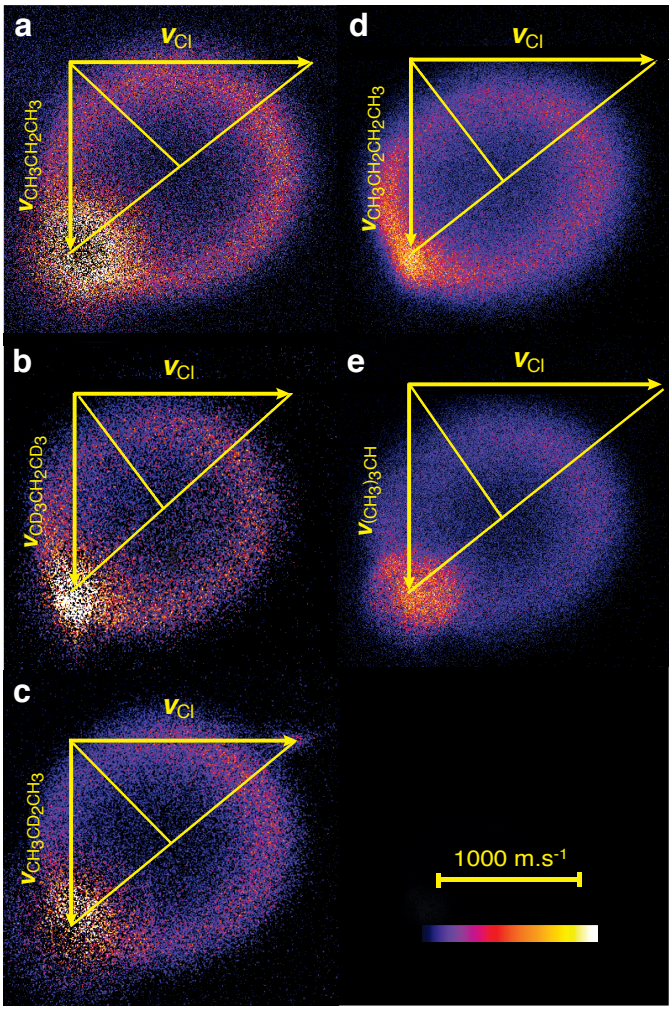

Figure 3.2. DC sliced raw images of reactive scattering and nominal Newton diagrams for the reactions of chlorine with propane and butane: a) propane, EC = 11.6 kcal.mol-1 b) propane D1, probe at m/z=49 (CD3CHCD3) EC = 11.8 kcal.mol-1, c) propane D2, probe at m/z=46, (CH3CDCH3) EC = 12.1 kcal.mol-1, d) n-butane, probe at m/z=57, EC = 13.4 kcal.mol-1, and e) isobutane, probe at m/z=57, EC = 13.6 kcal.mol-1. All images are shown after background subtraction and density-to-flux correction.

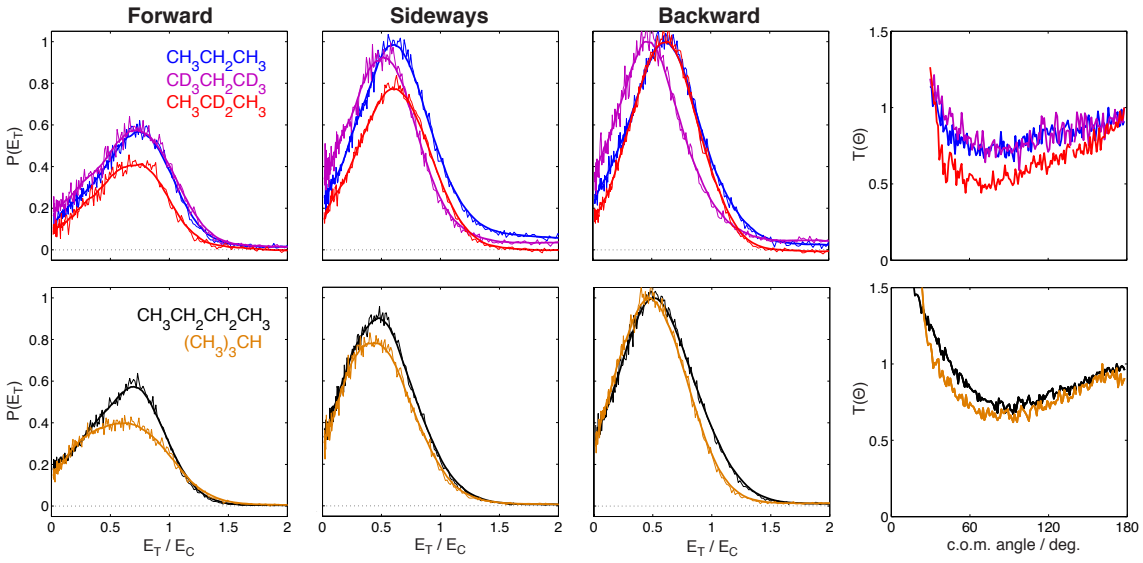

Figure 3.3: Reduced translational energy distributions for forward (30-60°), sideways (60-120°), and backward (120-180°) scattered products and the center-of-mass angular distributions. Top panel corresponds to propane reactions with propane in blue, D1 in purple and D2 in red. Bottom panel corresponds to butane reactions with n-butane in black and isobutane in gold. Each distribution is normalized to its backward component that dominates the translational energy distributions of all the systems in this range of integrated angles.

In the present study, no primary abstraction products were detected for selectively deuterated propane, whether labeled at the primary or secondary site. This is interpreted on the basis of the ionization energies (IEs) summarized in Table 3.1, which presents the adiabatic/vertical ionization energies (IEs) of the products of abstractions on the different sites along with the associated bond dissociation energies (BDEs) and enthalpies at 0K calculated at the CBS-QB3 level of theory.[98] As mentioned above, it is important to address the question of detection efficiency depending on the different radical products for each reaction. While the vertical IEs of the propyl and butyl products of secondary and tertiary abstractions lie below our detection limit of 7.9 eV, all the vertical IEs of the primary abstraction products for all systems lie above. One could expect to detect the latter, those undertaking important nuclear relaxation after ionization, if they were “hot” enough once the reaction occurred. However, experiments with partially

deuterated hydrocarbon are the opportunity to make a clear disentanglement here: the VUV probe does not ionize these products when its beam is unfocused. That is, no primary abstraction product is detected for the selectively deuterated propane systems. This is an indirect consequence of the radical source improvement that makes possible the use of an unfocused probe laser beam: although we could have access to primary abstraction products as already shown by multiphoton ionization with a focused VUV probe, [97, 99] we believe our results here are site-selective even in the case of non-labeled butanes, given the similarity in the vertical IEs of propane and butane. We will therefore discuss all velocity-flux maps as measured for secondary H(D) abstractions in propane and n-butane, and solely tertiary H abstraction in isobutane.

Fig.3.3 shows the reduced translational energy distributions for the forward (FW), sideways (SW) and backward (BW) scattering regions, along with the center-of-mass angular distributions for all systems. We choose to plot the E_T distributions reduced by $E_T^* = E_T/E_C$ to highlight the deviation from the *kinematic* dynamical picture of heavy-light-heavy reactive systems, for which the acute skew angle of the TS geometry implies the conservation of translational energy. Table 3.2 compiles the average translational energy release and fraction of the collision energy appearing in translation and of the available energy ($\boldsymbol{f}_C$ and $\boldsymbol{f}_{tot}$, respectively), obtained from the translational energy distributions shown in Fig.3-3. We emphasize that the narrower angular window over which the FW component is integrated underestimates the strength of this region, but we do not attempt to renormalize this. As mentioned previously, the integration over the entire angular distribution is however possible for the butane isomer data. Smoothed reduced translational energy distributions of 10° steps are thus plotted in Fig.3.4, along with the corresponding average translational energy distributions.

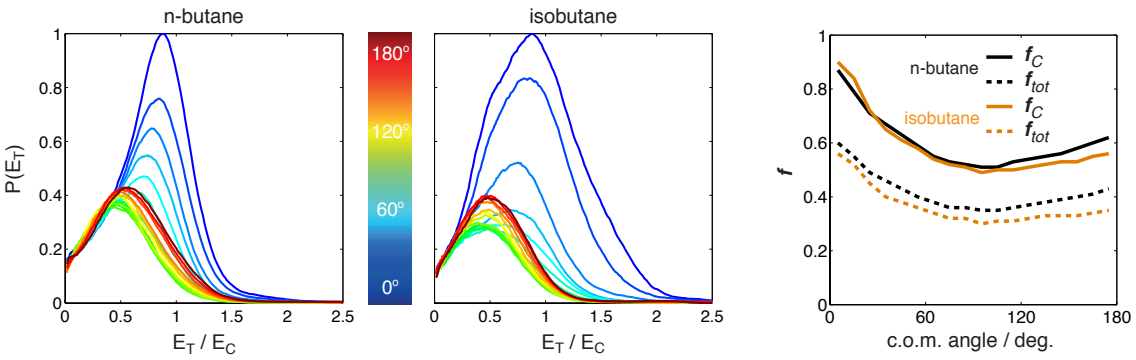

Figure 3.4: (Left) Reduced translational energy distributions for 10° steps of the angular distributions of reactions of chlorine with n-butane and isobutane. (Right) Fractions fC and ftot of collision energy EC and available energy Etot, respectively.

Before getting into details in the following discussion, here is a brief description of the main features of the measured scattering distributions. For all systems, the translational energy of the FW component peaks at higher energy than the SW/BW component. Again, even if the FW component looks less intense on Fig. 3.3 due to integration over a narrower angle window, the angular distribution is dominant in this region. The scattering signal is therefore maximal at low angles, then reaches a minimum in the 60-90° range, and increases steadily over 180°. These trends are consistent with previous work using similar methodology. [96, 97, 99]

3.4 Discussion

The discussion will begin with propane reactions. As mentioned in the Introduction, this is the first time that measurements of velocity-flux contour maps of these reactions are obtained by imaging. This system is indeed particularly challenging, due to low exoergicity and strong photochemical background. For normal propane, both translational energy and angular distributions are in agreement with the interpolated distributions reported by Blank et al.[96] at a similar collision energy. This confirms, as expected, that we can exclude the formation of a long-lived complex, i.e. a complex with a lifetime longer than its rotational period for which a FW-BW symmetric angular distribution would be expected. These results are consistent with a direct

reaction mechanism with little exit channel interactions, as inferred in general for these reactions based on the HCl rotational distributions. Furthermore, the increase in translational energy for FW scattered products compared to SW/BW products, also observed by Blank et al.,[96] gives credence to a spectator-stripping mechanism in the forward direction in which reactant to product momentum transfers are only marginal. This mechanism indicates a large impact parameter and weak interactions at the transition state. For SW/BW scattering components, translational energy distributions are consistent with collisions at smaller impact parameters that lead to a more effective partitioning of the available energy into internal degrees of freedom of the hydrocarbon radical product. State-resolved experiments have shown that HCl is rotationally cold, and this whatever the scattering angle.[10] This indicates that most of the available energy (app. 98%) that is not partitioned into translation is channeled into internal excitation of the propyl product. By referring to the line-of-centers model which helped the understanding of the dynamics of Cl+methane and Cl+ethane reactive scattering experiments,[2-5] Blank et al. suggested that a significant portion of the SW/BW components could be attributed to primary abstractions which are more sensitive to the effective reaction barrier. The remarkable similarity of our results however suggests that either primary abstraction only weakly contributed to the scattering signal probed with photons of higher energies or dynamics at primary and secondary sites are very similar.

We now consider the reactions of atomic chlorine with the two partially deuterated propane systems **D1** and **D2**. Although D abstraction is slightly less favorable than H abstraction (by 1 kcal.mol^{-1}), we believe that energetics criteria should not affect the comparison. Overall, the distributions show the same features as for the reaction with normal propane: the scattering signal is dominant in the FW region, a minimum is observed around 90° in the SW region, and

the scattering signal rises steadily over 180°**.** Significant differences can however be observed. Concerning translational energy recoil, FW and SW **D1** distributions peak at lower E_T^* than regular propane and **D2**, while all FW distributions peak at similar E_T^*. This reflects a more effective energy disposal into the CD_3CHCD_3 propyl degrees of freedom for the "rebound-like" mechanism. Also, the angular distribution of **D2** is affected by the deuteration. As the relative scaling of the angular curves is arbitrary, this could come from changes in the TS potential energy region that could modify the FW/BW balance or be a dynamical signature of the kinetic isotope effect described elsewhere.[100, 101] Interestingly, Estillore et al. also observed a slight increase of the BW component associated to D abstraction on primary site compared to H abstraction on secondary site in reaction of Cl with labeled 1,1,1,4,4,4-n-butane.

To gain insight into the origin of the differences in translational energy of the labeled isopropyl radicals, we invoke the impulsive model as used by Nesbitt and coworkers[102] to interpret the translational energy release of the ethyl product in the reaction of atomic fluorine with ethane. This simple model focuses on exit impact parameter solely, thus neglecting the initial angular momentum. This hypothesis is relevant for more exoergic reactions than Cl+alkane reactions, nevertheless it provides a guide to the trends we should expect in terms of coupling between translational and rotational degrees of freedom. This model is based on conservation of angular momentum and total energy and considers the radical product as a rigid body. The rotational excitation of the radical product is estimated to be:

$$E_{rot} \approx L^2/2I \approx M_{propyl} b^2 \sin^2\theta \, E_T$$

where L is the angular momentum and I the moment of inertia of the propyl radical. Moment arm b and angle θ for delivering torque are estimated to be 0.6 Å and 129° for non-labeled and labeled propyl structures at the CBS-QB3 level of theory, respectively. This gives 0.18 E_T for

reactions involving normal propane and **D2**, and 0.16 E_T for the reaction with **D1**. As one could expect by just considering the lower rotational constant of **D1** compared to those of propane and **D2**, the impulsive model predicts less energy to be channeled into the rotational degrees of freedom of the **D1** propyl product. This is an opposite trend to that of the scattering distributions presented here. The observed changes thus suggest that deuteration on the terminal carbons, which produces a more significant increase in the vibrational density-of-states than deuteration on the central carbon, could favor the overlap between the vibrational wave functions of the TS and the isopropyl products, promoting coupling of the collision energy into vibration, with the rotational energy distributions substantial but largely unchanged.

N-butane distributions are in good agreement with previous work on labeled n-butane[97], albeit the average translational energy is here slightly lower (f_C is between 0.5 and 0.6 for SW/BW components, while it is between 0.6 and 0.7 for secondary abstractions in labeled n-butane[97]). On Fig.3.3, n-butane and isobutane lead to BW distributions peaking at similar E_T^*, while n-butane distributions peak a higher E_T* in the FW and SW directions despite a greater exoergicity for tertiary abstraction in isobutane (by 2 kcal.mol^{-1}). In addition, we notice a higher integrated scattering signal for n-butane than for isobutane in FW/SW directions, in line with the greater number of H atoms to be abstracted on secondary sites in n-butane. While Fig.3.3 does not show the contribution of the 0-30° region, striking effects are observed when comparing n-butane and isobutane distributions in this region in Fig.3.4. Isobutane distributions exhibit a more sharply peaked angular distribution with a broader translational energy distribution in the FW direction, even possibly a bimodal distribution. There are two significant differences that could explain these changes: the greater exoergicity of abstraction on a tertiary site which might lead to a significant amount of HCl(v'=1), or a steric hindrance effect which could somehow result in

multiple collisions. State-resolved measurements on the HCl product will be helpful to disentangle these mechanisms.

As already mentioned elsewhere[1], a discrepancy is seen between crossed beam studies and PHOTOLOC studies concerning the fraction of the energy that is effectively channeled into the radical product. Bass et al. found 30% of available energy transferred to internal excitation of the butyl product (at Ec=7.4 kcal.mol^{-1}), while we find here about 60% when integrating the whole angular distribution. However, our data exhibit important changes depending on the scattering angle: from 40% at 0° to 60-65% between 60° and 180°. As mentioned by the authors themselves, results obtained in the latter scattering region with the PHOTOLOC technique have to be taken with caution due to strong background interferences. Indeed their inferred angular distributions show much less backward scattering than seen here and in the selectively deuterated butane study earlier. Universal crossed-beam studies on chlorine atom reactions with pentane isomers have revealed important changes in kinetic energy release depending on the collision energy, which may be another factor contributing to the differences seen in the crossed beam imaging compared with PHOTOLOC.[99]

Comparing the translational energy distributions of the propane and butane systems in Fig.3.3 finally strengthens our comments on the vibrational excitation of the propyl product. Among the systems studied here, the most similar distributions are those of propane **D1** and isobutane. These systems have a unique H abstraction site, and **D1** is the propane system with the highest vibrational density-of-states. The observed progression of translational energy release with hydrocarbon mass seems to indicate that C3 and C4 hydrocarbons are the last steps before convergence toward the internal energy transfer seen for larger saturated systems.

3.5 Conclusion

By taking advantage of an improved atomic chlorine source, we have measured velocity-contour flux maps of H/D abstractions in the reactions of chlorine with selected alkanes at an unprecedented level of detail. Angular and reduced translational energy distributions for the set of studied alkanes, namely propane, its two selectively labeled isotopologues **D1** ($CD_3CH_2CD_3$) and **D2** ($CH_3CD_2CH_3$), and butane isomers n-butane and isobutane for which none or only interpolated DCSs were measured in the past, show distinct differences that allow us to revisit the "reaction picture" of this family of reactions:

i. The role of vibrational excitation of the radical product has been invoked to explain the changes in recoil for the different reactive scattering distributions of the propane systems.

ii. The kinetic isotope effect has been proposed to account for the modification of the angular distribution associated to D abstraction in the $CH_3CD_2CH_3$ system, even if changes in the TS region cannot be excluded.

iii. The peculiar forward scattered distribution measured in the case of isobutane could be explained either by the formation of vibrationally excited HCl or a steric hindrance effect.

These results call for further investigations. Experiments at lower collision energies, with state-resolved detection to probe HCl/DCl, as well as dynamical calculations, should be helpful to shed light on the subtle energy partitioning in the radical products.

CHAPTER 4-REACTION DYNAMICS OF CHLORINE REACTION WITH BUTENE ISOMERS

4.1 Introduction

Reactions of chlorine atoms with hydrocarbons have become an important benchmark in the study of polyatomic reaction dynamics.[1] This is because these reactions are relatively fast, barrierless or nearly so, and because they afford the opportunity to explore distinct dynamics for different reactive sites [10, 11, 64, 95] and isomers, or to examine the influence of initial vibrational excitation[3, 6, 62] on the dynamics. Dynamical studies have ranged from state-resolved PHOTOLOC studies,[9, 103] to crossed-beam imaging with both universal [96, 99] and state-resolved detection,[104] to PHOTOLOC imaging[105] augmented by dynamical calculations. All of these studies have been interpreted with various simple models of the dynamics.

Although extensively investigated for their kinetics,[54, 106] reactions of Cl atoms with alkenes have been much less frequently reported in dynamical studies, yet they provide a fascinating opportunity to explore the influence of large variations in exoergicity for different target sites, and the possible influence of a strongly bound adduct (~1 eV) mediating the dynamics under some conditions. We recently reported a crossed-beam study of Cl reactions with 1-pentene and a number of hexene isomers at 4 and 7 kcal.mol^{-1} collision energies.[107] The chief findings in that study were that the reactions were dominated by complex formation at low collision energy while the high collision energy reactions began to show evidence of a stripping mechanism in the forward direction ascribed to direct abstraction of the alkylic H atom sites.

In this chapter we focus on the reaction dynamics for atomic chlorine with a series of butene isomers shown in Fig.4.1, with energetics referred to the reactants. The H abstraction and addition energetics have been calculated at the CBS-QB3 level of theory.[108, 109] In all cases, Cl addition to the double bond contributes about 20 kcal.mol^{-1} stabilization energy, with reaction at remote alkylic sites exoergic by 3-4 kcal.mol^{-1}, reaction at vinylic sites endoergic by 3-5 kcal.mol^{-1}, and reaction at allylic sites exoergic by 15-20 kcal.mol^{-1}. These are largely consistent with those we reported earlier for 1-pentene.

4.2 Experimental setup

The experiments were conducted in a crossed-beam imaging apparatus described in details in Chapter 2. Owing to intense photochemistry signal within 30° of the butene beams, reliable subtractions could not be obtained there and data in that region is not reported.

4.3 Results

DC sliced images of the C_4H_7 products for reactions of each of the four isomers are shown in Fig. 4.2, with the Newton diagrams superimposed. The collision energies were 12.5, 13.3, 13.8, and 13.5 kcal.mol^{-1} for 1-butene, trans-2-butene, cis-2-butene, and isobutene, respectively. The images are presented after background subtraction and density-to-flux correction. We emphasize that for visualization we show data with the threshold at zero, but the pixel counts are not necessarily positive after subtraction and the integrations over angle or velocity are thus reliable even in regions of substantial background.

Also shown in Fig. 4.2 are the total center-of-mass translational energy distributions, $P(E_T)$, for each image derived from the analysis. The thick solid lines are simply smoothed fits to the integrated data, while the fine lines are the integrated raw data. There is no deconvolution of the beam velocity spreads, but these contributions are relatively small and we would not expect to

resolve any underlying features owing to the high density of states in the products.

Slice imaging methods allow for direct inversion of the experimental data, allowing one to investigate the coupling of angular and translational energy release with no assumptions about the associated dynamics.[110] We have found it useful to show the translational energy release separately for forward, sideways and backscattered distributions, and these are presented in Fig. 4.3 along with the center-of-mass angular distributions. Owing to the background interference from C_4H_8 photodissociation by the probe laser, we omit the contribution within 30° of the butene beam for the forward distributions. The angular distributions are shown as insets in the translational energy distribution plots, color-coded for the different regions to match the appropriate $P(E_T)$ segments. Another useful aspect for interpreting the translational energy distribution plots is featured in Fig.4.3: Rather than giving the distributions in terms of total translational energy, we plot in terms of reduced translational energy, $E_T^*=E_T/E_{coll}$. This is useful because for heavy-light-heavy systems, the acute skew angle implies that conservation of translational energy is expected.[99] This is true both for near-collinear collisions, for which the light H atom is kinematically disfavored for coupling exoergicity into product recoil, or for large impact parameter collisions, for which the small momentum transfer also precludes product energy release appearing in translation. By plotting these distributions against E_T^*, we can see at a glance the nature of the deviation from the limiting cases.

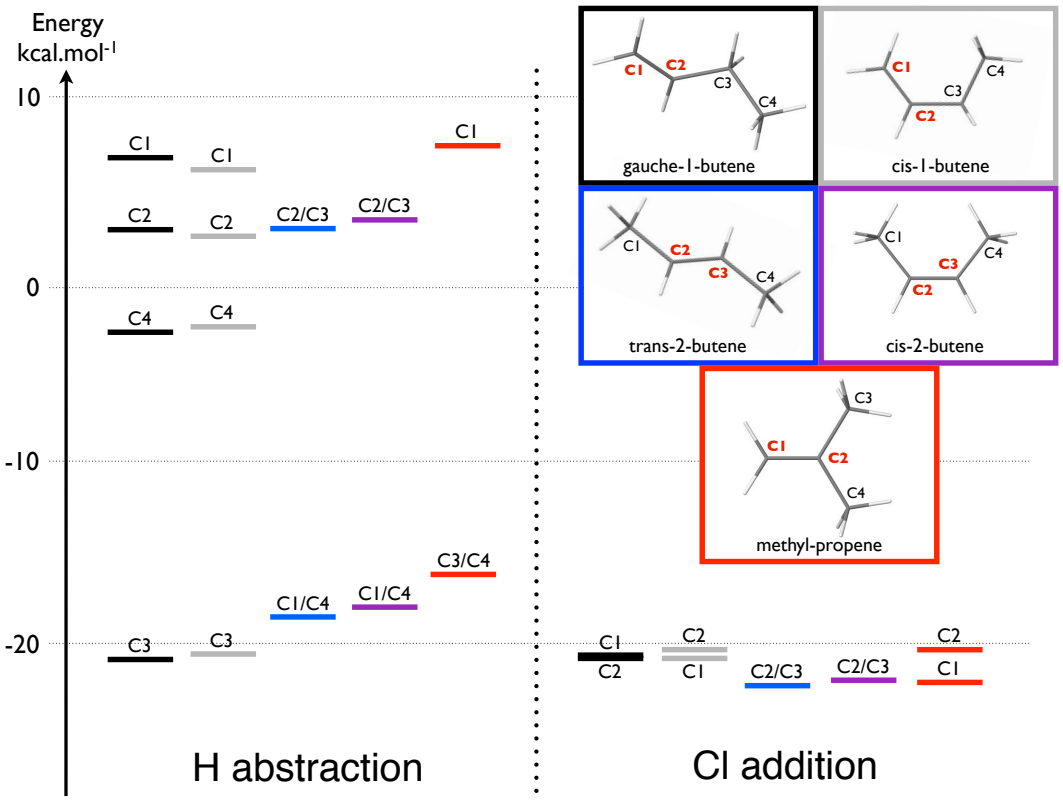

Figure 4.1: Energy diagram for Cl reaction with the indicated butene isomers. On the left are reaction enthalpies (0 K) for H abstraction at the indicated site. On the right are energy minima for Cl addition at the indicated site.

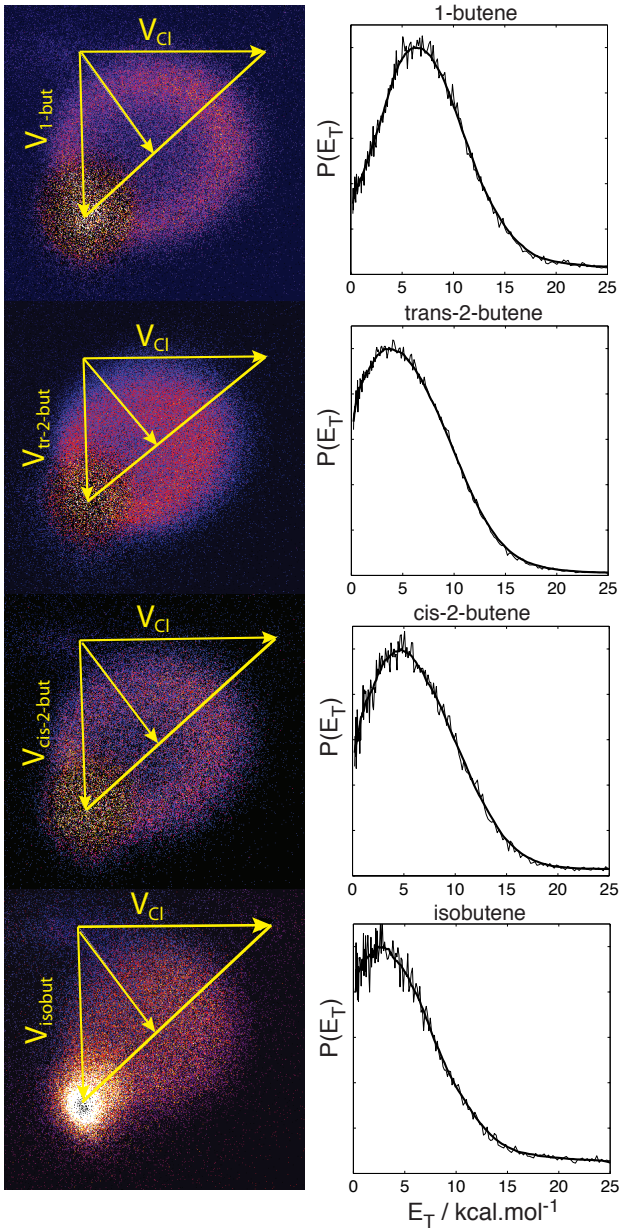

Figure 4.2: DC sliced images for the C4H7 product of reaction for the indicated target isomer with most probable Newton diagram superimposed (left) and global translational energy distributions obtained from the images.

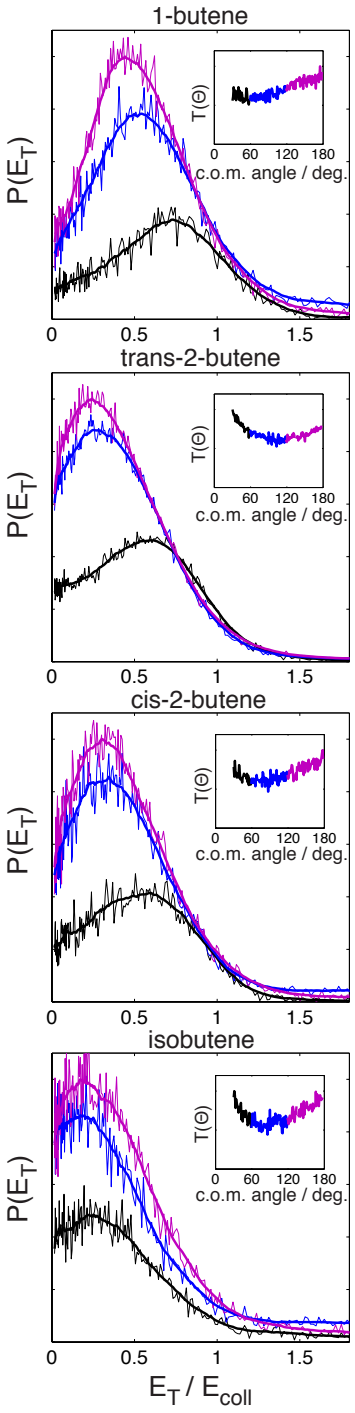

Figure 4.3. Reduced translational energy distributions for forward (black), sideways (blue), and backscattered (purple) reaction products, with the center-of-mass angular distributions inset in each plot.

The average translational energy release and fraction of the collision energy appearing in translation is compiled in Table 4.1, consistent with the translational energy distributions plotted in Fig. 4.2 and 4.3. We also show the total available energy assuming abstraction at the allylic site, and the corresponding fraction of the available energy appearing in translation. Owing to the large exoergicity, this fraction is substantially smaller than the fraction of collision energy that is conserved.

Table 4.1: Collision energy, available energy for allylic H abstraction, and average translational energy release (kcal/mol). The latter is given along with the fraction of collision energy or maximum available energy for indicated center-of-mass scattering regions.

	E_{coll}	E_{avail}	**Total (30°-180°)**			**Fwd (30°-60°)**		
			$\langle E_T \rangle$	$f_{T,}$	f_T	$\langle E_T \rangle$	$f_{T,}$	f_T
gauche-1-but	12.5	33.3	7.7	0.61	0.23	8.4	0.67	0.25
trans-2-but	13.3	31.3	6.2	0.46	0.20	7.4	0.55	0.23
cis-2-but	13.8	32.4	6.9	0.50	0.21	7.6	0.55	0.23
isobut	13.5	30.3	7.7	0.61	0.22	5.6	0.53	0.24

	E_{coll}	E_{avail}	**Side (60°-120°)**			**Back(120°-180°)**		
			$\langle E_T \rangle$	$f_{T,}$	f_T	$\langle E_T \rangle$	$f_{T,}$	f_T
gauche-1-but	12.5	33.3	7.7	0.61	0.23	7.0	0.56	0.21
trans-2-but	13.3	31.3	5.6	0.42	0.18	5.6	0.42	0.18
cis-2-but	13.8	32.4	6.4	0.46	0.20	6.7	0.48	0.21
isobut	13.5	30.3	6.0	0.44	0.20	6.9	0.51	0.23

4.4 Discussion

In the reactions of chlorine atoms with alkenes, there are several principal reactive processes that may occur[54, 68] falling into two categories: Electrophilic addition to the double bond followed by collisional stabilization or HCl elimination, or direct H abstraction without access to the adduct potential well. These two broad dynamical categories may be further subdivided, depending on target isomer, into addition at the more or the less substituted carbon of the double bond, and H abstraction at an allylic site (e.g., C1 or C2 in 1-butene), an alkyl site (C3 in 1-butene) or even at a vinylic site (C4 in 1-butene). All of these processes are energetically accessible at our collision energy, but reactions of the vinylic H atoms are so unfavorable that we can safely neglect them, and the products would not be detected by the 7.9 eV probe photons in any case. For abstraction at the alkyl sites, again the vertical ionization energy exceeds our photon energy, so although this is somewhat more feasible on energetic grounds (exoergic by 2 $kcal.mol^{-1}$and probably barrierless), the product is likely not detected in our study so we will also neglect this channel. We suspect this to be a minor channel but will examine this question more closely in future work described below.

Under single-collision conditions, the addition complex cannot be stabilized so it must decompose. Typically in a radical addition to an alkene, we have “anti-Markovnikov” behavior and the radical will add to the most energetically favored unsaturated carbon, which in general will be the least substituted site.[54] The biggest effect here is seen in isobutene, for which the C1 site is strongly favored (see Fig. 4.1). The addition complex may then decompose by H loss, which is endoergic by a few $kcal.mol^{-1}$, by Cl elimination returning to reactants, or by HCl elimination. For the latter reaction, the allylic site is strongly favored and the large exoergicity might suggest formation of vibrationally excited HCl. In fact, substantial vibrational excitation in

the HCl product has been used in kinetics studies as a marker for direct reaction, as this exoergic process would be characterized by an early transition state (TS).[68] The addition/elimination was assumed to give lower vibrational excitation owing to energy randomization in the long-lived adduct. On this basis, a large fraction of the direct component was inferred. This approach was developed by Setser and coworkers[68] and further considered by Taatjes and coworkers[54].

In our previous study with C5 and C6 monoalkenes under single-collision conditions, we inferred almost exclusive reaction *via* addition/elimination.[107] This was based on angular distributions that were nearly isotropic and translational energy distributions that peaked near zero. The highest collision energy studied in that work was 7 kcal.mol^{-1}, however, significantly less than what we employ here. Nevertheless, here we see significant variations in the behavior with different isomers, while in the earlier study even distinct molecules were largely indistinguishable from each other in their product distributions.

By examining the global translational energy distributions in Fig. 4.2, we see that 1-butene peaks farthest from zero at 6-7 kcal.mol^{-1}, the two 2-butene isomers are intermediate, peaking at 4-5 kcal.mol^{-1}, and isobutene shows the lowest energy peak at 2-3 kcal.mol^{-1}. If we assume that the lower translational energy peak is associated with a greater fraction of the indirect reaction, then the importance of adduct formation increases in the same order and is most important for isobutene. This is further supported by the angle-dependent translational energy distributions shown in Fig. 4.3 along with the angular distributions. Here, a distinction between the forward scattering and the backward and sideways scattering clearly indicates a direct component to the reaction. Again, this distinction is greatest for 1-butene, intermediate for the two 2-butenes, and absent for isobutene.

These trends are also reflected in the average translational energy release summarized in Table 4.I, and consistent with the relative stabilities of the adducts and abstraction reactions shown in Fig. 4.1. 1-butene (we consider only the gauche conformer[111]) has the shallowest well and the most exoergic abstraction channel, suggesting that the indirect reaction would be least important for this molecule. Isobutene has both the deepest well (for addition at the C1 site) and the lowest exoergicity for abstraction. On this basis alone we would anticipate the greater role for a long-lived intermediate for isobutene, which is consistent with the translational energy distributions in Figs. 4.2 and 4.3.

A crucial underlying question, and one that is implicit in the interpretation of Setser and raised by Taatjes et al., is the nature of the TS for HCl elimination from the adduct, both its height and its geometry. One would expect low vibrational excitation in the HCl product from adduct decomposition if one assumes product-like or intermediate geometry for the TS. A preliminary survey in 1-butene has failed to identify a TS for HCl elimination from the adduct.[112] One possible explanation for this is that the decomposition occurs primarily via a Cl atom roaming reaction.[26, 113] This picture is supported by earlier theoretical examination of H_2 addition to radicals.[114-116] For H_2 addition to vinyl radical, electron density must be donated from the singly occupied *p* orbital of σ character in the radical plane to the σ_u orbital in H_2, the most favorable interaction being in the collinear abstraction geometry. Mebel and coworkers argued that this is a general feature of H_2 addition to σ radicals, and similar arguments would apply to the reverse reactions. If we extend this picture to HCl as well as H_2, and allylic radicals as well as vinyl, then we infer that the favored C-H-Cl abstraction geometry would be accessed most readily by a roaming event. In this case, the vibrational excitation in HCl for the direct and indirect reactions at the allylic site could be very similar (and likely quite substantial).

This is analogous to the H_2 vibrational excitation seen in the roaming channel and the direct component of the H+HCO reaction reported by Bowman and coworkers.[117] If most adduct decomposition occurs via roaming, then the HCl vibrational excitation may be largely uncorrelated with the lifetime of the intermediate and low vibrational excitation may reflect reactions at alkyl sites or other aspects of the dynamics. Furthermore, the kinetic isotope effects (KIE) in these reactions[100, 101] examined by Finlayson-Pitts and coworkers will be complicated: The addition step would be characterized by an inverse KIE (the higher density-of-states in the deuterated molecule stabilizes the adduct compared to the undeuterated molecule), while the roaming-abstraction step would show a normal KIE owing to the difference in zero point energies. It is not clear how these opposing effects would manifest themselves in the observed KIE, but it is an interesting subject for investigation.

4.5 Conclusion

We have studied the reactions of chlorine atoms with a variety of butene isomers, namely 1-butene, trans-2-butene, cis-2-butene, and isobutene, using DC sliced imaging in a crossed-beam apparatus at collision energies of $\sim$13 kcal.mol^{-1}. The reactions showed distinct behavior for the various isomers that is interpreted as largely reflecting the relative importance of addition/elimination (complex formation) vs. direct reaction. The VUV probe at 157nm is sensitive only to reaction at the allylic site, which is likely to be the dominant reaction site for all isomers considered. A key question is raised concerning the decomposition of the complex, and whether it occurs via a roaming radical mechanism. If this is the case, then the HCl product vibrational distributions may not be a sensitive measure of direct vs. indirect reaction. We plan detailed energy-dependent crossed-beam studies and more extensive theoretical investigations to address these questions.

CHAPTER 5-ROAMING DYNAMICS IN RADICAL ADDITION-ELIMINATION REACTIONS

5.1 Introduction

Chlorine atom reactions with alkenes are an important prototype for the broad class of radical addition-elimination reactions: chlorine sources literally cover the Earth with both oceanic and anthropogenic origins and alkenes are among the most abundant atmospheric hydrocarbons [118]. These reactions play an important role in the oxidation of volatile organic compounds in marine boundary layers and Polar regions, [40, 44, 46]the burning of hazardous waste, [48]and possibly the aging of organic aerosols by heterogeneous processes.[50] In these bimolecular reactions that have become key in studying polyatomic reaction dynamics both in the gas phase [62] and in solution, [65] HCl formation is a major pathway for which addition-elimination competes with direct abstraction:

$$Cl + C_nH_{2n} \rightarrow (C_nH_{2n}Cl)^* \rightarrow C_nH_{2n-1}\cdot + HCl \qquad (1)$$

$$Cl + C_nH_{2n} \rightarrow C_nH_{2n-1}\cdot + HCl \qquad (2)$$

Direct abstraction and addition-elimination exhibit identical exoergicity (15-30 $kcal \cdot mol^{-1}$) and their decomposition is a long-standing challenge in both kinetics and dynamics studies for the obvious reason that they give rise to the same products. Nowadays, the kinetics of numerous Cl + alkene reactions seem to be well understood, with the gas-phase reactions exhibiting rate constants close to the gas kinetic limit, while evidence has been shown for addition-elimination involving a long-lived $C_nH_{2n}Cl$ intermediate. [53, 54, 67, 119] However, the details of the reaction mechanism and dynamics remain unknown. State-selected HCl measurements have not shown a distinct feature of addition-elimination in the product distributions.[68] Quantum

chemical calculations of reaction potential energy surfaces (PESs) have been enable to corroborate the addition-elimination mechanism [120, 121].

Recently, we have investigated the reactions of chlorine atoms with various alkenes such as butene isomers, 1-pentene, and various hexene isomers using a crossed-beam apparatus coupled to DC slice ion imaging [122, 123] We have found that the scattering distributions reflect the competition between direct H abstraction and Cl addition – HCl elimination. Our earlier preliminary theoretical calculations did not locate any typical transition states for HCl elimination, e.g., 3-center or 4-center transition states such as are generally seen for HCl elimination from closed-shell halides. This suggested the possibility that the decomposition of the C_4H_8Cl complexes might occur via a roaming radical mechanism.[16] Roaming dynamics are now widely recognized as an important pathway in unimolecular reactions [26, 28, 113, 124] but their role in bimolecular reactions remains an open question. In this work we show specifically for the case of Cl with isobutene that addition-elimination occurs by a mechanism involving Cl atom roaming.

5.2 Methods

5.2.1 Crossed-beam slice imaging experiment

The original crossed-beam imaging set-up has been described elsewhere.[123] In the following, we focus on the adopted experimental procedure, along with experimental modifications and improvements relevant for the present study. The two molecular beams were pulsed at 10 Hz with duration of 100 μs by using piezoelectric disk valves and backing pressures of 5 bar. The collision energy was varied by seeding the reactants in H_2, He, or Ne with less than 5% of percentage dilution. We note the present results for the highest collision energy were found to give improved collision energy definition compared to our earlier study. We used a

high-density chlorine radical source that consists in combining Cl_2 photolysis to ablation. [81]For this purpose, the third harmonic of an Nd:YAG laser (355 nm) is focused at the tip of the nozzle, which is embedded in an aluminum extension tube. The same laser pulse generates both photolysis and ablation. The speed ratios, directly measured by imaging the parent beams, are equal to 5 and 8 for Cl_2/Ne and Cl_2/He mixtures, respectively. In the reaction chamber, the isobutyl radical products are ionized at 157 nm with an unfocused excimer laser beam. Along the time-of-flight axis, the resulting ion cloud was stretched and accelerated via a four-electrode d.c. slice ion optics assembly to impact on a dual microchannel plate (MCP) detector coupled to a fast phosphor screen. The front plate of the MCP was held at constant potential, while the back plate "gates" the central slice of the reaction products at a specific m/z ratio by application of a high-voltage pulse. The images were recorded using a charged-coupled device (CCD) camera, and the megapixel acquisition program NuAcq was used to accumulate the raw images containing centroided data [125]. The data presented here are shown after background subtraction and density-to-flux corrections. Background substraction is performed by substracting the velocity-flux maps obtained with the Cl_2 photolysis laser off. These background images show a strong signal at m/z = 57 peaking in the forward directions at $\theta = 0°$ due to the photodissociaton of isobutene by the probe laser that cannot be substracted in the [0-30]° range at E_C = 14 and 8 kcal.mol^{-1} and in the [0-60]° range at E_C = 4 kcal.mol^{-1}. Finally, a small density-to-flux correction was performed by scaling the pixel intensity by the lab velocity at each point.

5.2.2 Computational methods

Ab initio calculations were performed using the CBS-QB3 method [108] implemented in the Gaussian09 quantum chemistry software package,[109] which involves geometry optimization

and evaluation of vibrational frequencies at the density functional B3LYP/6-311(2d,d,p) level of theory followed by a series of CCSD(T) and MP2 single-point calculations with various basis sets to extrapolate to the complete basis set limit. Connections between the transition state and local minima were verified by IRC calculations at the B3LYP/6-311(2d,d,p) level. The lifetimes of the $H_2CClC(CH_3)_2$ and $H_2CCCl(CH_3)_2$ radical complexes were estimated with Rice-Ramsperger-Kassel-Marcus (RRKM) calculations of energy-dependent rate constants for dissociation toward the reactants in single-collision conditions. The lifetimes of the HCl elimination process from the complexes at collision energies of E_C = 4, 8, and 14 kcal·mol^{-1} were estimated to be 5, 0.8, and 0.1 ns for $H_2CCCl(CH_3)_2$, to be compared to 72, 10, 2 ns for $H_2CClC(CH_3)_2$.

5.3 Results

5.3.1 Imaging Cl + isobutene dynamics in crossed-beams

The choice of isobutene as a target system should be noted before going into details of the reactive scattering distributions. There are two different sites that can lead to the formation of HCl and the alkenyl radical: The first one, the vinylic site, is directly located on the less substituted sp^2 carbon atom; the second one, the allylic site, is located on the two methyl groups adjacent to the double bond. Reactions at the allylic sites are thermodynamically very favorable with enthalpies of reaction ΔrH(0 K) ~ -16 kcal.mol-1, while H removal by Cl at the vinylic site is an endoergic process with ΔrH(0 K) ~ 7 kcal.mol-1.[123] The latter reaction is therefore unlikely to occur under our experimental conditions, although the highest collision energy could permit this reaction. Indeed, we use an unfocused probe laser in our present experimental configuration that avoids any non-resonant multiple photon ionization of the products. Given the ionization energies (IEs) of the two possible product radicals (IEs of allylic and vinylic C_4H_7

radicals are ~ 7.9[126] and 8.4 eV, respectively, with the latter value calculated at the CBS-QB3 level of theory), and the fact that H migration cannot occur in the energized radical product as established for similar systems (propene and isoprene)[121], we can confidently rule out the possible detection of radical products stemming from the abstraction directly at the double bond: The distributions presented here, and their changes with collision energies, correspond to reaction at the allylic sites only.

5.3.2 Direct vs. Addition/Elimination Pathways

Direct and indirect pathways for HCl production will appear very differently in the scattering distributions as illustrated in Fig.5.1. The product direction is taken as zero for the case of no momentum transfer, which corresponds in our case to the hydrocarbon beam direction. On this basis, we define for the radical product three different angular components in the center-of-mass frame, namely forward (FW, 0-60°), sideways (SW, 60–120°), and backward (BW, 120–180°). For direct H abstraction, the mechanistic picture is similar to the one in Cl + alkane reactions.[4, 64] The rebound component, associated to modest rotational and vibrational excitation, gives reactive scattering in the backward-sideways (BW-SW) directions; the stripping component involves little energy and momentum transfer and appears in the forward (FW) scattering direction. In all cases the direct reaction will tend to show translational energy release similar to the initial collision energy owing to the kinematics of H atom transfer. Moreover, for the direct reactions, the forward scattered distribution is sharply peaked and its intensity typically grows with collision energy as the fraction of the stripping component grows. Formation of a long-lived adduct shows very distinct scattering distributions: randomization of the internal energy over the vibrational degrees of freedom in the complex leads to product translational energy distributions that peak at low energy. Moreover, if the complex lifetime is significantly longer than its

rotational period, the system loses reference to the initial approach direction: the angular distributions show scattering that is symmetric in the FW and BW directions and the translational energy distributions in all directions will be identical. For systems in which the scattering is non-planar (such as often the case in more complex polyatomic systems) this symmetric scattering becomes fully isotropic.

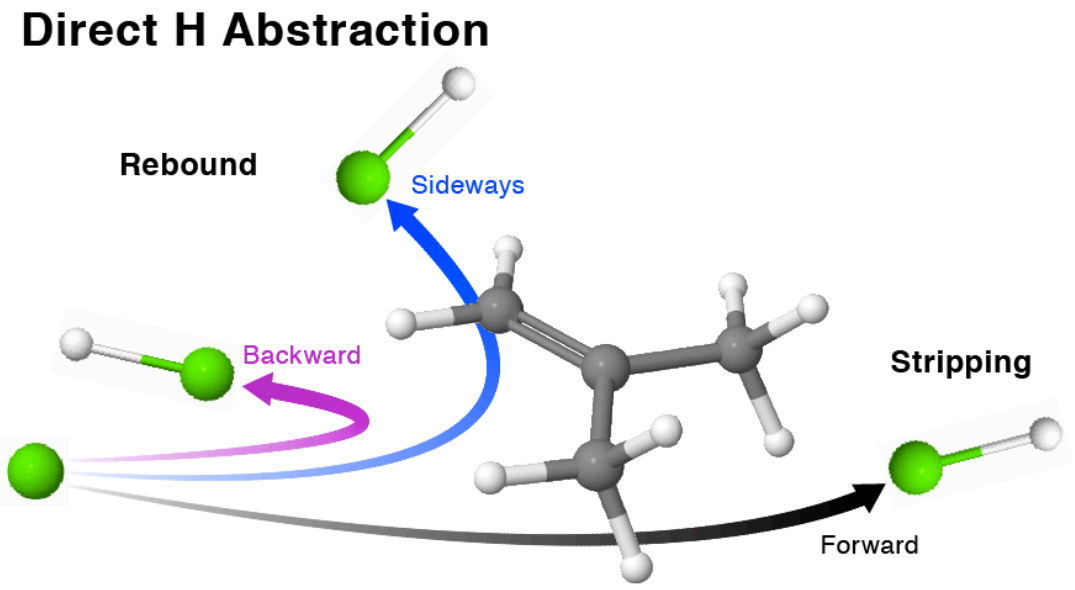

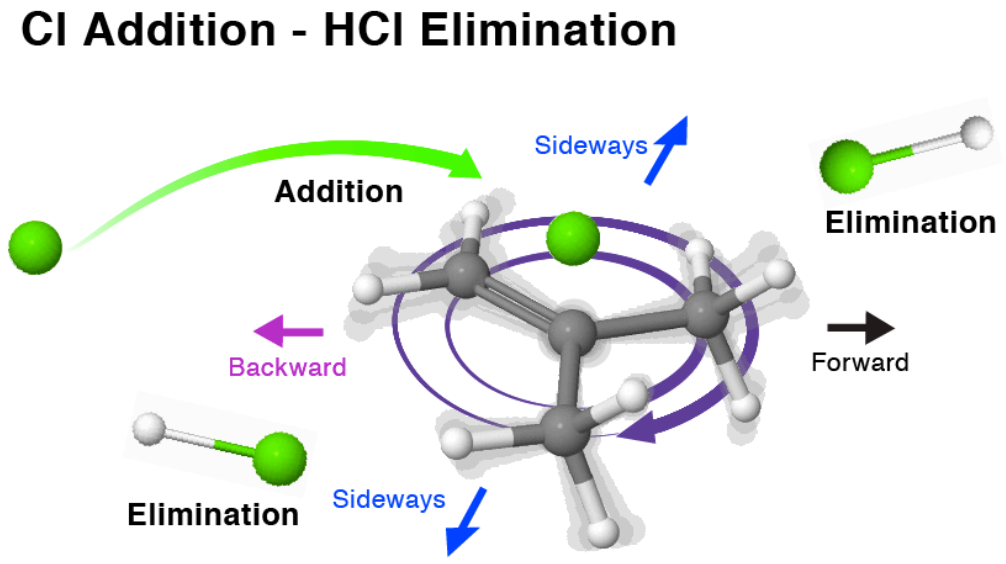

Figure 5.1: Cartoon illustrating the reaction dynamics Cl + alkene reactions. Direct H abstraction and addition-elimination are represented with the isobutene molecule. The reactive scattering components measured in the crossed-beam imaging set-up, namely forward, sideways, and backward, are highlighted.

The center-of-mass angular and translational energy distributions for reaction of Cl ($^2P_{3/2}$) with isobutene for collision energies of 14, 8, and 4 kcal·mol^{-1} are shown in Fig.5.2. In this case we see evidence of both characteristic distributions. At E_C = 14 kcal·mol^{-1}, the translational energy distribution in the FW direction peaks at substantially higher energy than in the SW and BW distributions, and the angular distribution shows a minimum around 90° and a modest enhancement of the FW scattering. This immediately indicates some direct component in the reaction, showing features reminiscent of the distributions observed for Cl + alkane reactions in this collision energy range. At the intermediate collision energy the angular distribution is slightly flattened, showing an evolution toward a more isotropic reactive scattering with decreasing collision energy. The distinction between the FW and SW/BW distributions is less pronounced and the BW translational energy release peaks at ~20% of the collision energy. At E_C = 4 kcal·mol^{-1}, the translational energy release peaks near 0 kcal·mol^{-1}, and the angular distribution is fully isotropic, although the center-of-mass is brought closer to the photochemical background and reliable data in the FW direction cannot be obtained. Nevertheless, these distributions tell a clear story: The complex-mediated mechanism plays a prominent role in these reactions, although it is not possible to decompose the precise relative contributions of direct vs indirect reactions from these experiments.

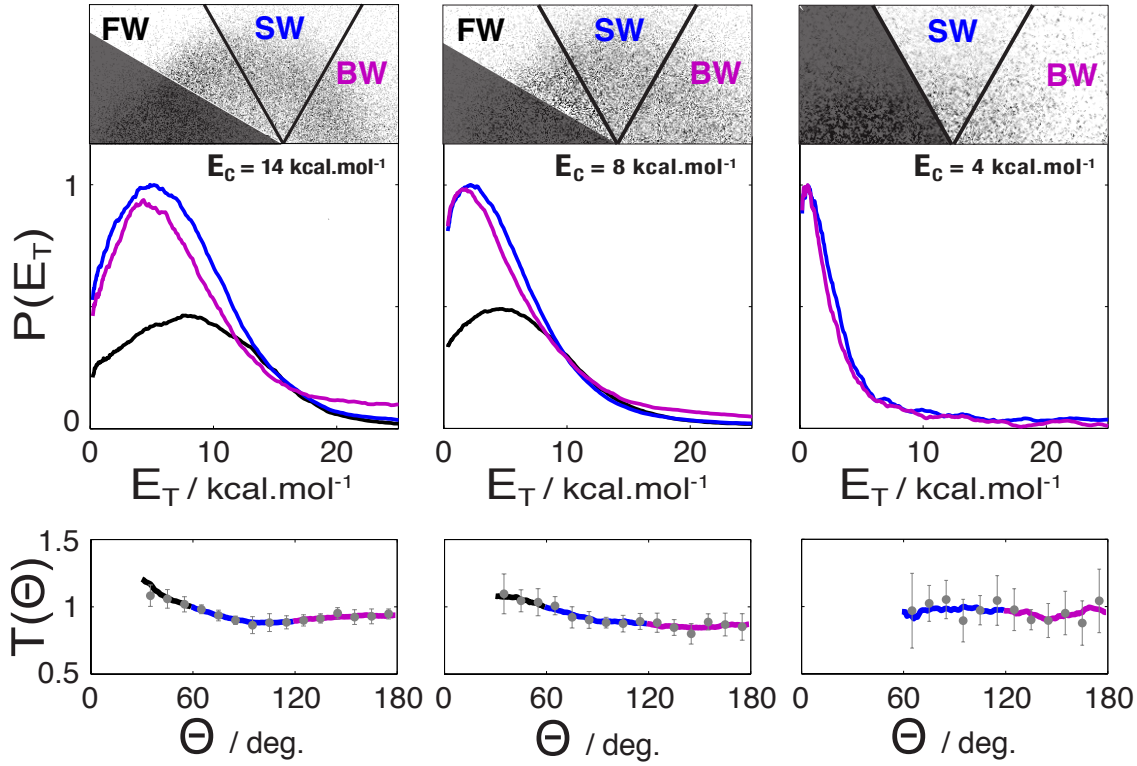

Figure 5.2: Center-of-mass distributions of the C4H7 radical for different collision energies. Translational energy distributions P(ET) and angular distributions T(Θ) are plotted for forward (30–60°, black), sideways (60–120°, blue), and backward (120–180°, purple) scattered products. The velocity-flux contour maps are shown with the photochemical background masked in the forward direction. Error bars were estimated each 10° via standard deviation.

The question now is the pathway for the decomposition of the adduct. Here, the translational energy distributions can provide insight. If the HCl elimination involved a conventional 3-center or 4-center transition state (TS), we would expect to see the translational energy distribution peak away from zero as the strained TS geometry relaxes to products. Instead we find, at the lowest collision energy, only 10% of the available energy appears in translation. This implies no experimental evidence for a conventional TS mediating the elimination, and this is strongly supported by the theoretical calculations below. We can also ask where the missing energy might be found. Pilgrim and Taatjes measured the HCl vibrational energy disposal in the Cl + propene reaction and found that significant amount of reaction exothermicity (28 ± 3%) was channeled

into HCl vibration with half of the population in vibrationally excited levels[119]. We expect a similar result here, and little total energy in rotation, implying that the greatest fraction of the unaccounted energy is retained in the internal energy of the hydrocarbon radical itself, holding more than 60% of the energy available for addition-elimination reactions. Again, this is the anticipated result for decomposition of a complex given the large number of internal degrees of freedom of the radical product.

5.3.3 Properties of the Addition Complex

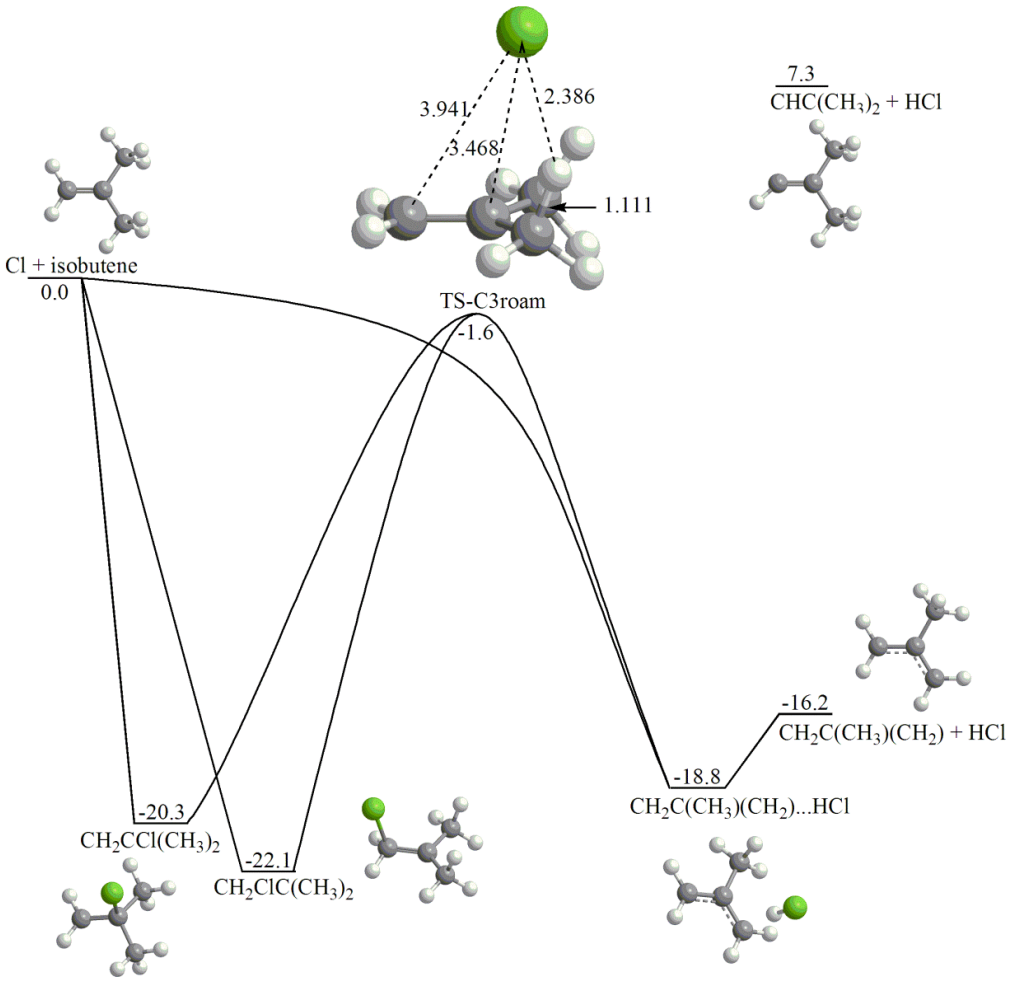

Figure 5.3: Key points on the potential energy surface of the Cl + isobutene reaction. Direct H abstraction is a barrierless pathway with a van der Waals complex in the exit channel. The two addition complexes undergo near dissociation to reach a unique roaming-type transition state (TS-C3roam) before eliminating HCl. The diagram has been calculated at the CBS-QB3 level of theory. Relative energies are shown in kcal·mol−1.

We now turn the discussion on the potential energy surface. Ab initio calculations were performed using the CBS-QB3 method [98], which provides a thermochemical accuracy of ~ 2 kcal·mol^{-1}. The key stationary points (minima and transition states) for the Cl + isobutene reaction are shown in Fig.5.3. Direct H abstraction is exoergic by 16.2 kcal·mol^{-1} at the allylic sites, and endoergic by 7.3 kcal·mol^{-1} at the vinylic site. Our calculations show that when Cl approaches isobutene from the side of the methyl groups, HCl elimination proceeds without any barrier. We also find there exist van der Waals C_4H_7…HCl complexes, which are bound by 2.6 kcal·mol^{-1}. The absence of barriers was confirmed via a careful scan of the minimal energy reaction path through partial geometry optimization with the critical H-Cl and C-H distances being frozen for the entrance channel and the exit channel, respectively. For reaction at the vinylic site, no transition state has been located.

5.3.4 The Roaming Transition State

The reaction can also proceed by barrierless addition of the Cl atom to C1 or C2 carbons leading to $H_2CClC(CH_3)_2$ or $H_2CCCl(CH_3)_2$ radicals, residing in deep potential wells of 20-22 kcal·mol^{-1}. Similar to the previous theoretical studies of Cl reactions with propene[11] and isoprene[12], we could not locate 'conventional', tight transition states for HCl elimination from the chlorobutenyl complexes. The reason for this is likely the same as for the absence of tight transition states for H_2 addition to radicals [115, 116] and may be understood on the basis of simple orbital symmetry arguments. For example, when H_2 adds to vinyl radical, electron density must be donated from the singly occupied *p* orbital to the antibonding σ_u orbital in H_2, the most

favorable interaction being in the collinear abstraction geometry. It was proposed that this may be a general feature of H_2 addition to radicals with an unpaired *p*-electron, and similar arguments would apply to the reverse reactions of H_2 elimination or HCl elimination considered here. Although no tight transition states were found, we were able to find pathways connecting these strongly bound C_4H_8Cl intermediates with the allylic C_4H_7 + HCl product channel. The structure of the transition state along the addition-elimination pathway, shown in Fig.5.3, is peculiar. The Cl-H distance for the forming H-Cl bond is 2.366 Å with the corresponding attacked C-H bond stretched only to 1.111 Å. The Cl atom is 3.468 and 3.941 Å away from C2 and C1 carbons, respectively. According to intrinsic reaction coordinate (IRC) calculations (cf. Fig.5.4), the transition state is connected to the van der Waals $H_2CCCH_3CH_2$…HCl product complex. In the reverse direction, IRC calculations return back to the C2 addition complex. However, since the Cl atom is located far from both C1 and C2, the downhill pathway from the transition state may also bifurcate to the C1 addition complex. Therefore, the Cl addition – HCl elimination transition state is both early, because the H-Cl bond barely starts to form and the breaking C-H bond is only slightly stretched, and late, because the C-Cl bond is already broken. Based upon its structure and the IRC path, this transition state is typical for a roaming radical mechanism, in which the Cl atom unlinks from the CC double bond, is about to be eliminated (returning to reactants), but wanders in the direction of the allylic site and picks up a hydrogen from a methyl group to form HCl. This observation is corroborated by vibrational frequencies computed for the transition state, which include a low imaginary frequency (317*i* cm^{-1}), two very low bound frequencies corresponding to motions of the Cl atom relative to the isobutene fragment (45 and 78 cm^{-1}) with the remaining frequencies being very similar to those of isobutene. The only exception is one C-H stretching frequency, which is reduced to 2706 cm^{-1} because this bond is

slightly elongated and thus begins to break in the transition state as the H atom is being abstracted by the roaming Cl radical. We have performed similar calculations for Cl reaction with all other butene isomers. Only roaming-type transition states for addition-elimination were found, although the PESs were complicated by additional H abstraction sites.

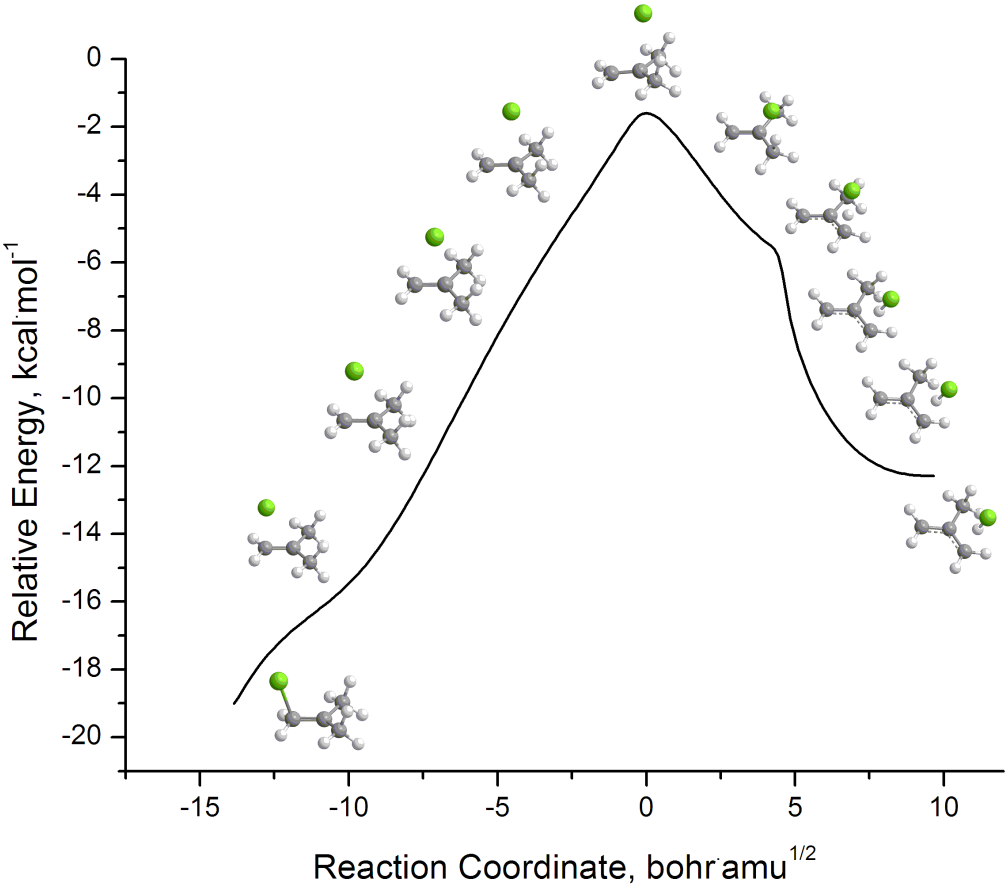

Figure 5.4: Lowest energy pathway linking the C1 addition complex and HCl elimination. Potential energy is plotted as a function of the intrinsic reaction coordinate with respect to the dissociation asymptote. Calculations are carried out at the B3LYP/6-311G(2d,d,p) level of theory. Relative energies are shown in kcal·mol^{-1}.

5.4 Discussion

Based upon the TS structure shown in Fig.5.3, both addition-elimination and abstraction mechanisms should be expected to produce HCl with similar vibrational excitation. The HCl

product vibrational distributions may therefore not be helpful for distinguishing between the direct and indirect reaction pathways. The statistical lifetimes of the Cl-complexes upon dissociation, estimated from energy-dependent rate constant calculations based on the Rice-Ramsperger-Kassel-Marcus theory[127], are too long at both low and high energies (72 and 2 ns, respectively) to account for the onset of the forward component when compared to the rotational period (~ 30 ps) of the complex. This observation, combined with the observed shift in the translational energy distribution in the forward direction, suggests that it is the appearance of the direct reaction at higher collision energy, bypassing the deep well, rather than an "osculating complex" that gives rise to the additional forward component.

We note that we make a distinction between the direct reaction that avoids the deep potential well, or other cases in which the reaction simply deviates from the minimum energy path [128, 129] and roaming dynamics that take place following adduct formation. The former dynamics are not unusual in bimolecular reactions: indeed they were seen in some of the earliest trajectory calculations [126] . Roaming dynamics as shown here and in many unimolecular reactions represent a distinct subset of those reactions that deviate significantly from the minimum energy path. They involve near-dissociation, in this case back to reactants, and a transition state located at a total potential energy and with vibrational frequencies near those of the reactants or products. This TS then leads to a configuration at which an intramolecular reaction may take place. These are precisely the conditions of the TS seen here, which is analogous to the roaming component in the H+HCO reaction[117] and in many other systems. A comparison of Cl-isobutene to that system, which has been studied using quasiclassical trajectories, is very instructive. For the H+HCO reaction, three outcomes were seen: a direct reaction and complex formation with two decomposition paths: either through a conventional 3-center transition state,

or by roaming. Both the direct reaction and the roaming reaction give rise to similar high vibrational excitation in the H_2 product. These two pathways are analogous to the direct and indirect reactions seen here, with the exception that in Cl-isobutene there is no 3-center TS for the indirect reaction. In fact, a key difference is that the present system involves a radical and a closed shell molecule exchanging the radical center along the reaction pathway, giving radical + closed shell products while the H+HCO reaction involves a radical pair giving a pair of closed shell molecules as products. We have recently learned of related work in the Orr-Ewing group at Bristol combining state-resolved velocity map imaging of the HCl product with direct dynamics calculations for this and related systems. Their results clearly support this roaming mechanism as the sole pathway from adduct to products, although they find greater branching for the direct reaction in their experiments than we see here. [130]

5.5 Conclusion

In summary, our experimental results show evidence for the important role played by indirect reactions in the total reaction cross-section of HCl formation in the reaction of Cl with isobutene *i*-C_4H_8. Addition-elimination proceeds through a long-lived complex in which the Cl addition to the double bond is followed by HCl elimination from the adjacent methyl groups. No evidence for a 3-center or 4-center transition state is seen in the experimental results, nor in a careful analysis of the ground-state potential energy surface. Instead we find a roaming-type transition state located 1-2 kcal·mol^{-1} below the energy of the reactant asymptote with greatly extended C-Cl and Cl-H bond distances and vibrational frequencies very similar to the reactants. The picture is therefore analogous to the roaming mechanism observed previously in unimolecular reactions. In this case the roaming dynamics are central to the addition-elimination reaction mechanism: Although abstraction is the only pathway to products, an indirect reaction can occur mediated by

the strong electrophilic interaction of the Cl atom with the alkene π cloud. The reactions remain fast and HCl elimination can compete with the Cl loss because of the loose roaming transition state combined with the slight enthalpic advantage.

CHAPTER 6-REACTION DYNAMICS OF FLUORINE REACTION WITH LINEAR ALKANES

6.1 Introduction

Polanyi's rules for atom + diatom reactions are core principles in reaction dynamics. If the barrier of an atom + diatom reaction is located in the entrance valley (the transition state structure is more like reactants than products), reactant translation is more effective than vibrational excitation in overcoming the barrier; alternatively, in late-barrier reactions, vibrational energy is more effective for reactivity.[131] For polyatomic species, with increased degrees of freedom and many vibrational modes, the extension of Polanyi's rule is complicated and calls for numerous experimental and theoretical investigations. Reaction dynamics studies replace the diatom with polyatoms, and much work has been done to investigate atom + methane (CH_4, CHD_3) reactions. [132-135] Experiments and theoretical work have explored whether we can simply extend Polanyi's rule to polyatomic targets and whether different vibrational modes have same impact on the reaction mechanism. X + CH_4 hydrogen abstraction reactions have been touchstone targets in these studies.

In 2002, Crim *et al.* reported that symmetric C-H stretching vibration drive the reaction CH_4 + Cl→CH_3 + HCl more efficiently than antisymmetric stretch. [134] Later Crim *et al.* observed excited symmetric C-H stretching mode increases Cl + CH_3D reactivity seven times while antisymmetric mode does not.[136] Liu and co-workers performed state-resolved pair-correlated differential cross section measurements of F, Cl, and O(^{3}P) + methane reactions in the past few years. In 2007 they found that the C-H stretching is no more efficient than an equivalent amount of translational energy in Cl + CHD_3→HCl + CD_3 reactivity, contrary to the extended Polanyi's rules. [137]In 2009 they observed C-H stretching excitation inhibits the CH bond cleavage in the

F + CHD_3 reaction. [138] The conclusion was confirmed by quasi-classical trajectory calculations.[139] In 2010 they published an experimental and theoretical study of the effects of CH bending in the F + CHD_3 reaction. Both experiment and theory show at low collision energy bending excitation promotes the reaction while at higher collision energy it diminishes. QCTs predict that v_6(e) and v_5(e) bending modes promote DF and HF channels respectively and v_5(e) is most efficient in increasing the reactivity. Experimental cross sections of F + CHD_3 (v_b = 1) show peak features for HF (v' = 3)+CD_3 (v_2 = 0,1), indicating possible reactive resonances. [140]

In 2005 Nesbitt *et al.* detected state-resolved HF(*v,J*) product states with IR laser absorption method to investigate the reaction dynamics of F + C_2H_6→HF(*v,J*) + C_2H_5. The results indicate a high-efficiency vibrational excitation with relatively modest rotational excitation, consistent with Polanyi's rules for early-barrier dynamics and in agreement with ab initio calculations. Their Doppler study of translational energy release into product quantum states revealed a linear correlation between HF (*v,J*) translational recoil and the available energy, which is the remaining energy that could be distributed into the translational energies of HF and ethyl fragment, as well as the rovibrational degrees freedom of ethyl fragment. A simple impulsive model based on conservation of energy and linear/angular momentum predicts a good agreement with experiment and the deviations are attributed to a Franck-Condon-like excitation of the CH_2 moiety.[102]

Layfield *et al.* published a theoretical study of the dynamics of F+CH_4, C_2H_6, C_3H_8 and *i*-C_4H_{10} reactions in 2009.[141] They derived a reparameterized Hamiltonian from ab initio information of the potential energy surfaces of all reactions studied to calculate direct quasiclassical trajectories. The accuracy of this Hamiltonian was tested by comparing the calculated dynamical properties with experimental results of fluorine + methane and ethane

reactions. Calculations on propane and isobutane reactions focused more on the differences at various abstraction sites. They found, as expected, energy distributed into HF vibration increases along primary, secondary and tertiary reaction sequence while tertiary abstraction reactions are more backward scattered than primary sites. Increasing sizes of the alkanes increase the energy partitioned into internal alkyl degrees of freedom. This work is very relevant to our study and will be discussed further below.

In the past few years, our group has conducted a series of crossed beam studies of Cl atom reaction with saturated and unsaturated C3 to C6 hydrocarbons reactions using DC slice imaging in a manner quite analogous to the reactions studied here.[80, 81, 97, 99] Here we present the latest results of our crossed-beam study on the reaction dynamics of F atom with saturated hydrocarbons targets, i.e. propane, n-butane and n-pentane. This is the first experimental F atom dynamics study of C3 and higher systems, where primary and secondary H sites are present. Raw scattering images of the abstraction products are collected with DC slice imaging in a universal crossed-beam apparatus via single photon ionization. After background subtraction and density-to-flux correction, the coupled differential cross section distributions, the translational energy distributions and center of mass angular distributions, are derived directly from the images without any convolution or assumptions.

6.2 Experimental method

Our apparatus is a crossed-beam machine[80] consisting of a main chamber and two source chambers fixed at 90° to each other. Both source beams are diluted in helium and expanded into the main chamber to react. The 5% fluorine mixture was pulsed into chamber through a piezoelectric stack valve [93] with a 120μm translation actuator pulsed for 50 μs. A pulsed discharge was fired in front of the valve body prior to the skimmer to generate F atoms. We

mount two electrode plates in front of the nozzle to create the discharge. An insulator plate is placed to prevent discharge between the first electrode and the nozzle plate. The first electrode plate is held at ground while the other one is given a pulsed high voltage (+800V). The pulse of the discharge is 2μs long and was set to discharge when the gas pulse is at its peak. The expanding F atom beam was skimmed through a 2mm diameter skimmer. Although it is not possible to visualize directly the F beam via our current DC slice imaging set-up, we have monitored a beam of N_2 in similar conditions showing a speed of ~ 1950 m/s with a speed ratio of 18. Hydrocarbon target beams were produced by seeding 2-10% alkanes in helium and expanding into the main chamber through a piezoelectric disk pulsed valve after a 2mm orifice diameter skimmer. In the present study, the beam speeds were measured at ~ 1600 $m.s^{-1}$ for propane, 1450 $m.s^{-1}$ for n-butane, and ~ 1320 $m.s^{-1}$ for n-pentane, with speed ratios of, 6, 5, and 4, respectively. The resulting collision energies E_C were equal to 10 ± 2 $kcal.mol^{-1}$.

The product radical was ionized by a VUV 157nm excimer laser in the interaction region, on the axis of a DC slice imaging [86] apparatus described previously, and then accelerated up via a set of four DC slice ion optics, through a 70cm flight tube perpendicular to the reaction plane to impact on a 75mm diameter dual mircochannel plate (MCP) detector coupled to a P-47 phosphor screen. The back plate of the MCP assembly is held at constant potential while a negative high-voltage pulse is given to the front plate to 'gate' the central slice of the products at a certain m/z ratio.

A CCD camera is used to record the raw images and data acquisition program is our own NUACQ-2 with event-counting and centroiding. We recorded images with F discharge on and off to obtain the photochemical background associated with the hydrocarbon targets. After background subtraction and density-to-flux correction, the experimental data is directly inverted

to the uncoupled center-of-mass angular and translational energy distributions.

6.3 Results

For reactions of hydrocarbons with VUV probe of the radical products, one needs to consider the detection efficiency for various product radicals (i.e., for particular abstraction sites.) In this paper, all the target alkanes contain primary and secondary hydrogens. We address this question by taking into account of product radicals' ionization energies. The enthalpies at 0 K and ionization energies of different H abstraction sites are shown in Fig.6.1, calculated at the CBS-QB3 level of theory. For propane and n-butane, the ionization energy of primary abstraction product is higher than our detection probe of 7.9 eV, while the secondary abstraction product is lower. It is possible both products are detected if these would possess some vibrational excitation. Experiments of F with partially deuterated propane and butane, which we do not present here, showed no primary abstraction product with our single photo ionization VUV probe. Thus, results here contain only secondary abstraction products of propane and n-butane. For pentane, we detect both primary and secondary abstraction products. Although secondary abstraction can give 2-pentyl or 3-pentyl radical, a previous study[142] of heptane isomer photodissociation at 157nm relative ionization efficiency shows less than 20% variation in various radical products detection efficiency; in the pentane case our detection likely does not favor 2-pentyl or 3-pentyl radicals.

propane C_3H_8

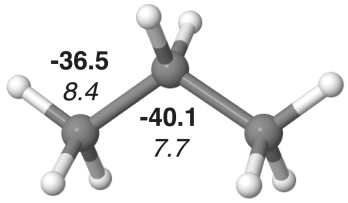

n-butane C_4H_{10}

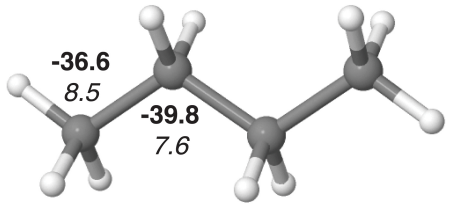

n-pentane C_5H_{12}

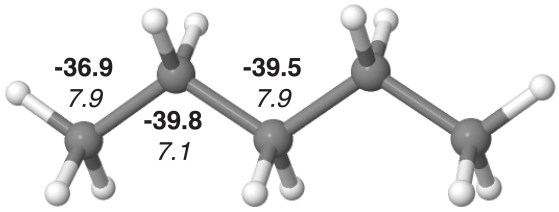

Figure 6.1: Lowest energy structures of propane, n-butane and n-pentane. Reaction enthalpies at 0 K (bold / kcal.mol-1) and ionization energies of the radical products (italic / eV) at different abstraction sites are calculated at the CBS-QB3 level of theory.

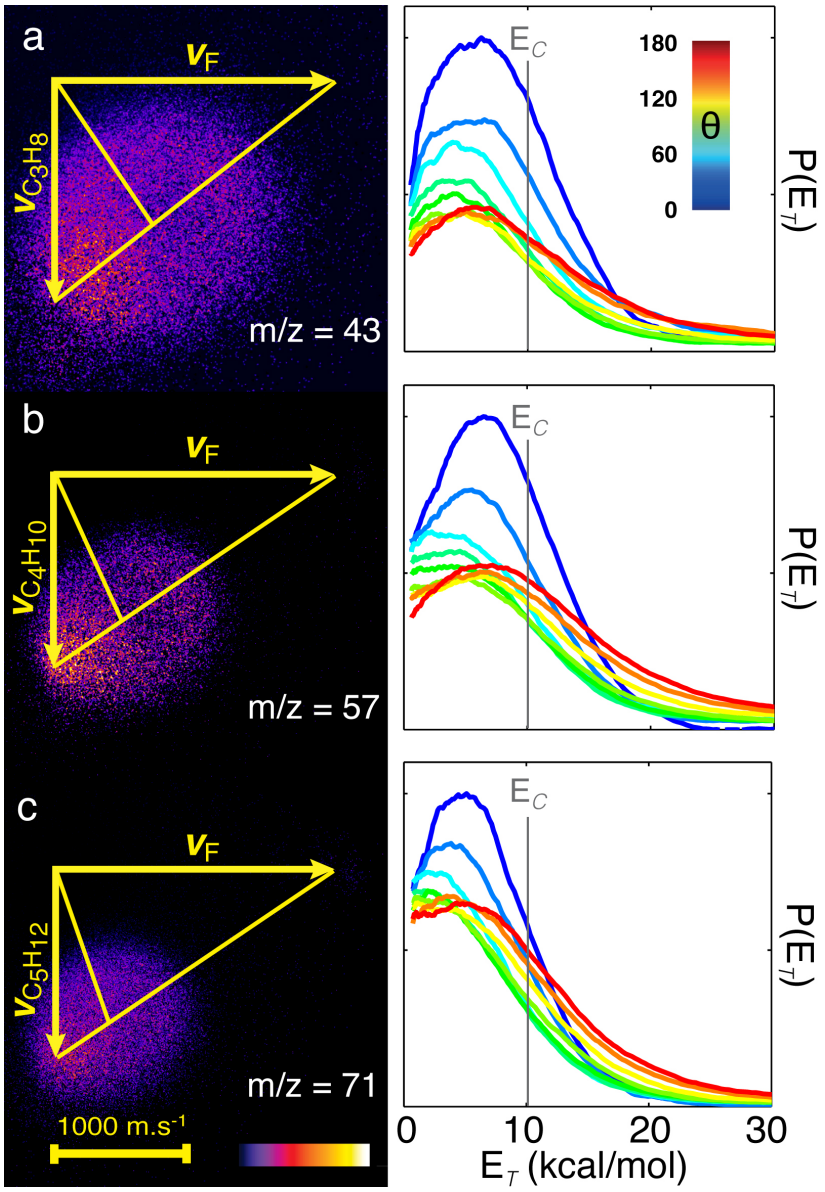

Figure 6.2: (Left) DC sliced raw images of reactive scattering after background subtraction and density-to-flux correction with newton diagrams superimposed. The collision energies of propane, n-butane and n-pentane are 10.2, 10.1, and 10.3 kcal.mol-1, respectively. (Right) Corresponding translational energy distributions for 20° angular steps.

Fig.6.2 presents the DC sliced raw images of reactive scattering of the F + alkane reactions after background subtraction and density to flux correction, with nominal Newton diagrams superimposed. Owing to the newly designed stack valve and the discharge, the F atom beam is stronger than the previous Cl beam we used for analogous studies; in addition, the pulse duration

of both F and alkane beams can be lowered to 50 μs, which helps to decrease the photochemistry of alkane background and allows us to present the full scattering distributions of the alkyl products. The translational energy distributions are integrated every 20°, shown in the right part of Fig.6.2. All the reactions have the same trends: (i) the scattering signal is maximal at low angles, (ii) the distribution peaks at higher translational energy (~ 5-7 kcal.mol^{-1}) for both 0° and 180° scattered angles, while it peaks at lower values (~ 1-3 kcal.mol^{-1}) near 90°, (iii) the high angle distribution is broader and thus extends to higher recoil.

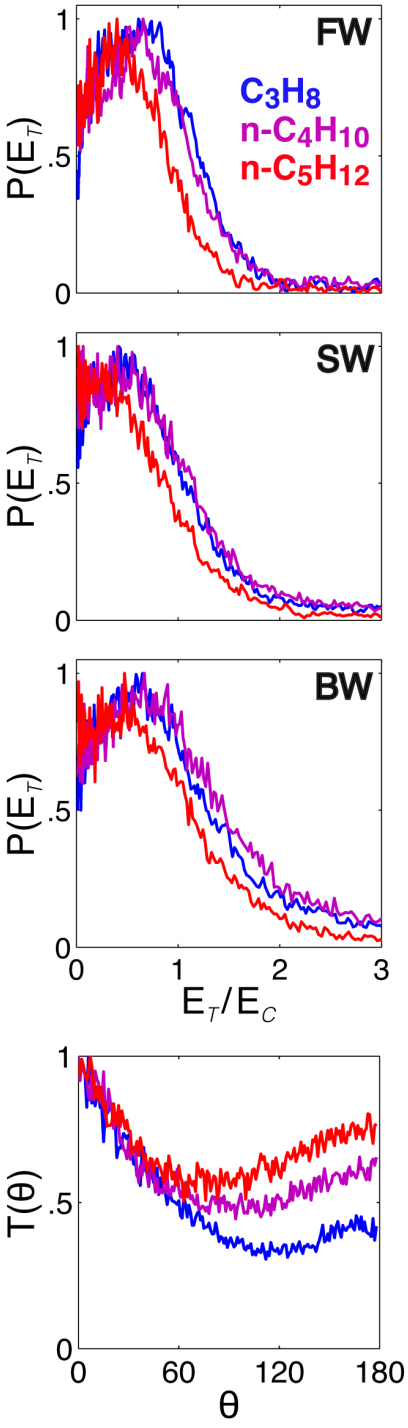

Figure 6.3: Reduced translational energy distributions of forward (FW), sideways (SW) and backward (BW) scattering regions of the alkyl products and their center-of-mass angular distributions.

Fig.6.3 shows the reduced translational energy distributions for forward (FW), sideways

(SW) and backward (BW) scattering of each target radical with their center-of-mass angular distributions on the bottom, which are all directly integrated from the raw data. The translational energy is reduced by collision energy, $E_T^* = E_T/E_C$. We plot E_T^* instead of E_T to give at a glance the deviation from the limiting cases for heavy-light-heavy systems: the acute skew angle favors the conservation of translational energy. The average translational energy release and the fraction of the collision energy in translation (f_c) and of available energy (f_{tot}) are shown in Table 6.1. The translational energy distributions of propane and n-butane are quite similar while n-pentane is different from the others, *i.e.* closer to zero than the other two. The BW scattering of all systems peak farthest from zero. The angular distributions have a strong forward component. As the size of the molecule increases, the backward scattering component increases.

Table 6.1: Most probable collision energies EC and available energies Etot = EC + ΔrH(0K) for primary and secondary H abstractions, along with the average energy release and the fractions of translational energy in collision energy (fc) and available energy (ftot) measured for the different scattering regions. For n-pentane, primary results are shown with an asterisk (*). Values are in kcal.mol-1.

			Total			**Forward**		
	E_C	E_{tot}	$\langle E_T \rangle$	f_C	f_{tot}	$\langle E_T \rangle$	f_C	f_{tot}
C_3H_8	10.2	50.3	8.3	0.81	0.16	8.4	0.82	0.17
***n*-C_4H_{10}**	10.1	49.9	7.6	0.76	0.15	7.1	0.71	0.14
***n*-C_5H_{12}**	10.3	50.1 47.2*	6.6	0.64	0.13 0.14	6.1	0.60	0.12 0.13

			Sideways			**Backward**		
	E_C	E_{tot}	$\langle E_T \rangle$	f_C	f_{tot}	$\langle E_T \rangle$	f_C	f_{tot}
C_3H_8	10.2	50.3	7.4	0.72	0.15	8.8	0.86	0.18
***n*-C_4H_{10}**	10.1	49.9	7.2	0.71	0.14	8.7	0.86	0.17
***n*-C_5H_{12}**	10.3	50.1 47.2*	6.3	0.61	0.13 0.13	7.3	0.71	0.15 0.15

6.4 Discussion

As shown in Fig.6.2, the translational energy distributions of the three target molecules share the same features: the scattering signal peaks at a higher translational energy release around 0°

and 180° while it shows a minimum around 90°. Comparing these results with a dynamics study published earlier in our group for Cl atom reactions with the corresponding alkanes, the Cl reactions showed a much stronger forward scattered than the present F atom results, suggesting for the latter, the stripping mechanism is less favored than the rebound mechanism despite the much greater exoergicity.[80]

The reduced translational energy distributions tell us more about the dynamics of these reactions. In Fig. 6.3, the translational energy release for the BW scattering peaks at 0.6 to 0.8 but extends significantly higher than do the FW/SW distributions. This is likely owing to the fact that for the close collisions leading to rebound scattering, there is an enhanced possibility for coupling of the substantial exoergicity into recoil. The FW scattering E_T* also peaks at 0.6-0.8 but shows much less extension to E_T^* >1 than the BW component. The SW scattering peaks at the smallest E_T^*.

The E_T^* of n-pentane is smaller than the other two in all directions, indicating that collision energy is more effectively partitioned into internal degrees of freedom of the pentyl radical. One possible reason for this difference is that the reaction enthalpies of propane and n-butane are almost the same and we do not detect the primary radicals, while for n-pentane two abstraction sites were probed here, and for primary, the exoergicity is about 3 kcal.mol^{-1} lower than secondary abstraction sites.

One rather puzzling feature is that all of our observed angular distributions show a sharp forward scattered feature that is not present in the direct dynamics trajectories of Layfield et al. However, the fractional translational energy release is in fair agreement. We believe the most likely explanation for this is that the trajectories were performed at a much lower collision energy (3.2 vs. ~10 kcal.mol^{-1}) than our experiment. The higher collision energy would certainly

enhance the contribution of a stripping component. A related aspect of the experimental result is that the relative yield of the backscattered component *increases* with the mass of the collision partner, regardless of whether results include only secondary abstraction (propane, butane) or both primary and secondary (pentane). This is contrary to what might be expected strictly based on expected impact parameter. It may be that this forward stripping component, not seen at the lower collision energy in the theoretical calculations, begins to appear and grows with the velocity, or with the "local" F-H-C collision energy, rather than the overall collision energy. Although we have normalized the angular distributions in Fig.6.3 to have the same maximum (in the forward direction) we could similarly scale them in the backward direction and note the relative decrease in the forward component with mass. We are planning future studies at a range of collision energies to probe these questions.

In addition, although we think of these as linear systems, there are additional conformers for butane and pentane that are somewhat populated at room temperature, and it is likely that they are, to some extent, frozen in the expansion and not fully relaxed to the linear minima. As discussed above, back-scattered products arise from small impact parameter collisions, which would allow more effective partitioning of available energy into internal degrees of freedom of alkyl radicals than FW/SW scattering, i.e. the energy channeled into alkyl internal energies increases with larger alkane molecules, in good agreement with the quasiclassical trajectories calculations in Layfield's paper.[141]

We find the fraction of available energy appearing in translation is about 0.13~0.18, while most of the available energy is likely partitioned into the vibrational excitation of HF; experiments for ethane and the trajectory calculations all suggest a maximum probability for HF (v=2). f_C is slightly smaller than in the work of Layfield et al., in which the fractions of available

energy into recoil is about 0.20~0.25 for F reactions with C1 to C4 systems. In Layfield's work, abstraction sites have no relative sensitivity in the distributions of alkyl internal energy. Although n-pentane was not included in the calculations, we can also speculate that the contribution from primary and secondary abstraction products will not change the energy partitioned into the internal freedom of alkyl fragments since the exoergicity of these three target alkanes at the same abstraction site is almost the same. The fraction decreases as the size of the reagent alkane molecules increases, consistent with the theoretical study. Their calculations show that the energy channeled into HF vibration, rotation and translation decreases for reactions from C1 to C4, with some of the energy going into alkyl internal degrees of freedom as the systems become larger. They plausibly attribute this to larger alkyl products have greater number of vibrational modes and a greater density of states; these modes effectively couple to the reaction coordinate and absorb more energy released in the reaction. For all target molecules, the fractions of BW scattering are larger than FW/SW scattering, in agreement with the translational energy distributions discussed above.

Qualitatively speaking, the result of high vibrational excitation in the products agrees with Polanyi rules for early-barrier dynamics in an atom+diatom systems.[143] Now we consider the distributions in a quantitative way by using the kinematic model of Evans *et al.*[144] While β is the reaction's skew angle, E_R is reaction exogercity, and E_C is the collision energy, the average translational energy release for backward scattering (collinear reaction) is given by

$$\langle E_T \rangle = sin^2\beta E_R + cos^2\beta E_C$$

For F + alkane reactions, as a heavy-light-heavy system, they produce very small skew angles around 10 to 20°, so $sin^2\beta$ is less than 0.10.[145] For all target molecules, the BW scattering fractions f_C is clearly smaller than 0.90, which means the translational energy release observed in

our experiment is lower than the values predicted by Evans' model. This is not surprising as our systems are atom + polyatom reactions with large numbers of degrees of freedom, while this model works well for three-atom reactions. Energy is converted from the F-H-C moiety into alkyl fragments via intramolecular vibrational redistribution, in addition to direct impulsive release of energy into product recoil which was also shown in the results of F + ethane by Nesbitt and coworkers. Alkyl radical products are likely to have significant rotational excitation. For FW scattered products, similar reduced translational energy release fractions lower than the model predictions are observed. Again, the large impact parameter collisions induce small momentum transfer, resulting in lower rotational excitation.

6.5 Conclusion

The reaction dynamics of F atom with propane, n-butane and n-pentane have been studied using a newly designed pulsed stack valve with single photon ionization via crossed beam DC slice imaging methods. Translational energy distributions of all the reactions have similar features, FW/BW scattering peaks at higher energy than does SW scattering. The center of mass angular distributions have a forward-scattered component that decreases with the size of the hydrocarbon target, possibly suggesting a velocity-dependent effect. The fraction of available energy into recoil falls with the size of molecule as a result of the large vibrational modes coupled to reaction coordinate and more effectively absorbing energy release.

CHAPTER 7-H ABSTRACTION CHANNELS IN THE CROSSED-BEAM REACTION OF F + 1-PROPANOL, 1-BUTENE AND 1-HEXENE BY DC SLICE IMAGING

7.1 Introduction

In recent years, there has been an increasing interest in oxidation of alcohols as renewable biofuels.[146-148] With a higher energy density and larger octane number, as well as fewer pollutants from combustion compared with gasoline, some are used specifically as transportation fuels. Moreover, the oxygenated hydrocarbon systems offer special dynamical interest to both theoretical and experimental research. Oxidation (i.e., hydrogen atom abstraction) from these molecules by ground state fluorine atoms offers a means of investigating aspect of these dynamics in detail.[149] As a result of the nonequivalent hydrogen atoms in C-H and O-H groups, abstraction can proceed through hydroxyl hydrogen removal and/or alkyl hydrogen removal. In addition, it is possible that the highly reactive product radicals initiate different subsequent reactions such as the chain reaction of CH_2OH with additional F_2 as well as interference with each other.[150] It is very important to understand the relative efficiency of these competing reaction channels and numerous studies were focused on the branching ratios of these parallel pathways. For many of the same reasons, F atom reactions with unsaturated hydrocarbons are of dynamical interest as an illuminating contrast to the analogous Cl or O atom reactions that have been studied in considerable detail. We describe our initial investigations into both of these systems in this report.

The CH_3OH + F reaction system was previsously studied by means of HF or radical emission spectra. [150-159]

$F + CH_3OH \rightarrow HF + CH_3O \qquad \Delta H = -32$ kcal/mol (1)

$\rightarrow HF + CH_2OH \qquad \Delta H = -41$ kcal/mol [160] (2)

Hydroxymethyl radical formation is about 10 kcal.mol^{-1} more exoergic than methoxy radical formation, indicating pathway (2) to be energetically favored. Furthermore, the 3:1 ratio of methyl to hydroxyl hydrogens suggests a statistically favored hydroxymethyl yield. Thus the prediction on the product branching fraction of methoxy radicals can be expected to be less than or equal to 0.25. However, although the reported branching ratios differ from one study to another, almost all the experimental results show a greater than 50% or at least larger than 25% methoxy yield fraction. Khatoon *et al.* reported the branching ratios of hydroxymethyl to methoxy radical pathways as 0.4 to 0.6 by studying fluorine atom reactions with normal and deuterated methanols using a fast discharge flow reactor with samples analyzed by a mass-spectrometer. [157] Durant's work also shows a 0.6 ± 0.2 methoxy branching ratio at room temperature which they ascribed to the fact that the hydroxyl-hydrogen potential energy surface is more attractive (although less exothermic) relative to the methyl-hydrogen abstraction surface.[159] Yet although experimental results of hydrogen abstraction from methanol with chlorine, bromine and hydroxyl and methyl radicals reported a dominance of the hydroxymethyl pathway; it is evident that fluorine reactions follow different mechanisms.[161-165] Jodkowski and co-workers explained this difference as the fluorine reaction branching ratios are determined by the activation entropy differences rather than activation energies for different channels.[166]

For hydrogen abstraction in higher alcohols the preferential attack was also found at the OH group. Several measurements on the alkoxy yield from reactions of F with normal and deuterated ethanols and propanols presented similar alkoxy product fractions.[160, 167, 168] The fraction yielding ethoxy radical is reported to be 0.5 although alkyl hydrogen abstraction is also energetically favored. The probability of attack on the C-H group was found to be five times less than attack on the O-H group for the reactions of F atoms with alcohols. (This ratio was also

observed in F + CH_3OD and F + CD_3OH reactions). Wagner *et al.* summarized that the low exothermicity Cl atom reaction channels happened following the order of exothermicity while the highly exothermic F atom reactions more controlled by steric factors.[167]

On the other hand, fluorine reaction with alkenes provides rich chemistry as a result of their large variations in exoergicity for different abstraction sites, as well as the presence of strongly bound adducts. Fluorine is the most electronegative element in the periodic table. It is possible for fluorine to replace hydrogen in organic compounds without grossly distorting the system geometry.[169, 170] Carbon-fluorine bond study has become a very important area of research in organic chemistry. [171] It is very interesting to take a detailed look at the reaction dynamics of F atom with unsaturated hydrocarbons, where both direct abstraction and long-lived complex formation with or without unimolecular decomposition mechanisms are possible.

Lee and co-workers conducted a comprehensive crossed molecular beam study on F atom reactions with a series of olefins.[172-176] For F + C_2H_4, C_2D_4 reactions, C_2H_3F (C_2D_3F) formation (H elimination) proceeded via a long-lived complex although the products' recoil energy distribution peaked about half of the available energy. Highly vibrationally excited DF suggested small internal excitation of the co-product, C_2D_3.[172] The symmetric angular distributions of C_2H_3F product indicated the lifetime of C_2H_4F was longer than the rotational period while the C_2H_3F product energy distribution was nonstatistical.[174] The complex formed in F + C_4H_8 reaction study showed, at least for complex configurations near the transition state, the internal energy randomization assumption broke down.[173] For reaction of F with propene, three reaction pathways were observed: H + C_3H_5F, CH_3 + C_2H_3F and HF + C_3H_5, and the relative branching ratios are estimated as 0.15:0.65:0.19.[175] The H pathway was inferred as proceeding through a direct reaction mechanism superimposed on a long-lived complex

formation as a result of the noticeable backward angular distribution; the forward-backward symmetric angular distribution suggested CH_3 formation mainly occurs via a long-lived complex formation mechanism. The clearly forward scattering angular distribution indicated a strong direct reaction channel for HF formation. This F + propene result was confirmed and further investigated by a theoretical study, where the doublet potential energy surfaces of fluorine atom reaction with propene were calculated at the UMP2 and CCSD(T) level of theory.[177] The most favorable reaction pathway was found to be CH_3 formation while at high temperature the H formation pathway is less favorable than CH_2F formation. On the potential energy surface no addition-elimination mechanism was seen, although the authors appeared to be looking exlusively for a cyclic 5-membered TS for HF elimination. This will be considered further below.

There are also various other experimental and theoretical studies for fluorine atom reactions with small alkenes[178-182] but few results have been reported for C4 or larger linear alkenes. Similarly, detailed experimental investigations on the kinetics of F + CH_3OH and ethanol, propanol reactions have been reported while little dynamical information is available for larger alcohols. Here we present a preliminary reaction dynamics study of H-abstraction reactions of F atom with 1-propanol, 1-butene and 1-hexene via crossed-beam dc slice imaging, focusing on minor pathways detected by single photon ionization at 157 nm. Scattering images of hydroxyalkyl and alkyl radicals were recorded and the results analyzed after density-flux correction and background subtraction. We also compare the fluorine atom results with analogous systems in which chlorine is the radical reagent.

7.2 Experimental

The experiments were conducted on a crossed beam imaging apparatus described in detail before.[123] Our machine consists of one main reaction chamber and two source chambers, perpendicular to each other. Both molecular beams were diluted in helium and were skimmed into the main chamber after supersonic expansion. A 5% fluorine mixture was pulsed from a piezoelectric stack valve with a 120 μm translation actuator and 50 μs pulse duration. F atoms were generated by a pulsed discharge fired just after the nozzle. Two electrode plates were mounted in front of the nozzle plate, as well as an insulator plate placed between electrodes to prevent unwanted discharge between first electrode and the nozzle. We created the discharge by giving a pulsed high voltage (+800 V) to the second electrode plate and keeping the first electrode at ground. A piezoelectric disk valve generated the target beams with helium as carrier gas. The product radical following reaction was ionized with a VUV beam at 157 nm from a F_2 excimer laser (7.9 ev) in the interaction region and then accelerated and stretched through a set of four DC slice ion optics lenses. After flying field-free along a 70 cm flight tube 90 degrees to the reaction plane, the ions would impact on a dual microchannel plate (MCP) detector coupled to a P-47 phosphor screen. A negative high-voltage pulse was given to the front plate to while the back plate of the MCP assembly was held at constant positive potential to gate only the central slice of the products at a certain m/z ratio.

Raw images were recorded using a CCD camera with F discharge on and off to discriminate the photochemical background associated with target molecules. Our home-built NUACQ-2 program is used to acquire the data with event-counting and centroiding. The intense F atom beam allow us to operate the VUV probe beam unfocused, and direct inversion of the experimental data is then achieved; only little density-to-flux correction was needed.

7.3 Computational Methods

CBS-QB3 method implemented in the Gaussian09 quantum chemistry software package was used to perform ab initio calculations on the reaction enthalpies and the transition states for HF loss following adduct formation for the F + butene reaction via the vinylic and allylic site.[183] The geometry optimization and vibrational frequencies were evaluated using density functional theory with B3LYP and M062X functionals using an 6-31+G(d,p) basis set. IRC calculations to verify the connections between TS and the local minima were conducted at both B3LYP/6-31+G(d,p) and M062X/6-31+G(d,p) level. The CBS-QB3 composite method was also used to gain a higher level of accuracy. Similar calculations were also performed for the reaction of F + propene and included in the supplementary information.

7.4 Results

Fig. 7.1 gives the reaction enthalpies (0 K) for H abstraction (black) and F addition (blue) at the indicated sites calculated at CBS-QB3 level of theory, as well as the vertical ionization energies (eV) of corresponding product radicals (in parentheses). As expected for the highly reactive F atom, the exoergicities are much higher compared to Cl atom reactions with the same targets.[80] All direct abstraction and addition sites are energetically accessible, and α hydrogen abstraction is the most energetically favored one. Based on our single photon ionization probe at 7.9 eV, according to the vertical ionization energies, we have high selectivity on the product radicals detected as will be discussed below.

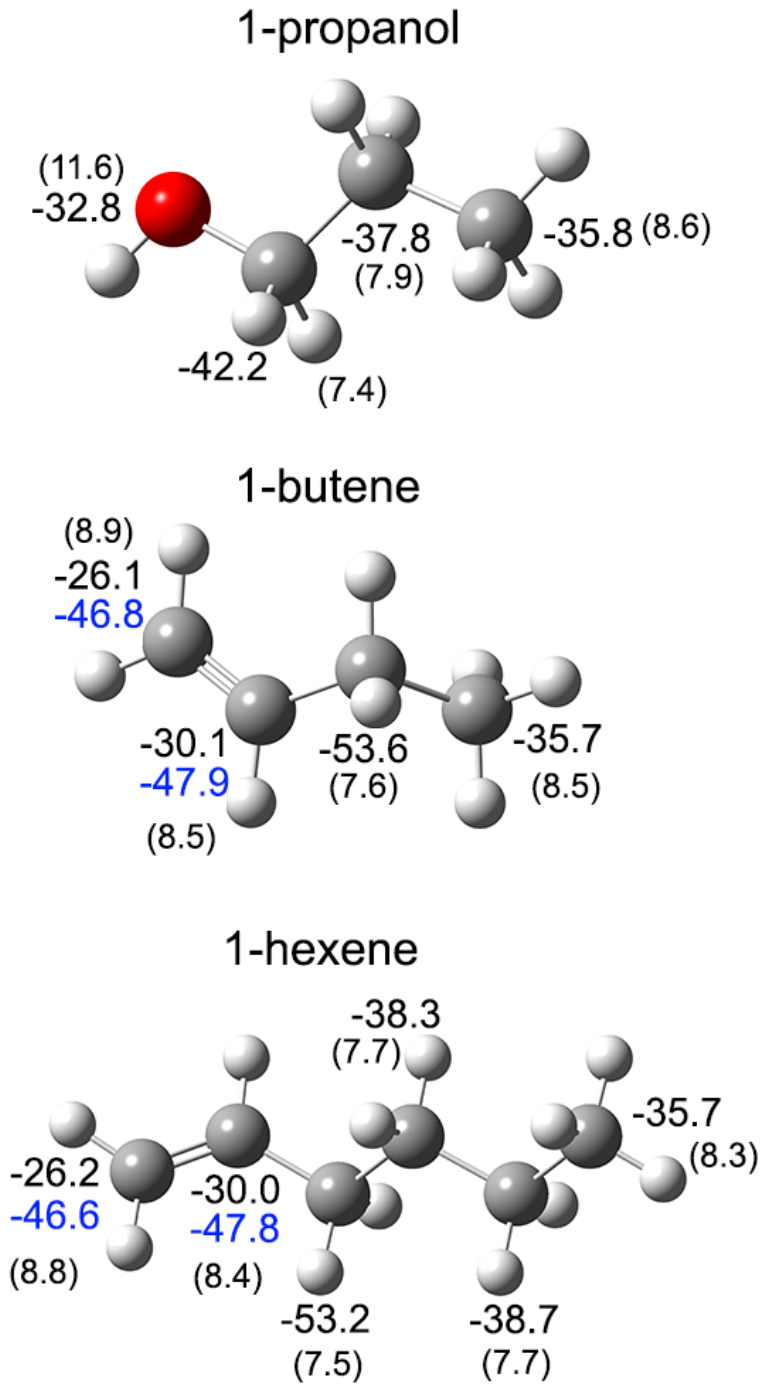

Figure 7.1: Lowest energy structures of 1-propanol, 1-butene and 1-hexene. Reaction enthalpies at 0 K (kcal.mol-1) at different abstraction sites are calculated at the CBS-QB3 level of theory. Numbers in blue are reaction energy release of complex formatting pathways; numbers in parenthesis are vertical ionization energies of corresponding product ions (eV).

The reactively scattered hydroxyalkyl radical from F atom reaction with 1-propanol is shown in the left side of Fig. 7.2 for a collision energy of 10.2 kcal.mol^{-1}. These raw images are background subtracted and density-to-flux corrected with Newton diagrams superimposed. 1-propanol has two types of abstraction sites: the primary and secondary C-H groups and the O-H site. The bond dissociation energy (at 298 K) is 104.7 kcal/mol for H_O elimination, about 89.6 kcal/mol for Hα elimination, 94.4 kcal/mol for Hβ elimination and 97.0 kcal/mol for Hγ elimination, consistent with the theoretical trends given in Fig. 1.[184] Previous experimental results of F + propanol reactions found evidence for the existence of all possible abstraction channels by determining the relative amount of HF and DF. [167] This kinetic study also reported that the possibility of alkyl H atom being attacked was 5 times less than hydroxyl H atom site.

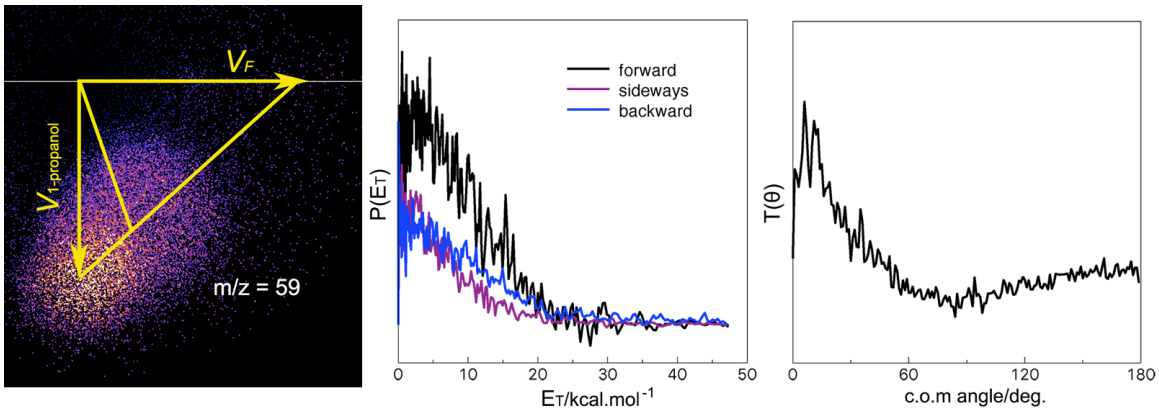

Figure 7.2: (Left) DC sliced image for the C3H7O product after background subtraction and density-to-flux correction at a collision energy of 10.2 kcal.mol-1, with Newton diagrams superimposed. (Center) Translational energy distributions for forward, sideways and backward scattered distributions of fluorine + 1-propanol. (Right) Center-of-mass angular distribution of F + 1-propanol reaction.

Fig.7.2 also shows the translational energy distributions integrated for forward, sideways and backward scattering regions and center-of-mass angular distributions for F reaction with 1-propanol. Despite the strong photochemistry background surrounding the alcohol parent beam,

we are able in this case to make reliable subtraction of the background signal, and are able to report results for the full scattering distribution. The sideways translational energy distribution peaks closer to 0 than the backward distributions and there is a strong forward component in the angular distributions.

Raw images for F atom reactions with 1-butene and 1-hexene are shown in Fig. 7.3 at collision energies of 10.4 kcal.mol^{-1} and 9.1 kcal.mol^{-1}, respectively. The corresponding translational energy distributions for alkene reactions are presented in the right part of Fig.7.3. The translational energy distributions are integrated every 20° and forward scattering is also omitted owing to background interference. Both 1-butene and 1-hexene scattered products show an increasing translational energy release with increasing angles, although 1-butene has a broader distribution than 1-hexene. The sideways and backward scattering reduced translational energy distributions are shown in Fig 7.4, as well as the angular distributions. The backward distributions peak farther from zero for both alkenes and 1-butene has broader peaks, in good agreement with the 20 degrees integrated results. The backward component dominates in the angular distributions.

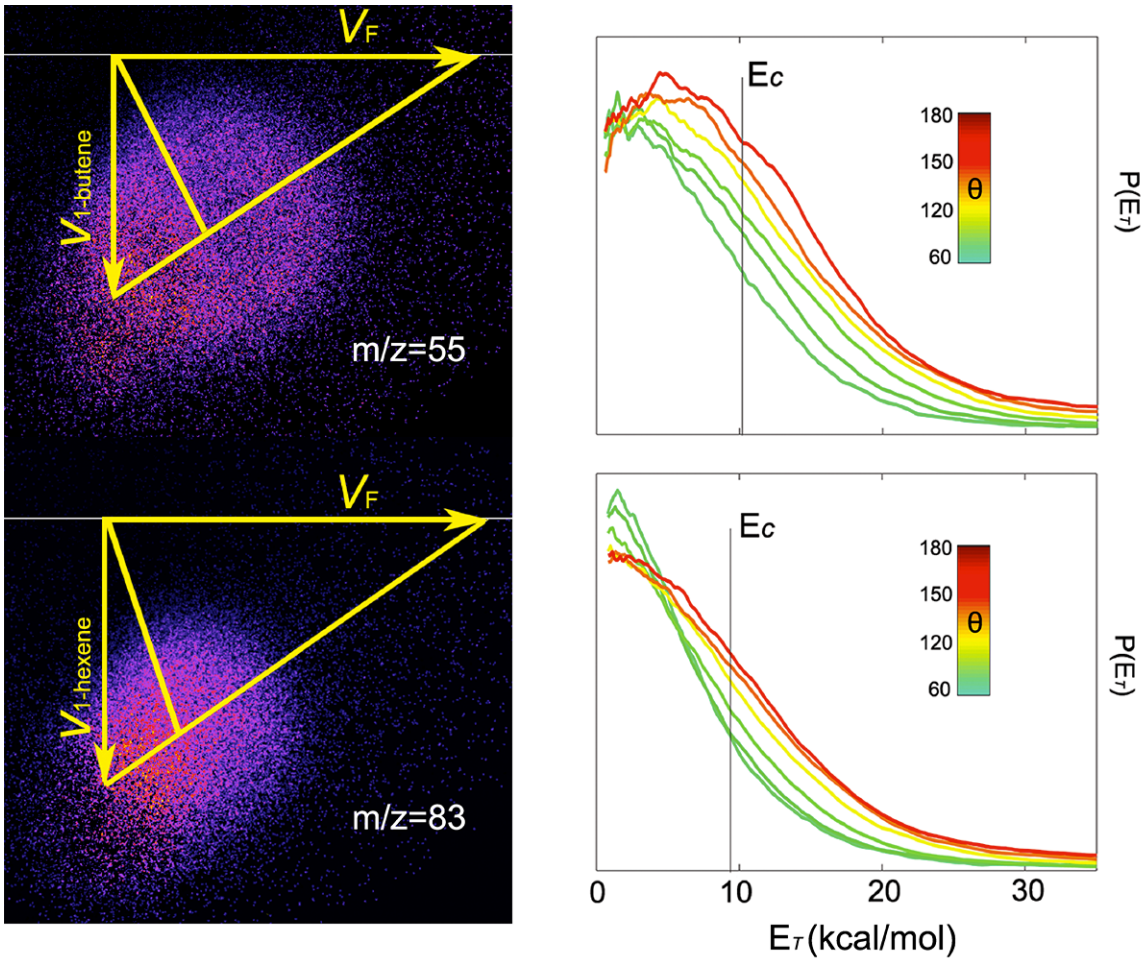

Figure 7.3: DC sliced images for C_4H_7 and C_6H_{11} products with newton diagrams superimposed (left) and translational energy distributions integrated every 20 ° (right).

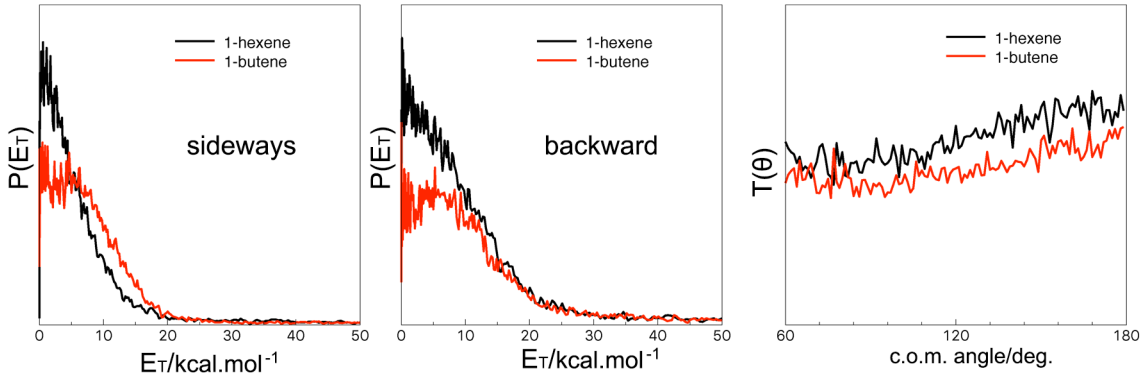

Figure 7.4: Sideways and backward translational energy distributions of F + 1-butene and F + 1-hexene reaction (left); right is the center-of-mass angular distributions of the targets.

Table 7.1: Most probable collision energies and average energy release for fluorine reaction with 1-propanol, 1-butene and 1-hexene; the latter is given along with the fraction of collision energy

appearing in translation for the indicated center-of-mass scattering regions. Values are in kcal.mol-1.

	Ec	**<E_T>sdw**	**<E_T>bwd**	**<E_T>*sdw**	**<E_T>*bwd**
1-propanol	10.2	9.1	12.4	0.89	1.22
1-butene	10.4	8.2	10.1	0.79	0.97
1-hexene	9.1	8.4	10.6	0.92	1.16

The average translational energy release and the fraction of the collision energy in translation are shown in Table 7.1. Here we also show the reduced translational energy release, P(E_T *), where E_T *= E_T/E_C to shed some light on the deviation from the heavy-light-heavy limiting cases, as the acute skew angle for H atom transfer favors translational energy conservation. The average reduced energy, <E_T *> of 1-butene is somewhat than the other two. The backward energy release is slightly higher than sideways for all target systems and the 1-propanol reaction shows higher translational energy release than the alkenes.

7.5 Discussion

A very interesting result here is the similarity of the distributions of F + 1-propanol with our previous results of F + 1-butane. Both backward translational energy distributions peak farther from 0 than sideways distributions and the center-of-mass angular distributions have a strong forward component, and are decreasing with increasing scattering angle. It is likely that C – H abstraction plays an important role in the F + alcohol process, as previous kinetic studies show the existence of all possible channels. On one hand, the kinematics and corresponding C-H abstraction reaction enthalpies lead to the speculation that the distributions of 1-propanol reaction results would show similar trends to that of 1-butane. On the other hand, according to the ionization energies, we only detect the H loss product on α and β hydrogen sites, not H loss on the hydroxyl site. This also helps to explain the similarity to results of F+1-butane, where only C-H sites exist. However, given multiple reactive sites, the substantial dipole moment in 1-

propanol (1.68 D), the strong hydrogen bonding interaction and the associated anisotropy of the potential energy surface, a simple interpretation of the results may not be forthcoming.

Let us now look at the portion of collision energy release in translation. Due to various attacking positions and corresponding variations in energy release we do not show the fraction of the total available energy appearing in translation. Instead we examine the fraction of the *collision energy* appearing as final translational energy (E_T*). Although most of the exoergicity would be disposed into the internal energy of HF, we find for sideways scattering $\langle E_T^* \rangle = 0.89$ and backwards 1.22, much higher than the corresponding fractions for F + n-butane, 0.71 and 0.86 respectively. One thing to mention is that both reactions have similar collision energies about 10 kcal.mol^{-1}, and in both systems only secondary abstraction products were detected.[82] As for alkane reactions the different collision energies can tell the relative importance of the stripping mechanism, it is very likely that the $\langle E_T^* \rangle$ difference between n-butane and 1-propanol come from C-O and O-H interference, which is in consistent with the results of the kinetic studies.[160, 167] The energy release of α H abstraction is 5 kcal.mol^{-1} more than β H abstraction, while their H numbers are 1:2; these two factors may compete with each other to determine the final branching. According to the kinetic studies on the branching ratios of F with alcohols, the O-H group abstraction is more favored over the attack on C-H groups, even though for propanol these H sites are in the ratio is 1:7. It may be that, because of the dominance of reaction at the OH site (which we do not detect) we are probing a subset of the reactive flux that excludes some geometries and impact parameters in comparison with the butane reaction. We find the appearance of O-H group causes a backward energy release factor exceeding 1.0, much higher than the factors in Cl + butanol isomers reactions. [185]

Khatoon *et al.* found that compared with abstraction from the OH group, the alkyl group H abstraction is less favored, and this preference is ascribed to steric factors rather than exothermicity differences to decide the reaction routes for F + alcohols.[167] Further theoretical characterization of the potential energy surfaces of fluorine reaction with propanol isomers will be important to understand the details of these reactions' dynamics.

In the reactions of fluorine atoms with 1-butene (we consider only the gauche conformer) and 1-hexene, the existence of the π system suggests addition to the double bond followed by unimolecular decomposition as a possible pathway in addition to direct abstraction.[111] Fluorine has both higher ionization energy and lower electron affinity than chlorine, and with the small and highly electronegative fluorine atom, the energy released during the reaction is much higher than chlorine atom reactions with corresponding alkenes. All abstraction sites and addition positions are easily energetically accessible while for chlorine, reaction at the vinylic sites is endothermic and highly disfavored. According to the anti-Markovnikov rule, we expect the radical to add to the least substituted unsaturated carbon. This effect can be seen in Cl + butene isomers, yet it is not the case with F reactions: the reaction enthalpies shown in Fig. 1 do not follow that the energetically favored sites are the more substituted ones.[123] The same was found by Li et al. for F addition to propene.[177] For unsaturated systems a dichotomy appears in the behavior of fluorine; in addition to inductive field effects, which leads to electron withdrawal to fluorine, Pauli repulsion occurs between electron pairs on π–electrons and fluorine leading to electron density return from fluorine.[171] In any case, with our selectivity on ionization energies, we only detect allylic H loss products, which are also the most favored on the basis of exoergicity. However, we show below that vinylic H abstraction may in fact dominate the addition/elimination channel.

For the F+ alkene reactions, both backward translational energy distributions showed higher energy release than sideways distributions, which is opposite to the results of chlorine.[107, 123] For chlorine reactions with C5-C6 monoalkenes, different targets showed indistinguishable distributions and the results were interpreted mainly as addition/elimination dominated mechanisms due to nearly isotropic angular distributions and nearly zero-peaked translational energy distributions, while for F + 1-butene and 1-hexene we see different behaviors. In Fig. 4 we can see the translational energy distributions for 1-hexene peaks near 0 while sideways distributions of 1-butene peaks around 5-7 kcal.mol^{-1}, backwards 7-9 kcal.mol^{-1}, and it is even clearer in Fig. 7.3 where the distributions are integrated every 20°. As a consequence, it is likely that adduct formation is more important for 1-hexene. However, reaction enthalpy variations between the corresponding pathways of 1-butene and 1-hexene are not substantial. A likely reason for the difference is the greatly increased density of states for the F-hexene adduct as well as greater conformational heterogeneity in hexene.

In the work of Ran *et al.* on F + propene*,* the HF channel clearly followed a direct abstraction reaction mechanism, although interestingly, the methyl loss channel clearly proceeded via a complex.[175] Huang and coworkers performed a detailed theoretical study of the F + propene reaction, determining geometries for minima and transition states at the UMP2(FULL)/6-311++G(d,p) level of theory. This was followed by CCSD(T)/cc-VTZ energy determinations.[177] While Ran et al. did not provide information on the site-specificity for the three chemically different hydrogen sites, Huang's calculations show that among various considered possible reaction paths including direct H abstraction and addition-isomerization-elimination reactions, F (^{2}F) attacking on the double bond to form a barrierless weakly bound complex, followed by F addition to the C=C forming a low-lying intermediate isomer

barrierlessly is the dominant channel. After this intermediate isomer the most competitive reaction pathway leads to CH_3 + $CHF=CH_2$. In the direct H abstraction channels, the dominant pathway was believed to be the F atom radical picking up the allylic hydrogen while the terminal vinyl hydrogen abstraction was less competitive, although these arguments were largely based on energetic considerations. Additionally, after F addition to the vinyl inner carbon (C2), the most favorable hydrogen atom elimination also is the vinyl inner hydrogen.

Li et al. argued that there was no pathway for HF elimination from the strongly bound F-propene addition complex. Apparently they were looking for a cyclic TS in that case from the C-1 adduct. However, based on the discovery of a roaming-type transition state in the Cl-butene system, we pursued a search for analogous features of the F+ propene and 1-butene potential energy surfaces, first using the CBS-QB3 composite method. The result is shown in Fig 7.5 for the 1-butene system; results for propene, which are very similar, are included as Fig.7.6. From the addition complex, which is bound by over 2 eV, the F atom may proceed over transition states in which both the C-F distance is very large (i.e., the old bond is broken) and the C-H distance is large (new bond is not yet formed). The system thus exhibits characteristics reminiscent of the Cl-butene system: In a sense, the F atom "redissociates" to permit H abstraction and HF elimination, although in contrast to the Cl case, the bond distances are not as large. One other remarkable feature of HF elimination from the adduct is seen both in Fig. 7.5 and Fig. 7.6: the TS leading to abstraction of the vinylic H from C2 is 5.5 kcal/mol *lower* than that for abstraction of the allylic H despite the much greater exoergicity for the latter channel. After zero point correction, the barrier for allylic HF elimination is 0.7 kcal/mol *above* the reactant asymptote, while the vinylic HF elimination pathway is nearly 4 kcal/mol below. We believe this suggests the C2 adduct as a likely intermediate that may lead via (2,2) HF

elimination to the much higher energy H_2CCCH_3 isomer. We find the IRC of the transition state structure optimized with B3LYP/6-31+G(d,p) for the allylic elimination does connect to the C2 adduct. The low TSs found at the CBS-QB3 level suggested to us, however, that the associated B3LYP geometries might be leading to an underestimation of the barrier heights. We ran further calculations using the M062X functional at the 6-31+G(d,p) level, and the results are also given in Fig. 7.5. After zero point correction, the allylic elimination is found to be much lower, but still 1.3 kcal above the vinylic pathway. Interestingly, the IRC at the M062X/6-31+G(d,p) level it leads to the C1 adduct with a structure very similar to that examined by Li et al. with CCSD(T). It appears that this barrier rises above the reactants at the higher level of theory; however, the vinylic HF elimination TS is much lower and very likely persists. In fact our observation of addition/elimination despite the selective allylic probe appears to indicate that this channel is operative despite the possible absence of a reaction path from the C-1 adduct. It may be that the C-2 adduct can follow either path as suggested by the CBS-QB3 results, although based on the barrier heights we expect the (2,2) vinylic elimination to dominate.

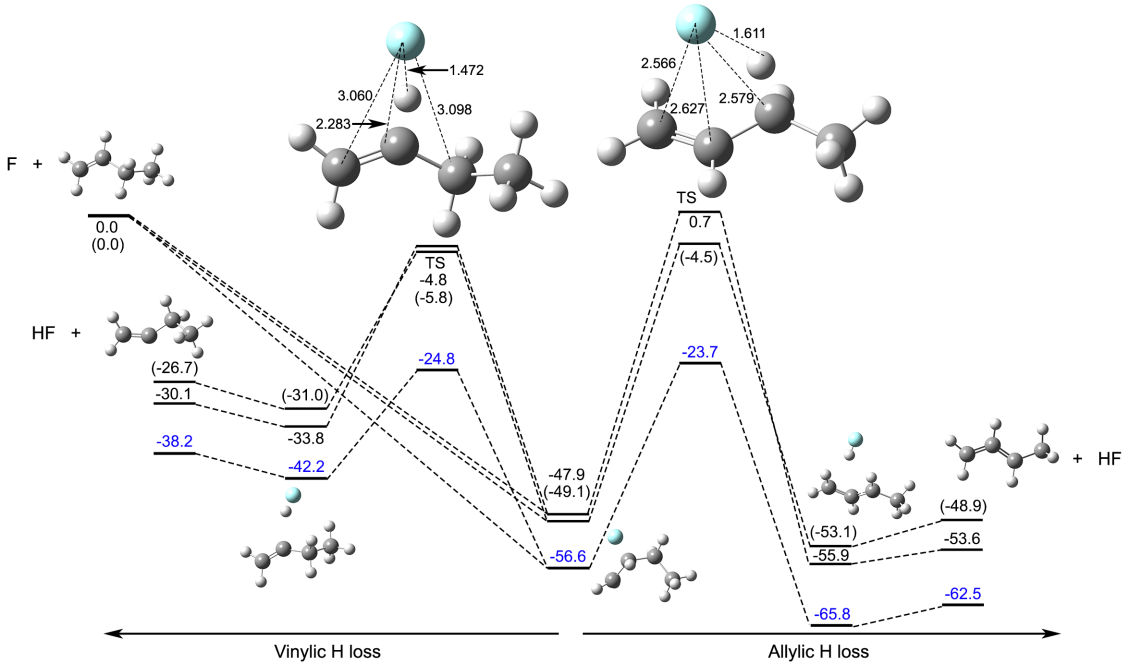

Figure 7.5: Key stationary points on the potential energy surface of the fluorine + 1-butene reaction. Numbers are relative energies at the CBS-QB3 level with zero point correction. Results at the M062X /6-31+G(d,p) level, also zero point corrected, are shown in parentheses. Results at the B3LYP /6-31+G(d,p) level zero point corrected are shown in blue. Structures are from CBS-QB3.

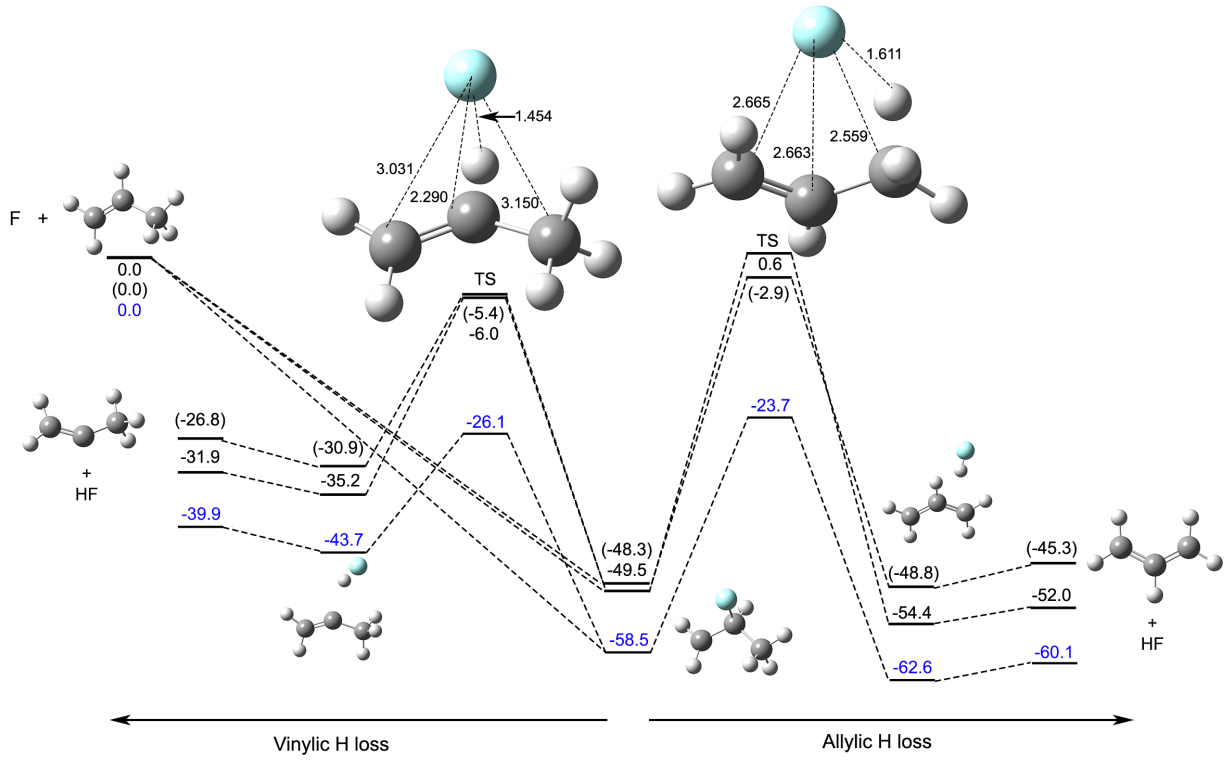

Figure 7.6: Key stationary points on the potential energy surface of the fluorine + propene reaction. Numbers are relative energies at the CBS-QB3 level with zero point correction. Results at the M062X /6-31+G(d,p) level, also zero point corrected, are shown in parentheses. Results at the B3LYP /6-31+G(d,p) level zero point corrected are shown in blue. Structures are from CBS-QB3.

This HF pathway will also be in competition with ethyl radical elimination (or butyl elimination in hexane). By analogy with methyl elimination in propene, we expect the latter to be a favored, lower energy pathway. Li et al. found this 10 kcal/mol below the reactants, and it is likely similar for the larger systems. However, as mentioned above, our present probe is not sensitive to the vinylic H abstraction nor to the ethyl elimination. In any case, the theoretical evidence for Markovnikov radical addition and the likely formation of the vinylic radical product despite the presence of an alternative pathway to a resonantly stabilized radical 1 eV lower in energy are two of the surprises that the fluorine atom brings. Future experiments that can probe these pathways directly will be very interesting to pursue.

7.6 Conclusion

The reaction dynamics of fluorine atom with 1-propanol, 1-butene and 1-hexene were studied by crossed beam DC slice imaging via single photon ionization. The distributions of F+ 1-propanol are quite similar to the previous F + 1-butane results: backscattered translational energy distributions peak at higher energy than does sideways scattering and the center-of-mass angular distribution has a strong forward component. The distributions of F + 1-butene and 1-hexene have higher backward translational energy distributions than SW scattering, opposite to Cl reactions and this is explained with distinct associated reaction mechanisms. The angular distributions show adduct formation is more important for F + 1-hexene than direct abstraction. The fraction of collision energy in product translation for all target systems are much higher than corresponding target reactions with chlorine. The theoretical calculations of stationary points on the potential surface for the butene system find a pathway for (2,2) HF elimination from the more stable C-2 adduct that leads to the vinylic isomer, $CH_3CH_2CCH_2$ far less stable compared to the resonantly stabilized allylic isomer. Our selective detection of the allylic product suggests, however, that that channel is present as well, and may also come from the C-2 adduct.

BIBLIOGRAPHY

1. Murray, C. and A.J. Orr-Ewing, *The dynamics of chlorine-atom reactions with polyatomic organic molecules.* International Reviews in Physical Chemistry, 2004. **23**: p. 435.
2. Simpson, W.R., A.J. Orr-Ewing, and R.N. Zare, *State-to-state differential cross sections for the reaction Cl (2 P)+ CH 4 (ν 3= 1, J= 1)→ HCl (v′ = 1, J′)+ CH 3.* Chemical Physics Letters, 1993. **212**: p. 163-171.
3. Simpson, W.R., et al., *Reaction of Cl with vibrationally excited CH4 and CHD3: State‐to‐state differential cross sections and steric effects for the HCl product.* Journal of Chemical Physics, 1995. **103**: p. 7313.
4. Simpson, W.R., et al., *Picturing the transition-state region and understanding vibrational enhancement for the Cl+CH4->HCl+CH3 reaction.* Journal of Physical Chemistry, 1996. **100**: p. 7938-7947.
5. Kandel, S.A., et al., *Dynamics for the Cl+ CH→ HCl+ CH reaction examined through state‐specific angular distributions.* Journal of Chemical Physics, 1996. **105**: p. 7550.
6. Kandel, S.A., et al., *Dynamical effects of reagent vibrational excitation in the Cl+ C 2 H 6 (ν 5= 1)→ HCl+ C 2 H 5 reaction.* Chemical Physics Letters, 1997. **265**: p. 121.
7. Kandel, S.A., et al., *Angular distributions for the Cl+ C2H6→ HCl+ C2H5 reaction observed via multiphoton ionization of the C2H5 radical.* Journal of Physical Chemistry A, 1998. **102**(13): p. 2270-2273.

8. Simpson, W.R., et al., *Core extraction for measuring state‐to‐state differential cross sections of bimolecular reactions.* Journal of Chemical Physics, 1995. **103**: p. 7299-7312.

9. Shafer, N.E., et al., *State-to-state differential cross sections from photoinitiated bulb reactions.* Chemical Physics Letters, 1993. **212**: p. 155-162.

10. Varley, D.F. and P.J. Dagdigian, *Comparison of the dynamics of abstraction of primacy vs secondary hydrogens in the Cl+CD3CH2CD3 reaction.* Chemical Physics Letters, 1996. **255**: p. 393.

11. Varley, D.F. and P.J. Dagdigian, *Product state resolved study of the Cl+(CH3)(3)CD reaction: Comparison of the dynamics of abstraction of primary versus tertiary hydrogens.* Journal of Physical Chemistry, 1996. **100**: p. 4365.

12. Bass, M.J., et al., *The dynamics of the Cl+C2H6 -> HCl(v';j')+C2H5 reaction at 0.24 eV: Is ethyl a spectator?* Journal of Chemical Physics, 2003. **119**(14): p. 7168-7178.

13. Bass, M.J., et al., *The dynamics of the Cl+ n-C4H10→HCl (v′, j′)+ C4H9 reaction at 0.32 eV.* Journal of Chemical Physics, 2004. **121**(15): p. 7175-7186.

14. Casavecchia, P., N. Balucani, and G.G. Volpi, *Crossed-beam studies of reaction dynamics.* Annual Review of Physical Chemistry, 1999. **50**: p. 347-376.

15. Casavecchia, P., et al., *Probing the dynamics of polyatomic multichannel elementary reactions by crossed molecular beam experiments with soft electron-ionization mass spectrometric detection.* Physical Chemistry Chemical Physics, 2009. **11**(1): p. 46-65.

16. Townsend, D., et al., *The roaming atom: Straying from the reaction path in formaldehyde decomposition.* Science, 2004. **306**(5699): p. 1158-1161.

17. Chang, Y.T., C. Minichino, and W.H. Miller, *Classical trajectory studies of the molecular dissociation dynamics of formaldehyde: H2CO→ H2+ CO.* Journal of Chemical Physics, 1992. **96**(6): p. 4341-4355.

18. Chen, W., W.L. Hase, and H.B. Schlegel, *Ab initio classical trajectory study of H2CO→ H2+ CO dissociation.* Chemical Physics Letters, 1994. **228**(4-5): p. 436-442.

19. Peslherbe, G.H. and W.L. Hase, *Semiempirical MNDO, AM1, and PM3 direct dynamics trajectory studies of formaldehyde unimolecular dissociation.* Journal of Chemical Physics, 1996. **104**(20): p. 7882-7894.

20. Li, X.S., J.M. Millam, and H.B. Schlegel, *Ab initio molecular dynamics studies of the photodissociation of formaldehyde, H2CO -> H2+CO: Direct classical trajectory calculations by MP2 and density functional theory.* Journal of Chemical Physics, 2000. **113**(22): p. 10062-10067.

21. Green, W.H., C.B. Moore, and W.F. Polik, *Transition-States and Rate Constants for Unimolecular Reactions.* Annual Review of Physical Chemistry, 1992. **43**: p. 591-626.

22. van Zee, R.D., M.F. Foltz, and C.B. Moore, *Evidence for a second molecular channel in the fragmentation of formaldehyde.* Journal of Chemical Physics, 1993. **99**(3): p. 1664-1673.

23. Houston, P. and S. Kable, *Photodissociation of acetaldehyde as a second example of the roaming mechanism.* Proceedings of the National Academy of Sciences, 2006. **103**(44): p. 16079-16082.

24. Heazlewood, B.R., et al., *Roaming is the dominant mechanism for molecular products in acetaldehyde photodissociation.* Proceedings of the National Academy of Sciences, 2008. **105**(35): p. 12719-12724.

25. Sivaramakrishnan, R., J. Michael, and S. Klippenstein, *Direct observation of roaming radicals in the thermal decomposition of acetaldehyde.* Journal of Physical Chemistry A, 2009. **114**(2): p. 755-764.

26. Bowman, J.M. and B.C. Shepler, *Roaming radicals.* Annual Review of Physical Chemistry, 2011. **62**: p. 531-553.

27. Herath, N. and A.G. Suits, *Roaming Radical Reactions.* Journal of Physical Chemistry Letters, 2011. **2**(6): p. 642-647.

28. Hause, M.L., et al., *Roaming-mediated isomerization in the photodissociation of nitrobenzene.* Nature Chemistry, 2011. **3**(12): p. 932-937.

29. Harding, L.B. and S.J. Klippenstein, *Roaming Radical Pathways for the Decomposition of Alkanes.* Journal of Physical Chemistry Letters, 2010. **1**(20): p. 3016-3020.

30. Sivaramakrishnan, R., et al., *Roaming radicals in the thermal decomposition of dimethyl ether: Experiment and theory.* Combustion and Flame, 2011. **158**(4): p. 618-632.

31. Sivaramakrishnan, R., et al., *Shock Tube and Theoretical Studies on the Thermal Decomposition of Propane: Evidence for a Roaming Radical Channel.* Journal of Physical Chemistry A, 2011. **115**(15): p. 3366-3379.

32. Zhao, Y.L., et al., *Hydrogen migration and vinylidene pathway for formation of methane in the 193 nm photodissociation of propene: CH3CH = CH2 and CD3CD = CD2.* Journal of Physical Chemistry A, 2007. **111**(34): p. 8330-8335.

33. Goncharov, V., N. Herath, and A.G. Suits, *Roaming dynamics in acetone dissociation.* Journal of Physical Chemistry A, 2008. **112**(39): p. 9423-9428.

34. Maeda, S., T. Taketsugu, and K. Morokuma, *Automated Exploration of Photolytic Channels of HCOOH: Conformational Memory via Excited-State Roaming.* Journal of Physical Chemistry Letters, 2012. **3**(14): p. 1900-1907.

35. Matsugi, A., *Roaming Dissociation of Ethyl Radicals.* Journal of Physical Chemistry Letters, 2013. **4**(24): p. 4237-4240.

36. Tsai, P.-Y., et al., *Roaming as the dominant mechanism for molecular products in the photodissociation of large aliphatic aldehydes.* Physical Chemistry Chemical Physics, 2015. **17**(35): p. 23112-23120.

37. Bowman, J.M. and A.G. Suits, *Roaming reactions: The third way.* Physics Today, 2011. **64**(11): p. 33-37.

38. Bowman, J.M., *Roaming.* Molecular Physics, 2014. **112**(19): p. 2516-2528.

39. Finlayson-Pitts, B.J. and J.N. Pitts, *Tropospheric Air Pollution: Ozone, Airborne Toxics, Polycyclic Aromatic Hydrocarbons, and Particles.* Science, 1997. **276**(5315): p. 1045-1051.

40. Atkinson, R. and J. Arey, *Gas-Phase Tropospheric Chemistry of Biogenic Volatile Organic Compounds: A Review.* Atmospheric Environment, 2003. **37**: p. 197-219.

41. Molina, M.J. and F.S. Rowland, *Stratospheric Sink for Chlorofluoromethanes: Chlorine Atom-Catalysed Destruction of Ozone.* Nature, 1974. **249**(5460): p. 810-12.

42. Solberg, S., et al., *Boundary-Layer Ozone Depletion as Seen in the Norwegian Arctic in Spring.* Journal of Atmospheric Chemistry, 1996. **23**(3): p. 301-332.

43. Platt, U. and G. Hönninger, *The Role of Halogen Species in the Troposphere.* Chemosphere, 2003. **52**(2): p. 325-338.

44. Wingenter, O.W., et al., *Hydrocarbon and Halocarbon Measurements as Photochemical and Dynamical Indicators of Atmospheric Hydroxyl, Atomic Chlorine, and Vertical Mixing Obtained During Lagrangian Flights.* Journal of Geophysical Research: Atmospheres, 1996. **101**(D2): p. 4331-4340.

45. Lawler, M.J., et al., *Pollution‐Enhanced Reactive Chlorine Chemistry in the Eastern Tropical Atlantic Boundary Layer.* Geophysical Research Letters, 2009. **36**(8).

46. Jobson, B.T., et al., *Measurements of C2‐C6 Hydrocarbons During the Polar Sunrise 1992 Experiment: Evidence for Cl Atom and Br Atom chemistry.* Journal of Geophysical Research: Atmospheres, 1994. **99**(D12): p. 25355-25368.

47. Ariya, P.A., et al., *Measurements of C2‐C7 Hydrocarbons During the Polar Sunrise Experiment 1994: Further Evidence for Halogen Chemistry in the Troposphere.* Journal of Geophysical Research: Atmosphere, 1998. **103**(D11): p. 13169-13180.

48. Hitchman, M.L., et al., *Disposal Methods for Chlorinated Aromatic Waste.* Chemical Society Reviews, 1995. **24**(6): p. 423-430.

49. Zimmermann, R., et al., *Emission of Nonchlorinated and Chlorinated Aromatics in the Flue Gas of Incineration Plants During and After Transient Disturbances of Combustion Conditions: Delayed Emission Effects.* Environmental Science & Technology, 2001. **35**(6): p. 1019-1030.

50. George, I.J. and J.P.D. Abbatt, *Heterogeneous Oxidation of Atmospheric Aerosol Particles by Gas-Phase Radicals.* Nature Chemistry, 2010. **2**(9): p. 713-722.

51. Liu, C.-L., et al., *The Direct Observation of Secondary Radical Chain Chemistry in the Heterogeneous Reaction of Chlorine Atoms with Submicron Squalane Droplets.* Physical Chemistry Chemical Physics, 2011. **13**(19): p. 8993-9007.

52. Mendez, M., et al., *Reactivity of Chlorine Radical with Submicron Palmitic Acid Particles: Kinetic Measurements and Product Identification.* Atmospheric Chemistry and Physics, 2013. **13**(23): p. 11661-11673.

53. Atkinson, R., *Gas-Phase Tropospheric Chemistry of Volatile Organic Compounds: 1. Alkanes and Alkenes.* Journal of Physical and Chemical Reference Data, 1997. **26**(2): p. 215-290.

54. Taatjes, C.A., *Time-resolved infrared absorption measurements of product formation in Cl atom reactions with alkenes and alkynes.* International Reviews in Physical Chemistry, 1999. **18**: p. 419.

55. Spicer, C.W., et al., *Unexpectedly High Concentrations of Molecular Chlorine in Coastal Air.* Nature, 1998. **394**(6691): p. 353-356.

56. Neufeld, D.A., et al., *Herschel Observations of Interstellar Chloronium.* Astrophysical Journal, 2012. **748**(1): p. 37.

57. Monje, R.R., et al., *Hydrogen Chloride in Diffuse Interstellar Clouds Along the Line of Sight to W31C (G10. 6-0.4).* Astrophysical Journal, 2013. **767**(1): p. 81.

58. DeSain, J.D., et al., *Product Formation in the Cl-Initiated Oxidation of Cyclopropane.* Journal of Physical Chemistry A, 2003. **107**(12): p. 1992-2002.

59. Glarborg, P., *Hidden Interactions - Trace Species Governing Combustion and Emissions.* Proceedings of the Combustion Institute, 2007. **31**(1): p. 77-98.

60. Liu, K., *Crossed-Beam Studies of Neutral Reactions: State-Specific Differential Cross Sections.* Annual Review of Physical Chemistry, 2001. **52**(1): p. 139-164.

61. Bechtel, H.A., et al., *Effects of Bending Excitation on the Reaction of Chlorine Atoms with Methane.* Angewandte Chemie-International Edition, 2005. **117**(16): p. 2434-2437.

62. Orr-Ewing, A.J., et al., *Scattering-angle resolved product rotational alignment for the reaction of Cl with vibrationally excited methane.* Journal of Chemical Physics, 1997. **106**: p. 5961.

63. Zhou, J., et al., *On the $Cl^*(^2P_{1/2})$ Reactivity and the Effect of Bend Excitation in the Cl + CH_4/CD_4 Reactions.* Journal of Physical Chemistry A, 2004. **108**(39): p. 7832-7836.

64. Varley, D.F. and P.J. Dagdigian, *Product State Distributions and Angular Differential Cross Sections from Photoinitiated Reactions of Chlorine Atoms with Small Hydrocarbons.* Journal of Physical Chemistry, 1995. **99**(24): p. 9843-9853.

65. Abou-Chahine, F., et al., *Vibrationally Resolved Dynamics of the Reaction of Cl Atoms with 2,3-dimethylbut-2-ene in Chlorinated Solvents.* Chemical Science, 2013. **4**(1): p. 226-237.

66. Ragains, M.L. and B.J. Finlayson-Pitts, *Kinetics and mechanism of the reaction of Cl atoms with 2-methyl-1,3-butadiene (isoprene) at 298 K.* Journal of Physical Chemistry A, 1997. **101**: p. 1509.

67. Kaiser, E.W. and T.J. Wallington, *Pressure Dependence of the Reaction Cl + C_3H_6.* Journal of Physical Chemistry, 1996. **100**: p. 9788.

68. Arunan, E., R. Rengarajan, and D.W. Setser, *INFRARED CHEMILUMINESCENCE STUDIES OF THE REACTIONS OF H-ATOMS WITH CCL3, CF2CL, AND CH2CH2CL RADICALS AT 300 AND 475 K - RECOMBINATION-ELIMINATION VS ABSTRACTION MECHANISMS.* Canadian Journal of Chemistry, 1994. **72**: p. 568.

69. Neumark, D.M., et al., *Experimental Investigation of Resonances in Reactive Scattering - the F+H2 Reaction.* Physical Review Letters, 1984. **53**(3): p. 226-229.

70. Neumark, D.M., et al., *Molecular-Beam Studies of the F+H2 Reaction.* Journal of Chemical Physics, 1985. **82**(7): p. 3045-3066.

71. Neumark, D.M., et al., *Molecular-Beam Studies of the F+D2 and F+HD Reactions.* Journal of Chemical Physics, 1985. **82**(7): p. 3067-3077.

72. Skodje, R.T., et al., *Resonance-mediated chemical reaction: F+HD -> HF+D.* Physical Review Letters, 2000. **85**(6): p. 1206-1209.

73. Lee, S.H., F. Dong, and K.P. Liu, *Reaction dynamics of F+HD -> HF+D at low energies: Resonant tunneling mechanism.* Journal of Chemical Physics, 2002. **116**(18): p. 7839-7848.

74. Manolopoulos, D.E., et al., *The Transition-State of the F+H2 Reaction.* Science, 1993. **262**(5141): p. 1852-1855.

75. Dong, F., S.H. Lee, and K. Liu, *Reactive excitation functions for F plus p-H-2/n-H-2/D-2 and the vibrational branching for F+HD.* Journal of Chemical Physics, 2000. **113**(9): p. 3633-3640.

76. Yang, X.M. and D.H. Zhang, *Dynamical resonances in the fluorine atom reaction with the hydrogen molecule.* Accounts of Chemical Research, 2008. **41**(8): p. 981-989.

77. Ren, Z.F., et al., *Probing the resonance potential in the F atom reaction with hydrogen deuteride with spectroscopic accuracy.* Proceedings of the National Academy of Sciences of the United States of America, 2008. **105**(35): p. 12662-12666.

78. Dong, W.R., et al., *Transition-State Spectroscopy of Partial Wave Resonances in the F plus HD Reaction.* Science, 2010. **327**(5972): p. 1501-1502.

79. Wang, T., et al., *Dynamical Resonances Accessible Only by Reagent Vibrational Excitation in the F + HD -> HF + D Reaction.* Science, 2013. **342**(6165): p. 1499-1502.

80. Joalland, B., et al., *Dynamics of chlorine atom reactions with hydrocarbons: insights from imaging the radical product in crossed beams.* Journal of Physical Chemistry A, 2014. **118**(40): p. 9281-95.

81. Joalland, B., et al., *Dynamics of Cl plus propane, butanes revisited: a crossed beam slice imaging study.* Physical Chemistry Chemical Physics, 2014. **16**(2): p. 414-420.

82. Shi, Y.Y., et al., *Crossed-beam DC slice imaging of fluorine atom reactions with linear alkanes.* Journal of Chemical Physics, 2015. **142**(18).

83. Houston, P.L., *Vector correlations in photodissociation dynamics.* Journal of Physical Chemistry, 1987. **91**(21): p. 5388-5397.

84. Chandler, D.W. and P.L. Houston, *Two-dimensional Imaging of State-selected Photodissociation Products Detected by Multiphoton Ionization.* Journal of Chemical Physics, 1987. **87**: p. 1445-1447.

85. Eppink, A.T.J.B. and D.H. Parker, *Velocity map imaging of ions and electrons using electrostatic lenses: Application in photoelectron and photofragment ion imaging of molecular oxygen.* Review of Scientific Instruments, 1997. **68**(9): p. 3477-3484.

86. Townsend, D., M.P. Minitti, and A.G. Suits, *Direct current slice imaging.* Review of Scientific Instruments, 2003. **74**(4): p. 2530-2539.

87. Kitsopoulos, T.N., C.R. Gebhardt, and T.P. Rakitzis, *Photodissociation study of CS2 at 193 nm using slice imaging.* Journal of Chemical Physics, 2001. **115**(21): p. 9727-9732.

88. Proch, D. and T. Trickl, *A high ‐ intensity multi ‐ purpose piezoelectric pulsed molecular beam source.* Review of Scientific Instruments, 1989. **60**(4): p. 713-716.

89. Proctor, D.L., D.R. Albert, and H.F. Davis, *Improved piezoelectric actuators for use in high-speed pulsed valves.* Review of Scientific Instruments, 2010. **81**(2): p. 023106.

90. Irimia, D., et al., *A short pulse (7 μs FWHM) and high repetition rate (dc-5kHz) cantilever piezovalve for pulsed atomic and molecular beams.* Review of Scientific Instruments, 2009. **80**(11): p. 113303.

91. Luria, K., N. Lavie, and U. Even, *Dielectric barrier discharge source for supersonic beams.* Review of Scientific Instruments, 2009. **80**(10): p. 104102.

92. Yan, B., et al., *A new high intensity and short-pulse molecular beam valve.* Review of Scientific Instruments, 2013. **84**(2): p. 023102.

93. Abeysekera, C., et al., *Note: A short-pulse high-intensity molecular beam valve based on a piezoelectric stack actuator.* Review of Scientific Instruments, 2014. **85**(11): p. 116107.

94. Atkinson, R., et al., Journal of Physical and Chemical Reference Data, 1999. **28**: p. 191.

95. Yen, Y.F., et al., *Site propensities for HCl and DCl formation in the reaction of Cl with selectively-deuterated alkanes.* Journal of Physical Chemistry, 1994. **98**: p. 4.

96. Blank, D.A., et al., *A Crossed Molecular Beam Investigation of the Reaction Cl + Propane → HCl + C_3H_7 Using VUV Synchrotron Radiation as a Product Probe.* Chemical Physics, 1998. **231**: p. 261.

97. Estillore, A.D., et al., *Dynamics of H and D Abstraction in the Reaction of Cl Atom with Butane-1,1,1,4,4,4-d6.* Physical Chemistry Chemical Physics, 2011. **13**(18): p. 8433-8440.

98. Montgomery, J.A., et al., *A complete basis set model chemistry. VI. Use of density functional geometries and frequencies.* Journal of Chemical Physics, 1999. **110**: p. 2822.

99. Estillore, A.D., L.M. Visger, and A.G. Suits, *Crossed-beam dc slice imaging of chlorine atom reactions with pentane isomers.* Journal of Chemical Physics, 2010. **132**: p. 164313.

100. Stutz, J., et al., *Rate constants and kinetic isotope effects in the reactions of atomic chlorine with n-butane and simple alkenes at room temperature.* Journal of Physical Chemistry A, 1998. **102**(44): p. 8510-8519.

101. Stutz, J., M. Ezell, and B. Finlayson-Pitts, *Inverse kinetic isotope effect in the reaction of atomic chlorine with C2H4 and C2D4.* Journal of Physical Chemistry A, 1997. **101**(49): p. 9187-9190.

102. Whitney, E.S., et al., *Reactive scattering dynamics in atom+ polyatomic systems: F+ CH → HF (v, J)+ CH.* Journal of Chemical Physics, 2005. **122**: p. 124310.

103. Murray, C., et al., *Stereodynamics of chlorine atom reactions with organic molecules.* Journal of Physical Chemistry A, 2005. **109**: p. 11093.

104. Li, W., et al., *State-resolved reactive scattering by slice imaging: A new view of the Cl+C2H6 reaction.* Journal of Chemical Physics, 2006. **124**: p. 11102.

105. Bass, M.J., et al., *Imaging photon-initiated reactions: A study of the Cl(2P3/2)+CH4 -> HCl+CH3 reaction.* Journal of Chemical Physics, 2005. **123**: p. 94301.

106. Tyndall, G.S., et al., *Kinetics and mechanisms of the reactions of chlorine atoms with ethane, propane, and n-butane.* International Journal of Chemical Kinetics, 1997. **29**: p. 43.

107. Estillore, A.D., L.M. Visger, and A.G. Suits, *Imaging the dynamics of chlorine atom reactions with alkenes.* Journal of Chemical Physics, 2010. **133**: p. 074306.

108. Montgomery, J.A., et al., *A complete basis set model chemistry. VII. Use of the minimum population localization method.* Journal of Chemical Physics, 2000. **112**: p. 6532.

109. Frisch, M.J., et al., *Gaussian 09, Revision A.02*. Gaussian, Inc. Vol. Revision A. 02. 2009, Wallington CT: Gaussian, Inc.

110. Townsend, D., et al., *Universal and state-resolved imaging of chemical dynamics.* Journal of Physical Chemistry A, 2005. **109**: p. 8661.

111. Kunitski, M., et al., *The conformational stability of gaseous 1-butene studied by femtosecond nonlinear spectroscopy and ab initio calculations.* Vibrational Spectroscopy, 2011. **56**(1): p. 13-18.

112. Mebel, A. 2013.

113. Suits, A.G., *Roaming atoms and radicals: a new mechanism in molecular dissociation.* Accounts of Chemical Research, 2008. **41**(7): p. 873-881.

114. Kim, G.-S., et al., *Ab Initio/RRKM Study of the Potential Energy Surface of Triplet Ethylene and Product Branching Ratios of the C (3P)+ CH4 Reaction.* Journal of Physical Chemistry A, 2003. **107**(11): p. 1788-1796.

115. Mebel, A., et al., *Theoretical study of potential energy surface and thermal rate constants for the C6H5+ H2 and C6H6+ H reactions.* Journal of Physical Chemistry A, 1997. **101**(17): p. 3189-3196.

116. Mebel, A.M., K. Morokuma, and M. Lin, *Ab initio molecular orbital study of potential energy surface for the reaction of C2H3 with H2 and related reactions.* Journal of Chemical Physics, 1995. **103**(9): p. 3440-3449.

117. Christoffel, K.M. and J.M. Bowman, *Three Reaction Pathways in the H+ HCO→ H2+ CO Reaction.* Journal of Physical Chemistry A, 2009. **113**(16): p. 4138-4144.

118. Finlayson-Pitts, B.J. and J.N. Pitts Jr, *Chemistry of the upper and lower atmosphere: theory, experiments, and applications*. 1999: Access Online via Elsevier.

119. Pilgrim, J.S. and C.A. Taatjes, *Infrared absorption probing of the Cl + C_3H_6 reaction: Rate coefficient for HCl production between 290 and 800 K.* Journal of Physical Chemistry A, 1997. **101**: p. 5776.

120. Brana, P. and J.A. Sordo, *Mechanistic aspects of the abstraction of an allylic hydrogen in the chlorine atom reaction with 2-methyl-1, 3-butadiene (isoprene).* Journal of the American Chemical Society, 2001. **123**(42): p. 10348-10353.

121. Brana, P. and J.A. Sordo, *Theoretical approach to the mechanism of reactions between halogen atoms and unsaturated hydrocarbons: The Cl + propene reaction.* Journal of Computational Chemistry, 2003. **24**(16): p. 2044-2062.

122. Estillore, A.D., L.M. Visger, and A.G. Suits, *Imaging the Dynamics of Chlorine Atom Reactions with Alkenes.* J. Chem. Phys., 2010. **133**: p. 074306.

123. Joalland, B., et al., *Crossed-beam slice imaging of Cl reaction dynamics with butene isomers.* Journal of Physical Chemistry A, 2013.

124. Grubb, M.P., et al., *No straight path: roaming in both ground- and excited-state photolytic channels of $NO_3 \rightarrow NO + O_2$.* Science, 2012. **335**(6072): p. 1075-1078.

125. Li, W., et al., *Megapixel ion imaging with standard video.* Review of Scientific Instruments, 2005. **76**: p. 63106.

126. Polanyi, J.C., J.L. Schreiber, and W.J. Skrlac, *Distribution of reaction products (theory). Part 12.–Microscopic branching in H + XY → HX + Y, HY + X (X, Y = halogens).* Faraday Discussions of the Chemcal Society, 1979. **67**: p. 66-89.

127. Fernandez-Ramos, A., et al., *Modeling the kinetics of bimolecular reactions.* Chemical Reviews, 2006. **106**(11): p. 4518-4584.

128. Marcy, T.P., et al., *Theoretical and experimental investigation of the dynamics of the production of CO from the CH_3 + O and CD_3 + O Reactions.* Journal of Physical Chemistry A, 2001. **105**(36): p. 8361-8369.

129. Pomerantz, A.E., et al., *Reaction products with internal energy beyond the kinematic limit result from trajectories far from the minimum energy path: an example from H + HBr→ H_2 + Br.* Journal of the American Chemical Society, 2005. **127**(47): p. 16368-16369.

130. Preston, T.J., et al., *Direct and Indirect Hydrogen Abstraction in Cl plus Alkene Reactions.* Journal of Physical Chemistry A, 2014. **118**(30): p. 5595-5607.

131. Polanyi, J.C., *Some Concepts in Reaction Dynamics.* Science, 1987. **236**(4802): p. 680-690.

132. Camden, J.P., H.A. Bechtel, and R.N. Zare, *Dynamics of the simplest reaction of a carbon atom in a tetrahedral environment.* Angewandte Chemie-International Edition, 2003. **42**(42): p. 5227-5230.

133. Kim, Z.H., et al., *Comparison of near-threshold reactivity of ground-state and spin-orbit excited chlorine atoms with methane.* Journal of Chemical Physics, 2001. **115**(1): p. 179-183.

134. Yoon, S., et al., *The relative reactivity of the stretch-bend combination vibrations of CH4 in the Cl (P-2(3/2))+CH4 reaction.* Journal of Chemical Physics, 2002. **116**(24): p. 10744-10752.

135. Lin, J.J., et al., *State-specific correlation of coincident product pairs in the F+CD4 reaction.* Science, 2003. **300**(5621): p. 966-969.

136. Yoon, S., et al., *The relative reactivity of CH3D molecules with excited symmetric and antisymmetric stretching vibrations.* Journal of Chemical Physics, 2003. **119**(18): p. 9568-9575.

137. Yan, S., et al., *Do vibrational excitations of CHD3 preferentially promote reactivity toward the chlorine atom?* Science, 2007. **316**(5832): p. 1723-1726.

138. Zhang, W.Q., H. Kawamata, and K.P. Liu, *CH Stretching Excitation in the Early Barrier F + CHD3 Reaction Inhibits CH Bond Cleavage.* Science, 2009. **325**(5938): p. 303-306.

139. Czako, G. and J.M. Bowman, *CH Stretching Excitation Steers the F Atom to the CD Bond in the F + CHD3 Reaction.* Journal of the American Chemical Society, 2009. **131**(48): p. 17534-17535.

140. Czako, G., et al., *Communication: Experimental and theoretical investigations of the effects of the reactant bending excitations in the F+CHD3 reaction.* Journal of Chemical Physics, 2010. **133**(13).

141. Layfield, J.P., A.F. Sweeney, and D. Troya, *Direct-Dynamics Study of the F + CH4, C2H6, C3H8, and i-C4H10 Reactions.* Journal of Physical Chemistry A, 2009. **113**(16): p. 4294-4304.

142. Silva, R., et al., *Photodissociation of heptane isomers and relative ionization efficiencies of butyl and propyl radicals at 157 nm.* Physical Chemistry Chemical Physics, 2009. **11**(23): p. 4777-4781.

143. Polanyi, J.C. and W.H. Wong, *Location of Energy Barriers .I. Effect on Dynamics of Reactions A+BC.* Journal of Chemical Physics, 1969. **51**(4): p. 1439-&.

144. Evans, G.T., E. van Kleef, and S. Stolte, *Chemical reaction dynamics: Combination of two models.* Journal of Chemical Physics, 1990. **93**(7): p. 4874-4883.

145. Picconatto, C.A., A. Srivastava, and J.J. Valentini, *Reactions at suprathreshold energy: Evidence of a kinematic limit to the internal energy of the products.* Journal of Chemical Physics, 2001. **114**(4): p. 1663-1671.

146. Chiaramonti, D., G. Liden, and J. Yan, *Advances in sustainable biofuel production and use.* Applied Energy, 2013. **102**: p. 1-4.

147. Cho, D.H., et al., *Alcohol-based biofuel production from waste wood hydrolysate.* Journal of Bioscience and Bioengineering, 2009. **108**: p. S45-S45.

148. Sawangkeaw, R., et al., *Biofuel production from palm oil with supercritical alcohols: Effects of the alcohol to oil molar ratios on the biofuel chemical composition and properties.* Bioresource Technology, 2011. **102**(22): p. 10704-10710.

149. Bogan, D., D. Setser, and J. Root. *Fluorine-containing free radicals*. in *ACS Symposium Series 66Am. Chem. Soc, Washington*. 1978.

150. Bogan, D.J., et al., *Laser-Induced Fluorescence Study of Methoxy Radical Formation from the Reactions of F(P-2) Atoms with Ch3oh, Cd3oh, and Ch3od.* Journal of Physical Chemistry, 1990. **94**(21): p. 8128-8134.

151. Smith, D., et al., *HF infrared chemiluminescence. Relative rate constants for hydrogen abstraction from hydrocarbons, substituted methanes, and inorganic hydrides.* Journal of Physical Chemistry, 1977. **81**(9): p. 898-905.

152. Macdonald, R.G., J. Sloan, and P. Wassell, *The dynamics of hydrogen abstraction from polyatomic molecules by fluorine atoms.* Chemical Physics, 1979. **41**(1): p. 201-208.

153. Dill, B. and H. Heydtmann, *Infrared chemiluminescent reactions of fluorine atoms with methanol and some deuterated analogs.* Chemical Physics, 1980. **54**(1): p. 9-20.

154. Agrawalla, B. and D. Setser, *Energy disposal in hydrogen atom abstraction reactions: energy in the radical fragment by laser-induced fluorescence.* Journal of Physical Chemistry, 1984. **88**(4): p. 657-660.

155. Wickramaaratchi, M., et al., *Evaluation of HF product distributions deduced from infrared chemiluminiscence. II. F atom reactions.* Chemical physics, 1985. **94**(1-2): p. 109-129.

156. Agrawalla, B. and D. Setser, *Infrared chemiluminescence and laser-induced fluorescence studies of energy disposal by reactions of fluorine and chlorine atoms with hydrogen sulfide, deuterium sulfide, hydrogen selenide, water, water-d2, and methanol.* Journal of Physical Chemistry, 1986. **90**(11): p. 2450-2462.

157. Khatoon, T. and K. Hoyermann, *The reactions of fluorine atoms with normal and deuterated methanols.* Berichte der Bunsengesellschaft für physikalische Chemie, 1988. **92**(6): p. 669-673.

158. Pagsberg, P., et al., *UV spectrum and kinetics of hydroxymethyl radicals.* Chemical Physics Letters, 1988. **146**(5): p. 375-381.

159. Durant Jr, J., *Anomalous methoxy radical yields in the fluorine+ methanol reaction. 1. Experiment.* Journal of Physical Chemistry, 1991. **95**(26): p. 10701-10704.

160. Bogan, D.J. and F.L. Nesbitt, *Ethoxy Radical Yield in the System C2d5oh Plus F(P-2) Plus F2 at P=1 Torr and T=223-423 K.* Journal of Physical Chemistry, 1994. **98**(4): p. 1151-1155.

161. Dobe, S., et al., *Fast Flow Kinetic Studies of the Reaction CH2OH+ HCl CH3OH+ Cl. The Heat of Formation of Hydroxymethyl.* Berichte der Bunsengesellschaft für physikalische Chemie, 1993. **97**(7): p. 877-883.

162. Dobe, S., et al., *Direct Kinetic Studies of the Reactions Br+ CH3OH and CH2OH+ HBr: The Heat of Formation of CH2OH.* Journal of Physical Chemistry, 1996. **100**(51): p. 19864-19873.

163. Hess, W.P. and F.P. Tully, *Hydrogen-atom abstraction from methanol by hydroxyl radical.* Journal of Physical Chemistry, 1989. **93**(5): p. 1944-1947.

164. Tsang, W., *Chemical kinetic data base for combustion chemistry. Part 2. Methanol.* Journal of Physical and Chemical Reference Data, 1987. **16**(3): p. 471-508.

165. Jodkowski, J.T., et al., *Theoretical study of the kinetics of the hydrogen abstraction from methanol. 3. Reaction of methanol with hydrogen atom, methyl, and hydroxyl radicals.* Journal of Physical Chemistry A, 1999. **103**(19): p. 3750-3765.

166. Jodkowski, J.T., et al., *Theoretical study of the kinetics of the hydrogen abstraction from methanol. 1. Reaction of methanol with fluorine atoms.* Journal of Physical Chemistry A, 1998. **102**(46): p. 9219-9229.

167. Khatoon, T., et al., *Rates and mechanisms of the reactions of ethanol and propanol with fluorine and chlorine atoms.* Berichte der Bunsengesellschaft für physikalische Chemie, 1989. **93**(5): p. 626-632.

168. Dill, B., et al., *Infrared chemiluminescence in the reactions of atomic fluorine with ethanol, propanol-(2) and some deuterated analogs.* Chemical Physics, 1981. **58**(2): p. 163-174.

169. Harper, D.B. and D. Ohagan, *The Fluorinated Natural-Products.* Natural Product Reports, 1994. **11**(2): p. 123-133.

170. O'Hagan, D. and D.B. Harper, *Fluorine-containing natural products.* Journal of Fluorine Chemistry, 1999. **100**(1-2): p. 127-133.

171. Chambers, R.D., *Fluorine in organic chemistry*. 2004: CRC Press.

172. Parson, J. and Y. Lee, *Crossed molecular beam study of F+ C2H4, C2D4.* Journal of Chemical Physics, 1972. **56**(9): p. 4658-4666.

173. Parson, J.M., et al., *Unimolecular decomposition of the long‐lived complex formed in the reaction F+ C4H8.* Journal of Chemical Physics, 1973. **59**(3): p. 1402-1415.

174. Farrar, J.M. and Y.T. Lee, *The question of energy randomization in the decomposition of chemically activated C2H4F.* Journal of Chemical Physics, 1976. **65**(4): p. 1414-1426.

175. Ran, Q., et al., *Dynamics of the F atom reaction with propene.* Journal of Chemical Physics, 2004. **121**(13): p. 6302-6308.

176. Robinson, G.N., R.E. Continetti, and Y.T. Lee, *The translational energy dependence of the F+ C2H4⟶H+ C2H3F reaction cross section near threshold.* Journal of Chemical Physics, 1990. **92**(1): p. 275-284.

177. Li, J.-L., et al., *A barrier-free atomic radical-molecule reaction: F+ propene.* Journal of Chemical Theory and Computation, 2006. **2**(6): p. 1551-1564.

178. Hase, W.L. and K.C. Bhalla, *A classical trajectory study of the F+ C2H4→ C2H4F→ H+ C2H3F reaction dynamics.* Journal of Chemical Physics, 1981. **75**(6): p. 2807-2819.

179. Sloan, J.J. and D.G. Watson, *The HF energy distribution in the reaction of F atoms with vinyl radicals.* Journal of Chemical Physics, 1981. **74**(1): p. 744-745.

180. Schlegel, H.B., K.C. Bhalla, and W.L. Hase, *Ab initio molecular orbital studies of atomic hydrogen+ ethylene and atomic fluorine+ ethylene. 2. comparison of the energetics.* Journal of Physical Chemistry, 1982. **86**(25): p. 4883-4888.

181. Dehe, K. and H. Heydtmann, *HF infrared chemiluminescence in the reactions of fluorine atoms with cis-butene-2, trans-butene-2 and 2,3-d(2)-butene-2.* Berichte Der Bunsen-Gesellschaft-Physical Chemistry Chemical Physics, 1996. **100**(7): p. 1226-1230.

182. Ran, Q., et al., *Molecular beam studies of the F atom reaction with propyne: Site specific reactivity.* Journal of Chemical Physics, 2005. **122**(4): p. 044307.

183. Frisch, M.J., et al., *Gaussian 09*. 2009, Gaussian, Inc.: Wallingford, CT, USA.

184. Zhou, W.D., Y. Yuan, and J.S. Zhang, *Photodissociation dynamics of 1-propanol and 2-propanol at 193.3 nm.* Journal of Chemical Physics, 2003. **119**(14): p. 7179-7187.

185. Estillore, A.D., L.M. Visger-Kiefer, and A.G. Suits, *Reaction dynamics of Cl + butanol isomers by crossed-beam sliced ion imaging.* Faraday Discussions, 2012. **157**: p. 181-91; discussion 243-84.

ABSTRACT

CROSSED BEAM IMAGING OF THE REACTION DYNAMICS OF HALOGEN ATOMS WITH SELECTED HYDROCARBONS

by

YUANYUAN SHI

December 2016

Advisor: Dr. Arthur G.Suits

Major: Chemistry (Physical)

Degree: Doctor of Philosophy

This dissertation presents results of applying dc slice imaging in crossed molecular beams to probe the dynamics of the reactions of halogen atoms (chlorine and fluorine) with polyatomic hydrocarbons and alcohols such as deuterated propanes, butane isomers, pentane, alkenes and propanol. The full velocity-flux contour maps of the radical products were measured with 157nm single photon ionization at various collision eneriges. Secondary and tertiary abstractions were found in Cl with normal and deuterated propanes and butane isomers and show distinct differences. The differences were explained in terms of the nature of abstraction sites, energy disposal of the radical product, and kinetic isotope effects. For Cl reaction with butene isomers, the coupling of translational energy and center of mass angular distributions reflect the energetics of competition between direct abstraction and addition/elimination pathways in accordance with ab initio thermochemical data. A possible Cl atom roaming mediating the

indirect mechanism is suggested and further addressed with investigations of Cl + isobutene reactions at various collision energies. For reaction of chlorine atoms with butenes, the combined experimental theoretical calculations result shows that Cl addition-HCl elimination occurs from an abstraction-like Cl-H-C geometry, rather than a conventional three-center or four-center transition state. This geometry is accessed exclusively by Cl atom roaming from the initial adduct.

For fluorine atom reaction with linear alkanes, i.e. propane, n-butane and n-pentane, little effect of reaction exoergicity appears in the reduced translational energy distributions. The fraction of available energy in translation for pentane is smaller than the other two. Sharp forward scattering were found in the center of mass angular distributions of all targets and the backscattering decreases in with the size of the molecule increasing. The analyzed data were compared with corresponding theoretical studies.

For fluorine atom reaction with 1-propanol, the translational energy distribution and center of mass angular distributions is quite similar to the results of F + n-butane; it is possible that the greater fraction of collision energy in translation comes from the existence of O-H group. The product scattering distributions of fluorine reaction with 1-butene and 1-hexene provide evidence of a long-lived complex mediated mechanism.

AUTOBIOGRAPHICAL STATEMENT

YUANYUAN SHI

Education:

Sep 2016 Ph.D., Chemistry (*anticipated*), Wayne State University
July 2011 B.S. Physical Chemistry, University of Science and Technology of China.

Recent Publications:

1. Joalland, B.; Van Camp, R. D.; Shi, Y.; Patel, N.; Suits, A. G., Crossed-beam slice imaging of Cl reaction dynamics with butene isomers. *J. Phys. Chem. A* **2013**. DOI: 10.1021/jp403030s
2. Joalland, B.; Shi, Y. Y.; Patel, N.; Van Camp, R.; Suits, A. G., Dynamics of Cl plus propane, butanes revisited: a crossed beam slice imaging study. *Phys Chem Chem Phys* **2014,** *16* (2), 414-420. DOI: 10.1039/c3cp51785c
3. Joalland, B., Shi, Y., Kamasah, A., Suits, A. G., & Mebel, A. M. (2014). Roaming dynamics in radical addition–elimination reactions. *Nature communications*, 5. DOI: 10.1038/ncomms5064
4. Joalland, B.; Shi, Y.; Estillore, A. D.; Kamasah, A.; Mebel, A. M.; Suits, A. G., Dynamics of chlorine atom reactions with hydrocarbons: insights from imaging the radical product in crossed beams. *J Phys Chem A* **2014,** *118* (40), 9281-95. DOI**:** 10.1021/jp504804n
5. Abeysekera, C.; Joalland, B.; Shi, Y.; Kamasah, A.; Oldham, J. M.; Suits, A. G., Note: A short-pulse high-intensity molecular beam valve based on a piezoelectric stack actuator. *Rev Sci Instrum* **2014,** *85* (11), 116107. DOI: 10.1063/1.4902153
6. Shi, Y. Y.; Kamasah, A.; Joalland, B.; Suits, A. G., Crossed-beam DC slice imaging of fluorine atom reactions with linear alkanes. *Journal of Chemical Physics* **2015,** *142* (18). DOI: 10.1063/1.4919099